UNIVERSITÀ DEGLI STUDI DI PADOVA

Dipartimento di Ingegneria Industriale

Laurea Magistrale in Ingegneria dell'Energia Elettrica

Tesi di Laurea Magistrale

MODELLI ANALITICI PER INDUTTORI PANCAKE E A MAGNETI PERMANENTI

Relatore
Prof. Fabrizio Dughiero

Laureando:
Alessandro Garaffa
1197566

Anno Accademinco 2019/2020

Alla mia famiglia,
che mi ha supportato
e ha creduto in me...

Sommario

La tecnologia di riscaldamento ad induzione trova una diffusione sempre maggiore in ambito medico, industriale e domestico ed è pressoché insostituibile in alcuni processi metallurgici. Il principio di funzionamento è basato sull'effetto termico generato da corrente indotte in un materiale ferromagnetico immerso in un campo magnetico alternato ad alta frequenza. I principali vantaggi del riscaldamento ad induzione sono l'alta efficienza di trasferimento del calore che è generato direttamente nel pezzo, l'elevata potenza specifica per unità di volume generata, la sicurezza del processo non essendo coinvolti processi di combustione a fiamma e la pulizia, in quanto sono eliminati tutti i prodotti di combustione. Una delle principali carenze di tale tecnologia sta nel bassissimo rendimento (sotto il 50%) nel riscaldamento di ottimi conduttori metallici non magnetici come rame e alluminio.

Il sistema di riscaldamento tramite magneti permanenti rappresenta una tecnologia ancora poco diffusa che invece presenta rendimenti altissimi e potenze specifiche in gioco maggiori rispetto alla classica induzione soprattutto per ottimi conduttori non magnetici.

Entrambe queste tecnologie sono realizzate appositamente per riscaldare determinati pezzi metallici distinti per forma, proprietà elettromagnetiche e tipologia di riscaldamento desiderato, proprio per questo si parla di sistemi e non dispositivi di riscaldamento ad induzione; il pezzo stesso agisce attivamente alla disposizione del campo magnetico e quindi del calore trasferito.

Sono dunque utilizzati modelli FEM elettromagnetici che rappresentano un' accurata soluzione per la modellizzazione ed analisi dei sistemi ad induzione e a magneti permanenti, tuttavia richiedono tempi di computazione molto lunghi, anche di giorni. Lo scopo di questa tesi è di elaborare un modello analitico che fornisca la potenza trasmessa al carico in funzione dei diversi parametri in gioco sia nel caso di induttori di tipo pancake che nel caso della tecnologia a magneti permanenti. Tali modelli analitici verranno poi implementati in un codice di calcolo Matlab e confrontati con i risultati FEM. La tesi si articola in sei capitoli:

- Capitolo 1: Riscaldamento ad induzione
- Capitolo 2: Induttori di tipo pancake
- Capitolo 3: Riscaldamento tramite magneti permanenti
- Capitolo 4: Tensore degli sforzi di Maxwell
- Capitolo 5: Appicazioni

- Conclusioni e prospettive

Il primo capitolo esamina come il riscaldamento ad induzione sia in alcuni campi di applicazione estremamente competitivo in termini di risparmio di energia primaria, costi di funzionamento e manutenzione rispetto al riscaldamento a fiamma. Sempre in questo capitolo viene esposto il principio di funzionamento e la parte impiantistica utilizzata in tale tecnologia. Viene inoltre affrontato il problema del basso rendimento per metalli con bassissima resistività elettrica.
Il secondo capitolo descrive matematicamente il modello analitico dellinduttore di tipo pancake che, nella configurazione implementata e grazie alla simmetria cilindrica del sistema, vengono risolte le equazioni di Maxwell nel potenziale vettore magnetico nella sola componente azimutale. Si ricava quindi lespressione analitica della resistenza equivalente del carico misurata ai capi dellinduttore. La potenza trasmetta al carico è il prodotto della resistenza per la il quadrato della corrente. Inoltre, modificando le condizioni al contorno del modello analitico precedente, si simula la presenza di uno strato di ferrite al di sotto dellinduttore. Tutti i risultati trovati sono poi comparati con il modello FEM nel caso di riscaldamento di dischi di alluminio e acciaio.
Al fine di generare una corrente indotta nel carico è necessario variare il campo magnetico allinterno di esso. Tale variazione può avvenire alterando il campo magnetico nel tempo come nel caso della bobina pancake alimentata da corrente sinusoidale oppure mantenere il campo magnetico fisso tramite un magnete permanente e farlo variare nello spazio. Il sistema più semplice da studiare è basato su un insieme di magneti permanenti magnetizzati assialmente e diposti a raggiera su un disco di ferrite che viene fatto rotare rispetto al carico; il terzo capitolo studia analiticamente tale sistema. Allo scopo di semplificare gli operatori differenziali indotti dalle equazioni di Maxwell ne viene studiato un sistema linearizzato, poi adattato al sistema rotante. Una volta trovato il campo magnetico in tutte le regioni dopo aver fissato le condizioni al contorno, si ricava la distribuzione delle correnti indotte allinterno del disco metallico. La potenza generata da tali correnti per effetto Joule è il risultato dellintegrale del quadrato della densità di corrente nel volume del carico per la propria conduttività elettrica. A partire dal campo magnetico, tramite il tensore degli sforzi di Maxwell si ricava la forza e momento cui è soggetto il disco. Si nota che, a differenza dal riscaldamento tramite bobina pancake, il riscaldamento a magneti permanenti genera unimportate forza assiale repulsiva ed un momento meccanico assiale che limitano estremamente lapplicabilità di tale tecnologia, specialmente in ambito domestico. Anche qui i risultati dei modelli sono confrontati con la simulazione FEM.
Nel quarto capitolo si spiega il motivo della presenza della forza assiale e del momento meccanico sul carico nel sistema a magneti permanenti, non presente invece nel pancake. Viene introdotto quindi il concetto di quantità di moto associata al campo elettromagnetico.
Nel quinto capitolo vengono proposti alcuni accorgimenti per eliminare il momento e la forza assiale cui è soggetto il disco metallico da riscaldare. Tali configurazioni trovano implementazione solo in ambito industriale e non domestico.
Nell'ultimo capitolo sono tratte le conclusioni e osservazioni sul lavoro di tesi e sono descritti i possibili studi futuri che possono rendere il riscaldamento a magneti permanenti in particolare una tecnologia implementabile anche in ambito domestico.

Contents

Chapter 1

Induction heating

Induction heating is the process of heating an electrically conducting object (usually a metal) by using electromagnetic induction, through heat generated in the object by eddy currents. An induction heater consists of an electromagnet and an electronic oscillator that passes a high-frequency alternating current (AC) through the electromagnet. The rapidly alternating magnetic field penetrates the object, generating electric currents inside the conductor, called eddy currents. The eddy currents flowing through the resistance of the material heat it by Joule heating. In ferromagnetic materials like iron, heat may also be generated by magnetic hysteresis losses. The frequency of current used depends on the object size, material type, coupling between the coil and the object to be heated and shape of the workpiece[1].
The basic principles of induction heating have been understood and applied to manufacturing since the 1920s. During World War II, the technology developed rapidly to meet urgent wartime requirements for a fast, reliable process to harden metal engine parts. More recently, the focus on lean manufacturing techniques and emphasis on improved quality control have led to a rediscovery of induction technology, along with the development of precisely controlled, all solid state induction power supplies[2]. The main success factors which lead to the spread of this technology and which make it often irreplaceable are basically the following:

- The heat is generated directly inside the workpiece
- Possibility to locate the heat in specific workpiece's zone in order to perform particular applications
- Rational use of electrical energy spent to produce heat
- Very high repeatability of thermal treatments i.e. high standardization of the final product with the consequent reduction of waste
- Possibility to have high specific power and therefore very low heating time, with consequentially the grown of the production
- High efficiency due by the almost absence of the environmental's heating

- High reliability of the induction heaters which reduces interruptions for fault or maintenance
- Elimination of environmental pollution due by the heating process with the consequent improvement of the healthiness of the working place

These characteristics make the induction heating a very competitive system with respect classical methods of heating by combustion. Induction heating finds mostly industrial applications but also in growing domestic applications as inductions hobs.
The main drawbacks or disadvantages are the following:

- Induction heating equipment is more complex than heating by flame and the initial cost is higher and it can be a real investment
- Poor adaptability and interchangeability, the induction heating system generally is designed only for determinate dimension of the workpiece
- Induction heating can't be used for complex shape workpieces

An other important downside of the induction heating is when we have to heat a good conductor workpiece as aluminium or copper, in fact this process has a relative low efficiency. The aim of this thesis is to develop an analytical model for pancake inductors and permanent magnets induction heating system which is a new high efficiency process to heat good conductors.

1.1 Primary energy and economical considerations

In the 1970s, as a result of the oil crises, the greatest concern on a global scale became the availability of primary energy sources, particularly fossil fuels. The energy economy became a major political goals. During the 1980s, however, the possible negative influence of human activities, particularly energy use, on the environment was recognised as an even more urgent problem. Energy programmes were reformulated with the aim of reducing energy consumption, but also to reduce environmental pollution. The electrothermal technologies (arc heating, resistance heating, plasma heating, electronica heating, induction heating, ...) play an important role in terms of greenhouse gas (GHG) reduction and energy saving [3].
In order to compare different energy sources it's necessary to get an arbitrary unit of measurement: the **primary energy** (PE). PE is an energy form found in nature that has not been subjected to any human engineered conversion process. It is energy contained in raw fuels, and other forms of energy received as input to a system. For example, coal can be converted to synthetic gas, which can be converted to electricity; in this example, coal is primary energy, synthetic gas is secondary energy, and electricity is tertiary energy. If we want to compare therefore electricity and natural gas which is a primary energy, it's necessary to relate the electricity to its primary energy consumption. Considering figure 1.1 taking into account the generation efficiency, the transmission losses, losses due by transformers and of the device supply, 10 MJ of primary energy generates the equivalent of 2.6 MJ of electrical energy. We can therefore say that 2.6 MJ of end-user electrical energy are equivalent to 10 MJ of primary energy. We have to note that

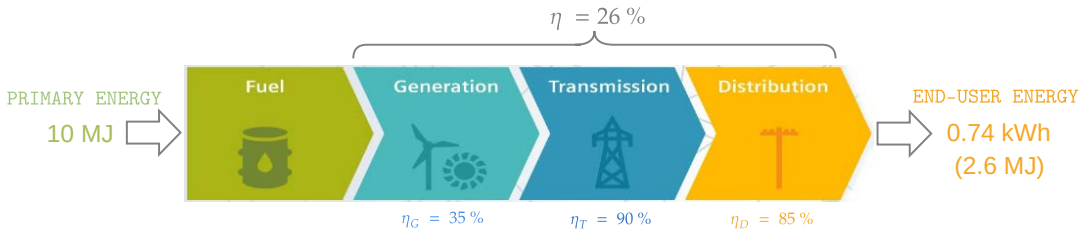

Figure 1.1: Electricity production to supply chain.

the PE equivalent for electricity could not seems convenient in terms of efficiency but electricity is one of the best energy carriers Electricity is one of the most common energy carriers, it can be transformed from various primary energy sources such as coal, oil, natural gas, and wind and used for in many applications as traction, heating, lighting and as well storage. The electrical energy found a huge spread for the following proprieties:

- usability
- convertibility
- transmissibility
- generability from different primary energy sources

If we wanna to compare for example two process A and B which supply the same "product X" and process A neds an amount of electrical energy in kWh E_A and an amount of MJ F_A of fuel while process B E_B and F_B as shown in figure 1.2.
It's useful to define the **replacement factor** γ:

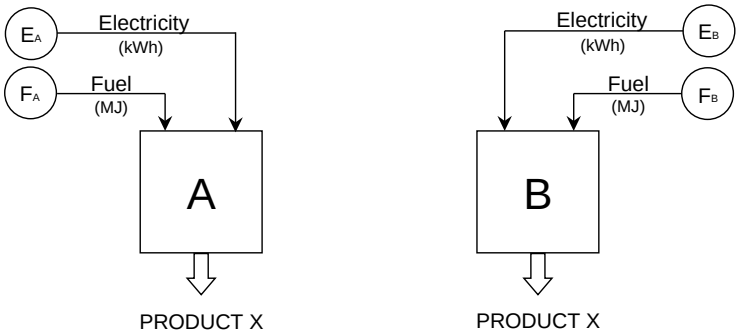

Figure 1.2: Comparison between two productive energy process.

$$\gamma = \left| \frac{F_A - F_B}{E_A - E_B} \right| \quad [\text{MJ/kWh}] \tag{1.1}$$

If we wanna switch from the process A to the process B where the last one absorbs a bigger amount of electricity but a smaller amount of fuel i.e.:

$$F_A > F_B$$
$$E_A < E_B$$

in this case the replacement factor expresses that the process B replace with γ MJ of fuel for each 1 kWh of electricity with respect process A. This means that considering the process in figure 1.2 where to produce 0.74 kWh of electricity is necessary 10 MJ of primary energy so to produce 1 kWh of electricity is necessary 13.5 MJ of primary energy, we will have a **primary energy saving** if:

$$\gamma > 13.5 \quad [\text{MJ/kWh}]$$

The value of γ^* where primary energy saving is null and in the case of electricity drawn from the grid, depends strongly by the share of renewable energy sources (RES) which was in EU 14.8% in 2005, 30% in 2017 and the forecast for the 2030 is 49% [4]. This means that primary energy saving is a dynamic concept and the value γ^* will drops with the implementation of new RES in the European grid and the estimated value of $\gamma^* = 13.5$ is absolutely an overestimated value cause it considers electricity produced only since fossil fuels. The calculation of the whole γ^* coefficient for the Italian or European grid is a complex task and can be done with different methodologies. In literature has been defined the **primary energy factor** (PEF) and indicates how much primary energy is used to generate a unit of electricity or a unit of useable thermal energy. Figure 1.3 shows the PEF in Europe from 2000 and the forecast until 2030 by using four different calculation methods. At the moment the PEF is about 2.00 therefore, in order to

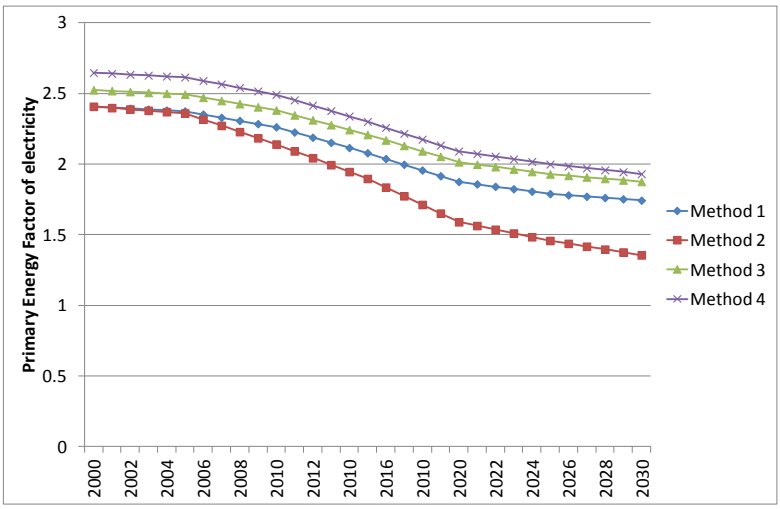

Figure 1.3: Comparison of the results for the different PEF calculation methods for European electricity production[5].

produce 1 kwh of electricity is necessary to deliver 2 kWh of primary energy and the efficiency $\eta = 50\%$, grater than the 26% with the process shown in figure 1.2 and γ^* is

7.2 MJ/kWh.
The primary energy saving however is not the only index to optimize cause the cost of the different forms of energy; in order to evaluate the if process B is cheaper than process A, it's useful to define the coefficient β:

$$\beta = K_E/K_F \quad [MJ/kWh] \tag{1.2}$$

where K_E is the electricity cost [€/kWh] and K_F the fuel cost [€/MJ], basically, the process B is cheaper than the process A if:

$$\gamma > \beta \tag{1.3}$$

1.1.1 Practical example

One interesting and actual comparison in a domestic application is among induction hobs and gas hobs. In Italy the price of the natural gas for the end user depends on region to region and is about 0.90 €/m^3 while the price for one kWh of electricity depends by contract type and can be assumed 0.20 €/kWh. Without considering the supplied energy due the transportation of the gas therefore assuming a primary energy, the average heating value of natural gas (methane) is 52 MJ/kg and the specific weight is 0.67 kg/m^3.
Let us suppose that the hobs have the following heating efficiency:

Type	**Input power (kW)**	**Efficiency**	**Delivered power (kW)**
Induction	1.11	90%	1.00
Gas	2.50	40%	1.00

Further assuming that the cooking time is 1 hour, the total supplied energy is:

Type	**Supplied energy**
Induction	1.11 kWh
Gas	2.50 kWh ≡ 9.00 MJ

which are equivalent to burn 173 g of methane therefore the cost of this heating process for the two types of energy source are:

Electricity	0.22 €/h
Gas	0.23 €/h

we can therefore see how the price for both the heating systems is almost the same, therefore it's difficult to say that induction heating is cheaper than gas because of the dynamic variation of electricity and fuel cost.
We can applying the tools shown before; we can calculate the β coefficient defined in equation 1.2 which results:

$$\beta = \frac{K_E}{K_F} = \frac{20 \text{ cent€/kWh}}{2.58 \text{ cent€ /MJ}} = 7.75 \text{ MJ/kWh}$$

while the replacement factor defined in equation 1.1 labelling the induction heating as the process B and gas A, γ results:

$$\gamma = \frac{F_A}{E_B} = \frac{9.00 \text{ MJ}}{1.11 \text{ kWh}} = 8.11 \text{ MJ/kWh} \tag{1.4}$$

We can notice that γ is slightly grater than β therefore the process B (induction heating) is cheaper than process A (gas).
Regarding the primary energy saving $\gamma > \gamma^* = 7.2$ MJ/kWh therefore the process A neds more primary energy to supply the same product than process B i.e. induction heating process saves primary energy. As already said, the increase of RES in the grid decreases the value of γ^* therefore the induction heating will be more and more competitive in the future.
Summarizing we can say that induction heating in terms of operative cost is similar to the gas heating and the investment cost and actually the initial investments (higher for induction hobs) can't be amortise for domestic use. In term of primary energy saving for induction heating, cause the higher heating efficiency, is better than the flame one and the future trend is going to getting better.
Induction hobs have other advantages such as easy cleaning, safety, no combustion but on the other hand they need special pots to work. In fact, aluminium and copper pots or non-magnetic metals have a low efficiency. In this thesis therefore we will study a system based on permanent magnets which allows to heat with high efficiency aluminium or copper pots as well.

1.2 Heating demand

Heating and cooling (H/C) of ambient and objects requires a huge share of energy demand. In fact, as shown in figure 1.4 the end-user energy demand in the EU28 in 2012 was 12,821 TWh whose 6,497 (51%) TWh used for heating and cooling. The remanent 6,323 TWh of the energy demand are the non H/C comprises end-uses like transportation, mechanical energy in industry as well as residential and service sector appliances. From these data we can say that the increase the heating efficiency in terms of primary energy saving would have a big impact on the total energy demand. The cooking heating neds the 2% of the whole energy demand while processing heating the 15%. From figure 1.5 we can see how the natural gas leads the primary energy demand with 45% of share followed by coal with 15%; as already said in this pie chart electricity is not present, because is considered a secondary energy. As we talked in subsection 1.1.1, induction heating allows to save primary energy than gas in domestic applications and this can be even more valid in industry where the process heating energy demand is eight times bigger than household.
With equal final energy demand, less primary energy can be consumed by substituting fossil fuel heating system with electric heating system which have the advantage to be a zero emission technology. Moreover, with the installation of a private photovoltaic power plant also financed by government incentives, industries can improve drastically the primary energy saving and also the heating process cost.
The development of a new high-efficiency electricity-based heating system can find a

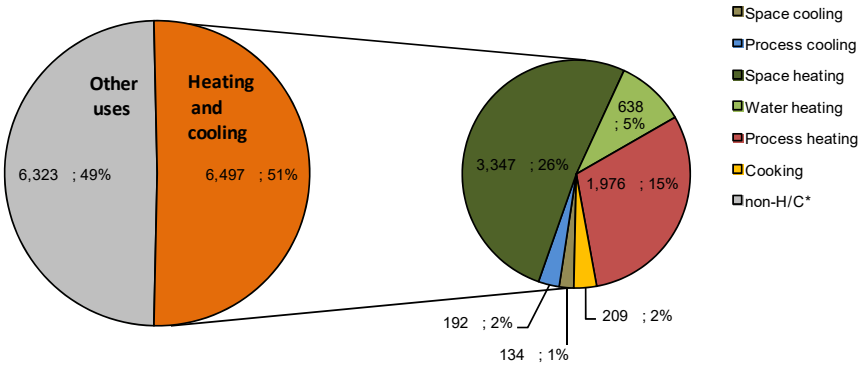

Figure 1.4: Primary energy demand for EU28 by energy carrier for H/C in all sectors in 2012 [TWh][6].

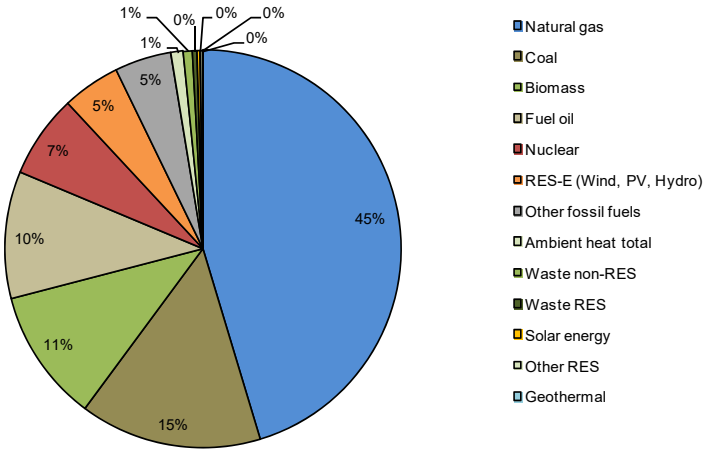

Figure 1.5: Primary energy demand for EU28 by energy carrier for H/C in all sectors in 2012 [TWh][6].

wide field of application in industry but also in household and will be always more competitive with the grown of the RES share in the grid.

1.3 Working principle of induction heating

The working principle of the induction heating is a non-contact process which is a combined recipe of Electromagnetic induction and Joule heating therefore is based on three physical principles, here below explained:

1. Transfer of energy from the inductor to the piece to be heated (workpiece or billet),

by means of **Electromagnetic Fields**.

2. Transformation of the electric energy into heat due to **Joule effect** ($P = RI^2$).
3. Transmission of the heat inside the workpiece by means of **Thermal Conduction**.

Considering figure 1.6, an alternating current flows into the coil which generates an electromagnetic field which surrounds the entire space. If the coil has an optimized

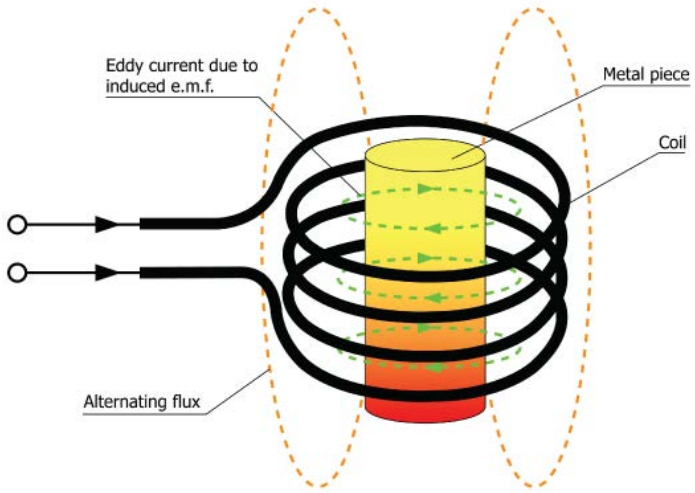

Figure 1.6: Induction heating working principle [7].

shape i.e. is well coupled with the workpiece, the electromagnetic field is strong into the workpiece space. The magnetic flux density generated in a point P distant **r** by a infinitesimal wire of length dL where flows an oriented current **I** is described by Biot-Savart' law:

$$\mathbf{B} = \int \frac{\mu_0}{4\pi} \frac{(dL\ \mathbf{I}) \times \hat{\mathbf{r}}}{r^2} \tag{3.5}$$

The key principle of the induction heating is the **Faraday's Law** which says that the instantaneous electromotive force (e.m.f) along a generic closed path Γ is opposite to the variation of magnetic flux in a arbitrary surface Σ which lies on Γ with respect the time, in formula:

$$e.m.f.\big|_{\Gamma}(t) \ = \ -\frac{d\Phi_{\Sigma}}{dt} \ = \ -\frac{d}{dt}\int_{\partial\Gamma} \mathbf{B} \cdot \hat{\mathbf{u}}_N d\Sigma \tag{3.6}$$

Equation 3.6 is applicable for each closed path, in air but also inside the workpiece; right inside the conductor workpiece since the Ohm's law the Faraday's e.m.f. generates a current proportional to the conductivity σ of the metal. The induced currents inside the workpiece (eddy currents) generate heat for Joule losses directly in the billet body. The base working principle is the variation of magnetic flux inside the workpiece with respect the time as expressed in the Faraday's Law. This means that in order to heat the billet it's necessary a variation of Φ_{Σ} which derives by the sinusoidal variation of magnetic flux density with respect the time. Basically the stronger the applied magnetic field, or the greater the electrical conductivity of the conductor, or the faster the

field that the conductor is exposed to changes, then the greater the currents that are developed and therefore the heating.
The Faraday's law tell us in addition that what is really important is the variation of Φ_Σ with respect the workpiece in the time; in particular if we consider a permanent magnet in motion with a relative speed v_x with respect the workpiece along the x-direction, manipulating equation 3.6 we obtain:

$$e.m.f.\Big|_\Gamma(t) = -\frac{d\Phi_\Sigma}{dt} = -\frac{d\Phi_\Sigma}{dx}\frac{dx}{dt} = -\frac{d\Phi_\Sigma}{dx}v_x \tag{3.7}$$

The electromotive force is still generated even if the magnetic field is maintained constant in the time therefore we can say that in order to generate heat into the billet:

- The magnetic flux density varies over *time*.
- The magnetic flux density varies over *space*.

The actual induction heating systems with the coils are based of the variation of the magnetic flux density over the time by supplying an alternating current. The aim of this thesis is also to study a new induction heating system based on the space-variation of the magnetic flux density.

1.4 Elements of induction heating

There is a particular frequency of the sinusoidal current which supplies the coil called *resonance frequency* where the load seen from the coil terminal is particular resistive i.e. the $\cos\phi$ reaches the maximal value. In order to obtain the resonance frequency which depends by the load type as metal type, shape, heating required, the coil has to generate high frequency magnetic field therefore has to be supplied with high frequency current. Figure 1.7 shows the simplified block diagram of an induction heating unit where, starting from AC 50 Hz and passing through DC stage, we obtain the final AC-HF.

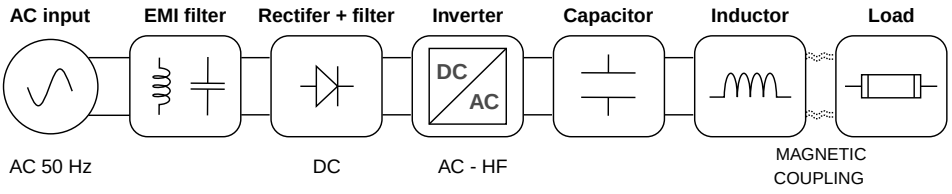

Figure 1.7: Simplified block diagram of an induction heating unit.

All the basic steps of system are shown below:

- **AC input**: An induction heater is powered by the electric grid which works at 50/60 Hz. For industrial applications the grid generally is three-phase with a low or medium voltage while single-phase for the domestic or for limited power applications.

- **EMI filter**: Cause of the distorting load which induction heater system is, in order to decrease the harmonic contribution which would affects the grid, it is necessary to connect EMI filters. The major contributor to harmonic is the rectifier which generates 2^{nd} order harmonics for single-phase input and 3^{rd} order for three-phase input and second contributor to higher-order harmonics is the inverter. A basic EMI filter is a capacitor-inductor which short circuits to ground the harmonics; more sophisticated filters are based on an active electronic which generate an out of phase harmonic in order to delete the harmonic total contribution.

- **Rectifier**: In order to supply the inverter, it's necessary to convert the AC 50 Hz source into a DC source. This task is performed by the rectifier which can be single or three phase as shown in figure 1.8. If instead of diodes we use thyristors, it's

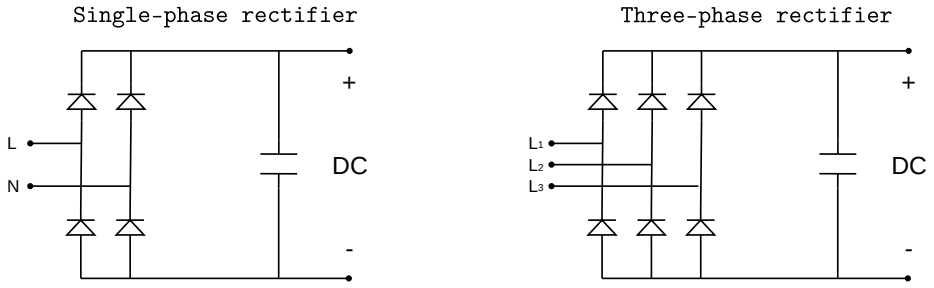

Figure 1.8: Schematic representation of single and three phase rectifier.

possible to control the conduction of component and therefore control the final DC voltage value which then will supply the inverters and therefore the inductor. The capacitor (filter) in the DC stage allows to decrease the ripple level and guarantees a better quality output voltage decreasing the harmonics.

- **Inverter**: is one of the main part of an induction heating system and starting from the DC power supply, convert into AC HF; the inverter is rated by its operating frequency range and power. There are various types of inverters supplies which are line-frequency supplies, frequency multipliers, motor-generators, spark-gap converters, and solid-state inverters. Solid-state inverters have the most efficiency between the power supplies.
  The DC current goes to the inverter, where solid-state switches, such as IGBTs or MOSFETs convert it into a current, this time at a high frequency (typically in the range of 10kHz-600kHz). According to figure 1.9 IGBTs can work at a higher power level and lower frequency versus MOSFETs operating at a lower power level and higher frequencies [8].

- **Capacitor**: The natural behaviour of the load is inductive so the $\cos\phi$ is particularly low and, in order to control the apparent power supplied from the inverter and rectifier, it's necessary the power factor correction with a capacitor. The capacitance C to connect in parallel to the inductor has to be calculated since the

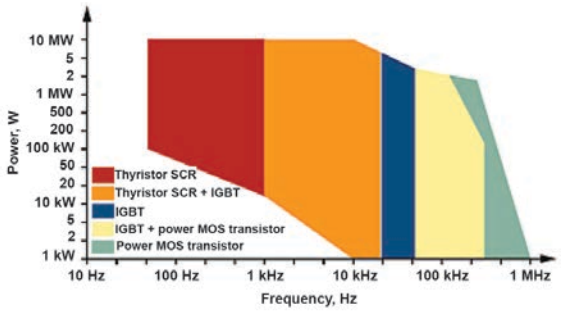

Figure 1.9: Power vs frequency for commercial solid-state power supplies [9].

resonant frequency f_R:

$$f_R = \frac{1}{2\pi\sqrt{LC}} \tag{4.8}$$

where L is the inductance of the induction coil. The necessity to the power factor correction capacitor is to decrease the size of the inverter which will supply about the active power transferred through heat to the load with a consecutive reduction of the cost of the plant.

- **Inductor**: The induction heating coil is specifically shaped copper tubing or other conductive material which alternating electrical current is passed through, creating a variable magnetic field. Metal parts or other conductive materials (load) are placed within, through or close to the induction heating coil, without touching the coil and the variable magnetic field that is generated creates eddy currents within the metal causing it to heat. In order to transfer to the metal as much power as possible, the inductor has to be well coupled with the load thus it has to be particularly shaped. Figure 1.10 shows the most common coil shapes. The magnetic

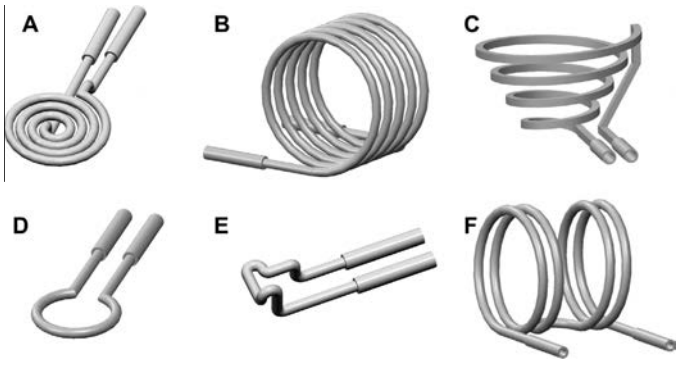

Figure 1.10: Common coil designs applied for the inductive heating of composites (A) pancake coil, (B) helical coil, (C) conical coil, (D) single-turn coil, (E) irregular coil adapted to the workpiece shape, (F) double-helical coil (Helmholtz coil) [10].

field generated from the coil, as already said, depends by the current which flows

inside it. In order to increase the current capability, the inductor presents a hole inside its section where water flows to keep the copper temperature low.

- **Load**: The load itself is part of the induction system which is customized in base on the basis of metal kind, shape, heating treatment kind.

1.5 The problem of the low efficiency for good conductors

Without going into detail, considering a cylindrical billet with constant resistivity and permeability around which a coil is wrapped where flows a sinusoidal current with angular frequency ω. With reference to the system in figure 1.11 the billet has radius R, electrical resistivity ρ and relative permeability μ_r. The coil has N turns with radius $R_c = \alpha R$, radial length s and axial length a.

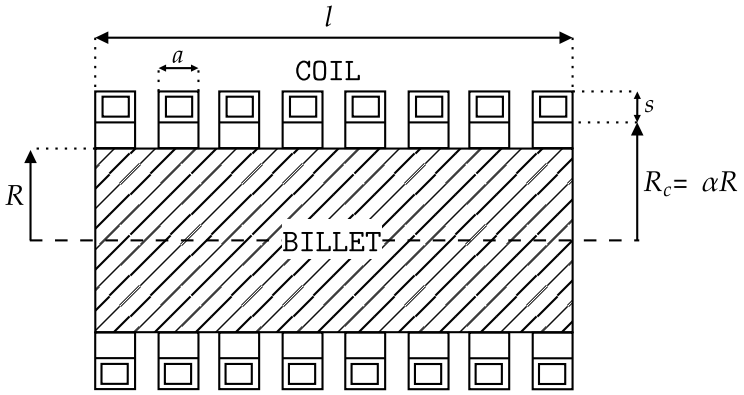

Figure 1.11: System consisting of the inductor and the cylindrical load.

From this geometrical configuration it's possible to derive the electrical efficiency of the system η[11]:

$$\eta = \frac{r'_L}{r'_L + r_c} = \frac{1}{1 + r_c/r'_L} \tag{5.9}$$

where r'_L is the resistance of the load reported at the coil terminals and results:

$$r'_L = N^2 \rho \frac{2\pi R}{l\delta} \sqrt{2} P \tag{5.10}$$

and δ is the penetration depth, quantity with a key role in induction heating and defined as following:

$$\delta = \sqrt{\frac{2\rho}{\mu_0 \mu_r \omega}} \tag{5.11}$$

while the quantity P is defined as:

$$P = \Re\mathfrak{e}\left\{ -\sqrt{-j} \frac{J_1(\sqrt{-j}m)}{J_0(\sqrt{-j}m)} \right\} \quad \text{with } m = \frac{\sqrt{2}R}{\delta} \tag{5.12}$$

where J_0 and J_1 are the firs kind Bessel function of order 0 and 1 respectively.
The quantity r_c is the resistance of the coil without the load (billet) and results:

$$r_c = N^2 \rho_c \frac{2\pi R_i}{l\delta_c} A_c k_c \tag{5.13}$$

where ρ_c is the electrical resistance of the coil, k_c is a parameter which takes into account the density of the turns and is defined for a rectangular axial section of the coil with dimension $a \times s$:

$$k_c = \frac{l}{Na} \tag{5.14}$$

it has to note that figure 1.11 shows an hollow conductor, the hole is necessary to the cooler (generally water) flowing but in this case of study we assume that the turns have rectangular section with no hole. δ_c is the penetration depth of the coil calculated with the resistivity of the coil. The quantity A_c is defined as following:

$$A_c = \Re\mathfrak{e}\left\{(1+j)\frac{\cosh\left(\sqrt{2j}s/\delta_c\right)}{\sinh\left(\sqrt{2j}s/\delta_c\right)}\right\} \tag{5.15}$$

Equation 5.9 becomes by replacing r'_L with equation 5.10 and r_c with 5.13:

$$\eta = \frac{1}{1+\alpha\sqrt{\frac{\rho_c}{\rho\mu_r}}\frac{A_c k_c}{\sqrt{2}P}} \tag{5.16}$$

The electrical efficiency increases with the decreasing of α which has the minimal theoretical value equal to 1 i.e. the coil is wrapped around the billet without air gap. The same is still valid for the parameter k_c which reaches its minimal value of 1 when the turns axial pitch is a. Both those two conditions are equivalent to say that the inductor is well coupled with the load. If this is verified and assuming to have sufficiently high values of m, the maximal electrical efficiency is:

$$\eta_{max} = \frac{1}{1+\alpha\sqrt{\frac{\rho_c}{\rho\mu_r}}} \tag{5.17}$$

Figure 1.12 show the electrical efficiency in function of m for $\alpha = 2$ and $k_c = 1$ for different material listed in table 1.1. We suppose the coil is made up copper with resistivity $\rho_c = 1.68\times10^{-8}\ \Omega m$. It's easy to note that for m>2.5 the efficiency is mostly independent by m i.e. the frequency and reach the value η_{max}, while below 2.5 η strongly drops to zero with m equal to zero. We can also note that for the magnetic steel below the Curie's temperature, the efficiency is higher than the steel above the Curie's temperature even if the resistivity is higher. In fact in the transaction from magnetic to non-magnetic steel μ_r pass from 500 to 1 while the resistivity grows just of the 30% and the whole effect is a reduction of the efficiency. An other important term which play a key role for the efficiency is the coefficient α express basically how the coil is radially close to the billet. Figure 1.13 shows the dependence of the efficiency in function of m for different values of α from 1.5 to 3.0 for steel above the Curie's temperature and for copper.

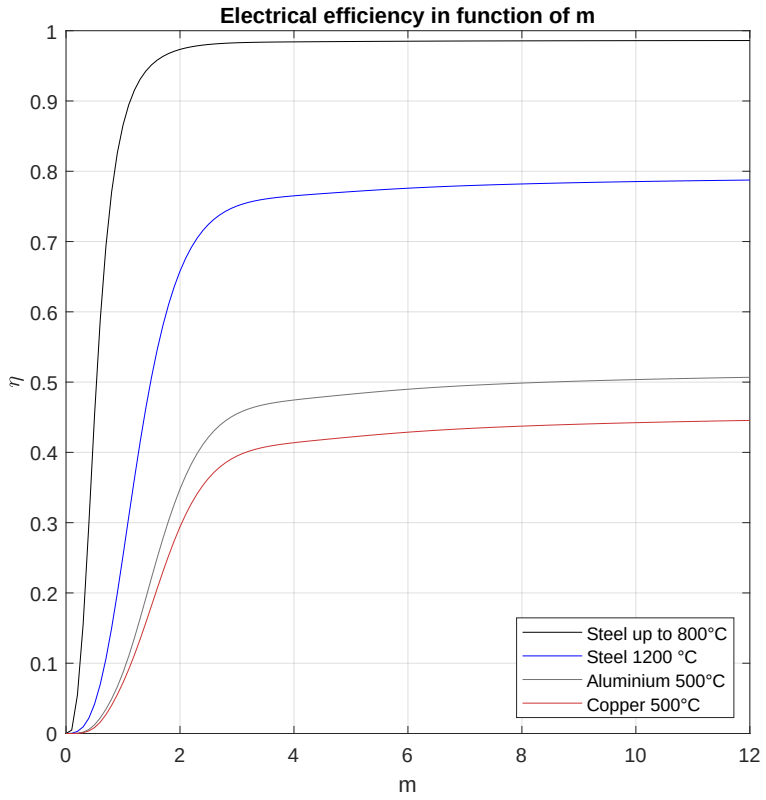

Figure 1.12: Electrical efficiency of coil-load system in function of m ($\alpha = 2,\ k_c = 1$).

Material	**Electrical resistivity** ρ **[**Ω**m]**	**Relative permeability** μ_r
Steel (up to 800 °C)	0.756e-6	500
Steel (1200 °C)	1.04e-6	1
Aluminium (500 °C)	8.03e-8	1
Copper (500 °C)	4.91e-8	1

Table 1.1: Resistivity and permeability for different materials.

We can see how for good no-magnetic conductors like copper or aluminium, the electrical efficiency is poor. This is due because the current in the coil heats the coil itself i.e. the maximal theoretical efficiency to heat the same copper which constitutes the coil is:

$$\eta_{max}^{Cu} = \frac{1}{2} \tag{5.18}$$

while the maximal theoretical efficiency to heat aluminium is:

$$\eta_{max}^{Al} = \frac{1}{1 + \sqrt{\frac{\rho_{Cu}}{\rho_{Al}}}} \simeq 0.56 \tag{5.19}$$

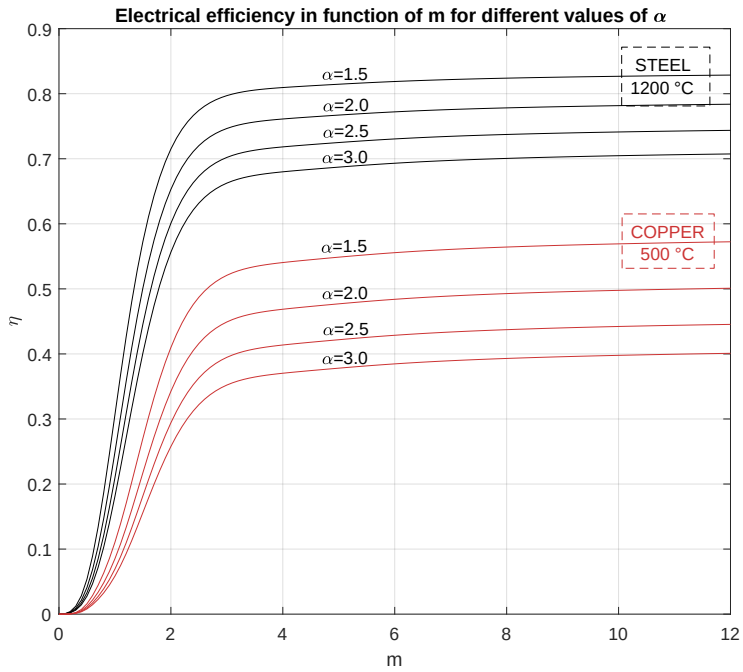

Figure 1.13: Electrical efficiency of coil-load system for different values of alpha.

Heating a copper or aluminium billet by using induction is a extremely poor in therms of efficiency and this outcome is valid for axial inductors but also for pancake inductor or, in general, for every kind of coil shape.
This issue limits the spread of the induction hobs because of the necessity to replace normal pots with magnetic steel pots which guarantees a sufficient level of heating. As already told we speak of induction heating system not induction heating device cause the load interacts directly with the power supplied and gradually with the increasing of the temperature in the billet, increase the resistivity and the efficiency as well. Depending on the operation to be carried out, it is therefore necessary to carry out a specific analysis to identify the ideal generator for induction heating. Frequency is one of the decisive factors for successful induction heating. However, the material, the heating temperature and the quantity of parts to be treated also have a decisive influence on the planning of the induction heating solution.

Chapter 2

Pancake inductor

A pancake inductor is made up of a flat spiral copper coil which allows to generate a magnetic field with a big radial component around it. The magnetic field is therefore generated in a flat region and, for this reason, pancake inductors are used to heat steel foils, flat metal disks and are installed in the induction hobs (see figure 2.1).

Figure 2.1: Pancake inductor used in induction hobs.

The principal characteristic of this kind of inductor is the number of turns N, the internal and the external radius R_i and R_e and the space between the turns. An other feature of the device is the diameter of the turns which contributes also to the ampacity. Is the current which generates the magnetic fields so it has to be as high as possible without overheating the inductor. Since the current varies with frequency of some tens of kHz the skin effect affect the wire and, in order to distribute the current along all the conductor it is made up Litz wire which replace the mono-wire by numerous smaller single insulated wires resulting the same cross section.

2.1 Mathematical model

In order to have a mathematical model of the pancake inductor-load system we consider the inductor made up by a concentric planar circular coil of negligible axial thickness characterized by N concentric adjacent turns as show in figure 2.2. The innermost turns has radius R_i while the outermost turn R_e. The position of the coil is parallel to the x-y plane, at a coordinate $z = s$. At $z = r+s$ there is a soft magnetic yoke with ideally infinite permittivity which shield the upper space by the magnetic field however it hasn't considered in the mathematical model. In $z = 0$ is present a supposed infinite long metal disk with electrical conductivity σ an thickness h, over the disk is present air again.

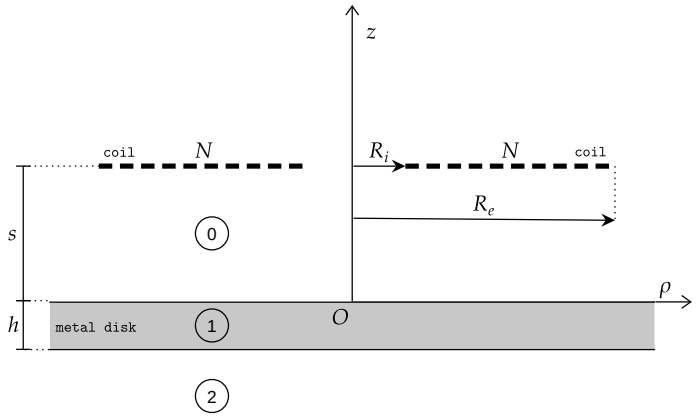

Figure 2.2: Schematic configuration of the system.

We can therefore define three regions which will have different solutions:

- Region ⓪ : air gap region ($0 < z < s$);
- Region ① : metal region ($-h < z < 0$);
- Region ② : air region ($z < -h$);

A sinusoidal current flows in the coil with the time-dependent law $i(t) = I\sin(\omega t)$ which can be written in terms of the phasor $\underline{I}$:

$$i(t) = \mathrm{Im}(\underline{I}) = \mathrm{Im}(Ie^{j\omega t}) \tag{1.1}$$

where $I = \sqrt{2}I_{rms}$ is the peak current value and I_{rms} is the root mean square value of the current. In order to simplify the study we will operate with phasors, in particular, in sinusoidal steady state the magnetic flux density $\mathbf{B}$ generated by the current will follow the same law of the current and can be represented as phasor $\underline{\mathbf{B}} = \mathbf{B}e^{j(\omega t+\phi)}$. Phasors are also the components of a phasor vector but, in order to reduce the complexity of notation, the underline of the components will be avoided. Due to the geometrical

symmetry, we choose to use cylindrical coordinates (ρ, θ, z) and in this coordinate system the magnetic flux density for physical considerations has the azimuthal component equal to zero:

$$\underline{\mathbf{B}} = \begin{pmatrix} B_\rho \\ B_\theta \\ B_z \end{pmatrix} = \begin{pmatrix} B_\rho \\ 0 \\ B_z \end{pmatrix} \tag{1.2}$$

Since:

$$\underline{\mathbf{B}} = \nabla \times \underline{\mathbf{A}} \tag{1.3}$$

where $\mathbf{A}$ is the magnetic potential vector which is perpendicular to $\mathbf{B}$ and has only the azimuthal component:

$$\underline{\mathbf{A}} = \begin{pmatrix} A_\rho \\ A_\theta \\ A_z \end{pmatrix} = \begin{pmatrix} 0 \\ A_\theta \\ 0 \end{pmatrix} \tag{1.4}$$

If we study the system in terms of magnetic potential vector we reduce the numbers of unknown to one. Still taking advantage of geometric symmetry $A_\theta = A_\theta(\rho, z)$ i.e. it doesn't depend by the azimuthal coordinate. We can therefore write the equations which govern the system starting from the Ampere's law:

$$\nabla \times \underline{\mathbf{H}} = \underline{\mathbf{J}} \tag{1.5}$$

J is the current density which can be expressed with the Ohm's law $\underline{\mathbf{J}} = \sigma \underline{\mathbf{E}}$ where σ is the electrical conductivity and $\underline{\mathbf{E}}$ is the electric field. Considering also that $\underline{\mathbf{B}} = \mu \underline{\mathbf{H}}$ where μ is the magnetic permittivity, equation 1.5 becomes:

$$\nabla \times \frac{\underline{\mathbf{B}}}{\mu} = \sigma \underline{\mathbf{E}} \tag{1.6}$$

Taking into account the relation between $\underline{\mathbf{B}}$ and $\mathbf{A}$ we can write:

$$\nabla \times \nabla \times \frac{\underline{\mathbf{A}}}{\mu} = \sigma \underline{\mathbf{E}} \tag{1.7}$$

Remembering that $\nabla \times \nabla \times \mathbf{A} = \nabla(\nabla \cdot \mathbf{A}) - \nabla^2 \mathbf{A}$ and considering the Coulomb gauge ($\nabla \cdot \mathbf{A} = 0$) we obtain:

$$\nabla^2 \underline{\mathbf{A}} = -\sigma \mu \underline{\mathbf{E}} \tag{1.8}$$

Starting from the MaxwellFaraday equation we can express the electric field in terms of the magnetic vector potential:

$$\nabla \times \underline{\mathbf{E}} = -\frac{\partial \underline{\mathbf{B}}}{\partial t} = -\frac{\partial}{\partial t} \nabla \times \underline{\mathbf{A}} = \nabla \times \left(-\frac{\partial \mathbf{A}}{\partial t} \right) \Rightarrow \underline{\mathbf{E}} = -\frac{\partial \underline{\mathbf{A}}}{\partial t} \tag{1.9}$$

We said that in sinusoidal steady state all the time-dependent variables are expressed by phasors and a time-derivate is replaced with $j\omega$ i.e. $\frac{\partial}{\partial t} \rightarrow j\omega$. The final expression becomes:

$$\nabla^2 \underline{\mathbf{A}} = j\omega\sigma\mu \underline{\mathbf{A}} \tag{1.10}$$

In cylindrical coordinate system the Laplacian operator has the following structure:

$$\nabla^2 \underline{\mathbf{A}} = \begin{pmatrix} \nabla^2 A_\rho - \frac{A_\rho}{\rho^2} - \frac{2}{\rho^2}\frac{\partial A_\theta}{\partial \theta} \\ \nabla^2 A_\theta - \frac{A_\theta}{\rho^2} + \frac{2}{\rho^2}\frac{\partial A_\rho}{\partial \theta} \\ \nabla^2 A_z \end{pmatrix} \tag{1.11}$$

In our case of study $A_\rho = A_z = 0$ therefore equation 1.10 becomes:

$$\begin{pmatrix} -\frac{2}{\rho^2}\frac{\partial A_\theta}{\partial \theta} \\ \nabla^2 A_\theta - \frac{A_\theta}{\rho^2} \\ 0 \end{pmatrix} = \begin{pmatrix} 0 \\ j\omega\sigma\mu A_\theta \\ 0 \end{pmatrix} \tag{1.12}$$

Note that if the magnetic vector potential has only the azimuthal component and equation 1.10 is true, A_θ is constant along θ as we already said. The operator $\nabla^2 A_\theta$ can be developed as:

$$\begin{aligned} \nabla^2 A_\theta = \nabla \cdot (\nabla A_\theta) = \nabla \cdot \begin{pmatrix} \frac{\partial A_\theta}{\partial \rho} \\ \frac{1}{\rho}\frac{\partial A_\theta}{\partial \theta} \\ \frac{\partial A_\theta}{\partial z} \end{pmatrix} = \nabla \cdot \begin{pmatrix} \frac{\partial A_\theta}{\partial \rho} \\ 0 \\ \frac{\partial A_\theta}{\partial z} \end{pmatrix} &= \frac{1}{\rho}\frac{\partial}{\partial \rho}\left(\rho \frac{\partial A_\theta}{\partial \rho}\right) + \frac{\partial^2 A_\theta}{\partial z^2} \\ &= \frac{1}{\rho}\frac{\partial A_\theta}{\partial \rho} + \frac{\partial^2 A_\theta}{\partial \rho^2} + \frac{\partial^2 A_\theta}{\partial z^2} \end{aligned} \tag{1.13}$$

where it's used the divergence in cylindrical coordinates ($\nabla \cdot \mathbf{A} = \frac{1}{\rho}\frac{\partial \rho A_\rho}{\partial \rho} + \frac{1}{\rho}\frac{\partial A_\theta}{\partial \theta} + \frac{\partial A_z}{\partial z}$) and the chain rule for the partial derivate. For the only azimuthal component, equation 1.10 by using equations 1.11 and 1.13 becomes:

$$\frac{\partial^2 A_\theta}{\partial \rho^2} + \frac{\partial^2 A_\theta}{\partial z^2} + \frac{1}{\rho}\frac{\partial A_\theta}{\partial \rho} - \frac{A_\theta}{\rho^2} = j\omega\sigma\mu A_\theta \tag{1.14}$$

We can solve the differential equation using the method of the separation of the variable, we can therefore write the solution with the structure:

$$A_\theta(\rho, z) = P(\rho)Z(z) \tag{1.15}$$

equation 1.14 can be rewritten as:

$$Z\frac{\partial^2 P}{\partial \rho^2} + P\frac{\partial^2 Z}{\partial z^2} + \frac{Z}{\rho}\frac{\partial P}{\partial \rho} - Z\frac{P}{\rho^2} = j\omega\sigma\mu PZ \tag{1.16}$$

dividing by Z we obtain:

$$\frac{\partial^2 P}{\partial \rho^2} + P\frac{1}{Z}\frac{\partial^2 Z}{\partial z^2} + \frac{1}{\rho}\frac{\partial P}{\partial \rho} - \frac{P}{\rho^2} = j\omega\sigma\mu P \tag{1.17}$$

It's possible to simplify the expression by defining:

$$\zeta^2 := \frac{1}{Z}\frac{\partial^2 Z}{\partial z^2} \tag{1.18}$$

Equation 1.17 by using eq. 1.18 becomes:

$$\frac{\partial^2 P}{\partial \rho^2} + P\zeta^2 + \frac{1}{\rho}\frac{\partial P}{\partial \rho} - \frac{P}{\rho^2} = j\omega\sigma\mu P \tag{1.19}$$

which can be rewritten:

$$\rho^2 \frac{d^2 P}{d\rho^2} + \rho \frac{dP}{d\rho} + P\left(\rho^2(\zeta^2 - jm^2) - 1\right) = 0 \tag{1.20}$$

where $m = \sqrt{2}/\delta$ where δ is the *penetration depth* $\delta := \sqrt{\frac{2}{\omega\sigma\mu}}$. The solution of the differential equation 1.18 is:

$$Z(z) = A_1'(\zeta)e^{\zeta z} + A_2'(\zeta)e^{-\zeta z} \quad A_1', A_2' \in \mathbb{R} \tag{1.21}$$

while the differential equation 1.19 has solution[1]:

$$\begin{aligned} P(\rho) &= B_1' J_1(k\rho) + B_2' Y_1(k\rho) \quad B_1', B_2' \in \mathbb{R} \\ &= B'(k) J_1(k\rho) \end{aligned} \tag{1.22}$$

where $k^2 := \zeta^2 - jm^2$, J_{11} and Y_{11} are Bessel functions respectively of first and second kind, first order. The general solution for the magnetic vector potential is:

$$A_\theta(\rho, z) = P(\rho)Z(z) = J_1(k\rho)\left[C_1(k)e^{\zeta z} + C_2(k)e^{-\zeta z}\right] \tag{1.23}$$

where $C_1(k) = B'(k)A_1'(\zeta)$ $C_1(k) = B'(k)A_2'(\zeta)$ depends only by k because ζ can be assumed as dependent variable of k. We found now the expression of A_θ which depends by the variable k. If the solution extends radially, so that there are no restrictions on the radial function $P(\rho)$, there are correspondingly no restrictions also on k and the solution involves an integral over all k[13]:

$$A_\theta(\rho, z) = \int_0^\infty J_1(k\rho)\left[C_1(k)e^{\zeta z} + C_2(k)e^{-\zeta z}\right] dk \tag{1.24}$$

The solution changes for the various regions of the system.

- Region 0, $(0 < z < s)$:
  This region is composed by air $\sigma = 0$ and $\mu = mu_0$ therefore $k = \zeta$. The solution can be splitted in two terms:

$$\begin{aligned} A_{\theta 0} &= A_{0e} + A_{0r} \\ &= \frac{\mu_0 NI}{2(R_e - R_i)} \int_0^\infty C_0(k) J_1(k\rho) e^{-k(s-z)} dk + \int_0^\infty C_{01}(k) J_1(k\rho) e^{-kz} dk \end{aligned} \tag{1.25}$$

  where:

$$C_0(k) = \int_{R_i}^{R_e} \rho J_1(k\rho) d\rho \tag{1.26}$$

[1] $x^2 \frac{d^2 y}{dx^2} + (2p+1)x\frac{dy}{dx} + (a^2 x^{2r} + \beta^2)y = 0$ has solution: $y = x^{-p}\left[C_1 J_{q/r}(\frac{a}{r}x^r) + C_2 J_{q/r}(\frac{a}{r}x^r)\right]$[12]

the term A_{0e} represents the exiting field potential vector i.e. the potential vector of the inductor coil field in the absence of conducting material in region 1. The second term, A_{0r}, represents te so-called *reaction field potential* of the load[14]. The splitting of the solution is corrected on the basis of the superposition principle.

- Region 1, $(-h < z < 0)$:
  This is a conductive region with conductivity $\sigma_1 \neq 0$ and permeability μ_1 therefore $k \neq \zeta$ and the solution is:

$$A_{\theta 1} = \int_0^\infty \left[C_{11}(k) e^{\zeta_1 z} + C_{12}(k) e^{-\zeta_1 z} \right] J_1(k\rho) dk \tag{1.27}$$

  where $\zeta_1^2 = k^2 + j\omega\sigma_1\mu_1$.

- Region 2, $(z < -h)$:
  Here we have air again, the conductivity is zero an the solution has the same behaviour of the region 0 but in this case the magnetic potential vector for $z \to -\infty$ must be zero thus the constant of the term e^{-kz} is zero and the solution has the following form:

$$A_{\theta 2} = \int_0^\infty C_2(k) e^{kz} J_1(k\rho) dk \tag{1.28}$$

2.2 Boundary conditions

The unknown coefficients C_{01}, C_{11}, C_{12} and C_2 can be derived by applying the continuity conditions of the magnetic field and the magnetic flux density. Considering figure 2.3 the perpendicular component at the boundary of **B** is direct along z-direction while the parallel component to the boundary of **B** is direct along ρ-direction. Across the

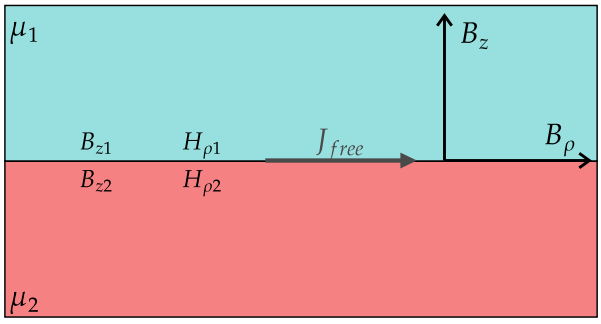

Figure 2.3: Magnetic flux density and magnetic field through material with different permeability.

boundary there is the conservation of the z-component of the magnetic flux density ($B_{z1} = B_{z2}$). Since the free current density $J_f ree$ is zero along the boundary surface, we have the conservation of the ρ-component of the magnetic field ($H_{\rho 1} = H_{\rho 2}$). From

the considerations of the section 2.1 we have to express the magnetic flux density in function of **A**; by using equation 1.3 we obtain in cylindrical coordinates:

$$\mathbf{B} = \begin{pmatrix} B_\rho \\ B_\theta \\ B_z \end{pmatrix} = \begin{pmatrix} -\frac{\partial A_\theta}{\partial z} \\ 0 \\ \frac{1}{\rho}\left(\frac{\partial(\rho A_\theta)}{\partial \rho}\right) \end{pmatrix} \tag{2.29}$$

By using the conservation of the component of the magnetic flux density wa have:

$$\begin{gathered} B_{z1} = B_{z2} \\ \frac{1}{\rho}\left(\frac{\partial(\rho A_{\theta 1})}{\partial \rho}\right) = \frac{1}{\rho}\left(\frac{\partial(\rho A_{\theta 2})}{\partial \rho}\right) \quad \forall \rho \quad \Longleftrightarrow \quad A_{\theta 1} = A_{\theta 2} \end{gathered} \tag{2.30}$$

From the conservation of the component of the magnetic field (no free current density is present) we have:

$$\begin{gathered} H_{\rho 1} = H_{\rho 2} \\ \frac{B_{\rho 1}}{\mu_1} = \frac{B_{\rho 2}}{\mu_2} \\ \frac{1}{\mu_1}\frac{\partial A_{\theta 1}}{\partial z} = \frac{1}{\mu_2}\frac{\partial A_{\theta 2}}{\partial z} \end{gathered} \tag{2.31}$$

We can now apply conditions 2.30 and 2.31 to our case of study firstly imposing the continuity of **A** and of its z-derivate in $z = 0$ and then in $z = -h$. We obtain the system:

$$\begin{cases} A_{\theta 0}\Big|_{z=0} = A_{\theta 1}\Big|_{z=0} \\ \frac{\partial A_{\theta 0}}{\partial z}\Big|_{z=0} = \frac{\partial A_{\theta 1}}{\partial z}\Big|_{z=0} \\ A_{\theta 1}\Big|_{z=-h} = A_{\theta 2}\Big|_{z=-h} \\ \frac{\partial A_{\theta 1}}{\partial z}\Big|_{z=-h} = \frac{\partial A_{\theta 2}}{\partial z}\Big|_{z=-h} \end{cases} \tag{2.32}$$

which can be written in matrix form:

$$\begin{bmatrix} 1 & -1 & -1 & 0 \\ k & \frac{\zeta_1}{\mu_{r1}} & -\frac{\zeta_1}{\mu_{r1}} & 0 \\ 0 & e^{-\zeta_1 h} & e^{\zeta_1 h} & -e^{-kh} \\ 0 & \frac{\zeta_1}{\mu_{r1} e^{-\zeta_1 h}} & -\frac{\zeta_1}{\mu_{r1} e^{\zeta_1 h}} & -k e^{-kh} \end{bmatrix} \cdot \begin{bmatrix} C_{01} \\ C_{11} \\ C_{12} \\ C_2 \end{bmatrix} = \begin{bmatrix} -\frac{\mu_0 N I}{2(R_e - R_i)} C_0(k) e^{-ks} \\ \frac{\mu_0 N I}{2(R_e - R_i)} k C_0(k) e^{-ks} \\ 0 \\ 0 \end{bmatrix} \tag{2.33}$$

We can in particular express the coefficient C_{01} which has the explicit expression derived from 2.33:

$$C_{01} = \frac{\mu_0 N I}{2(R_e - R_i)} C_0(k) F(k) \tag{2.34}$$

where

$$F(k) = -\frac{\left(e^{2h\zeta_1} - 1\right)\zeta_1^2 + \left(1 - e^{2h\zeta_1}\right)k^2 \mu_{r1}^2}{\left(e^{2h\zeta_1 + ks} - e^{ks}\right)\zeta_1^2 + \left(2\,e^{2h\zeta_1 + ks} + 2\,e^{ks}\right)k\,\mu_{r1}\,\zeta_1 + \left(e^{2h\zeta_1 + ks} - e^{ks}\right)k^2 \mu_{r1}^2} \tag{2.35}$$

It has to note that the electric and the magnetic field in region 0 is computable with only the coefficient C_{01} while to compute current density and power distribution inside the load it's necessary to find also C_{11}, C_{12} and C_2.

2.3 Impedance of inductor-load system

Focussing now on the region 0 we wanna calculate the e.m.f. at the ends of the coil. By using equations 1.10 and the Ohm's law:

$$\underline{\mathbf{E}}(\rho,z) = \frac{1}{\sigma}\underline{\mathbf{J}}(\rho,z) = -j\omega\underline{\mathbf{A}}(\rho,z) \tag{3.36}$$

From equation 3.36 we can calculate the e.m.f $\underline{V_e}$ on an elementary turn Γ_r of radius r of the coil in the conductive region:

$$\underline{V_e} = \oint_{\Gamma_r} \underline{\mathbf{E}} \cdot \mathbf{dl} = \int_0^{2\pi} \underline{A_0}(\rho,z) r d\theta = -j2\pi\omega r \underline{A_0}(\rho,z) \qquad (R_i < r < R_e) \tag{3.37}$$

the total e.m.f. of N turns $\underline{V}$ is:

$$\underline{V} = \int_{R_i}^{R_e} \underline{V_e} \frac{N}{R_e - R_i} d\rho = -j2\pi\omega \frac{N}{R_e - R_i} \int_{R_i}^{R_e} \rho \underline{A_0}(\rho,z) d\rho \tag{3.38}$$

It's possible therefore to calculate the value of impedance of the coil-load system. This value of impedance $\dot{Z}$ is intend as the variation of impedance with the load assuming zero the resistance of the coil and by using equations 1.25, 2.34 and 3.38 we obtain:

$$\dot{Z} = -\frac{\underline{V}}{\underline{I}} = j\pi\omega\mu_0 \frac{N^2}{R_e - R_i} \left\{ \int_0^\infty [C_0(k)]^2 dk + \int_0^\infty [C_0(k)]^2 F(k) e^{-ks} dk \right\} \tag{3.39}$$

The first integral gives the reactance of the coil in air, with no load while the second which is a complex number, gives the variation of impedance due by the load. It's useful to have an analytical expression of them:

$$X_{air} = \pi\omega\mu_0 \frac{N^2}{R_e - R_i} \int_0^\infty [C_0(k)]^2 dk \tag{3.40}$$

$$\Delta\dot{Z} = R + j\Delta X = j\pi\omega\mu_0 \frac{N^2}{R_e - R_i} \int_0^\infty [C_0(k)]^2 F(k) e^{-ks} dk \tag{3.41}$$

The complexity of the equation 3.39 derives from the integral overall k. We can therefore evaluate this integral with te Gauss-Laguerre quadrature formulae[2]:

$$\dot{Z} = j\frac{\pi\omega\mu_0 N^2}{(R_e - R_i)^2} \left\{ \sum_{i=1}^n w_i e^{x_i} [C_0(x_i)]^2 + \frac{1}{s} \sum_{i=1}^n w_i \left[C_0\left(\frac{x_i}{s}\right) \right]^2 F\left(\frac{x_i}{s}\right) \right\} \tag{3.42}$$

In figure 2.4 is shown the behaviour of the resistance and the reactance variation in function of the ratio between h and δ_1 with parameters shown in table 2.1.

We have to note that the variation of reactance due by the load ΔX is lower than zero in fact the reactance of the system with the load decreases its inductance. In the graphic is plotted $X = X_{air} + \Delta X$.

---

[2] $\int_0^{+\infty} e^{-x} f(x) \approx \sum_{i=1}^n w_i f(x_i)$
where x_i is the i^{th} root of Laguerre polynomial $L_n(x)$ and the weight w_i is given by: $\frac{x_i}{(n+1)^2[L_{n+1}(x_i)]^2}$ [15]

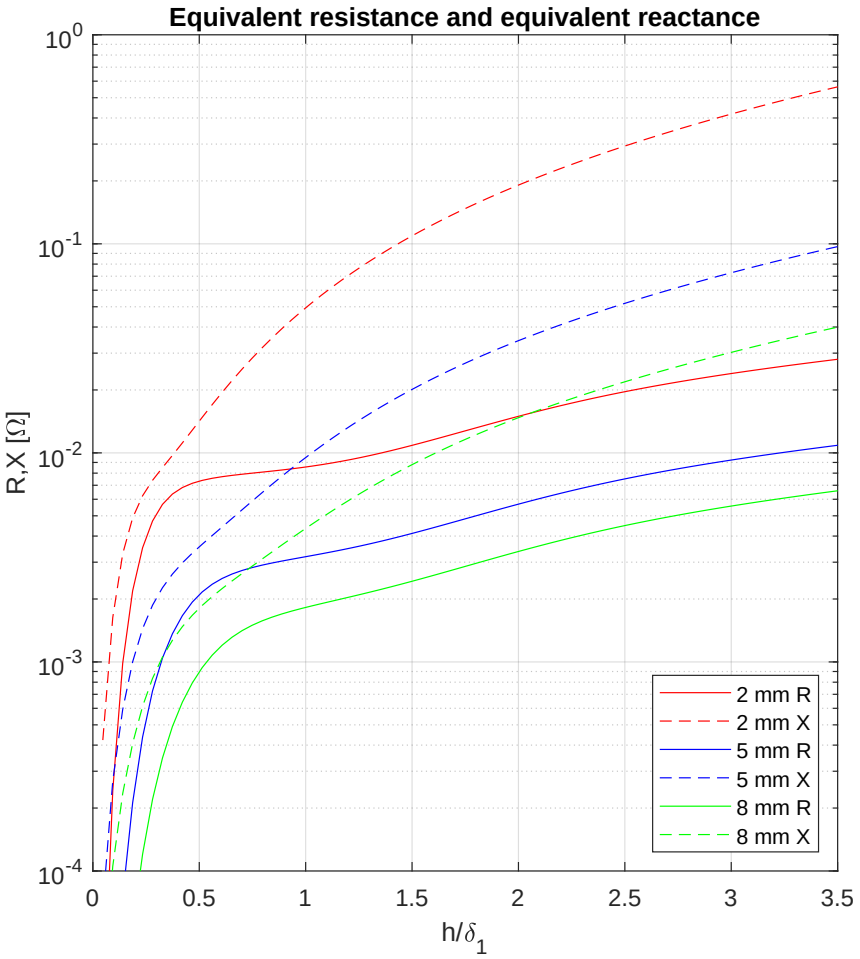

Figure 2.4: Equivalent resistance R and equivalent reactance X as function of the ratio h/δ_1 for various values of thickness h of the metallic disk.

Symbol	Description	Value
R_e	External radius of the coil	100 mm
R_i	Internal radius of the coil	0 mm
N	Number of turns	20
s	Inductor load distance	5 mm
σ	Conductivity of the copper disk	57 MS
μ_{r1}	Relative permittivity of the copper disk	1
n	Sum limit of Laguerre polynomials	100

Table 2.1: Parameters of the case of study.

2.4 Power transmitted in the billet

We found the variation of resistance of the coil due the load, it's possible to evaluate the power generated by the eddy currants in the metallic disk using the relation:

$$P + jQ = \dot{Z}I^2 = RI^2 + j(X + \Delta X)I^2 \tag{4.43}$$

There is another expression for the active power transmitted into the metallic disk starting from the current density:

$$P = \int_V \frac{J^2}{\sigma} dV \tag{4.44}$$

The computation of the power with this method is computationally complicated with respect the method described by equation 4.43 but it's interesting to understand how induced current flows in the metal. We can therefore compute the current density in the disk as previously seen using the equation:

$$\underline{\mathbf{J}}_1(\rho, z) = \sigma \underline{\mathbf{E}}(\rho, z) = -j\sigma\omega \underline{\mathbf{A}}(\rho, z) \tag{4.45}$$

The current density $\underline{\mathbf{J}}_1$ has only the azimuthal component as the magnetic vector potential. By using equation 1.27 we obtain:

$$\underline{J_1}(\rho, z) = -j\sigma\omega \int_0^\infty \left[C_{11}(k)e^{\zeta_1 z} + C_{12}(k)e^{-\zeta_1 z}\right] J_1(k\rho)dk \tag{4.46}$$

where:

$$C_{11}(k) = \mu_0 \frac{NI}{2(R_e - R_i)} C_0(k)G(k) \tag{4.47}$$

$$C_{12}(k) = \mu_0 \frac{NI}{2(R_e - R_i)} C_0(k)H(k) \tag{4.48}$$

with:

$$G(k) = \frac{e^{2h\zeta_1} k\,\mu_{r1}\,\zeta_1 + 2\,e^{2h\zeta_1} k^2\,\mu_{r1}^2}{\left(e^{2h\zeta_1+ks} - e^{ks}\right)\zeta_1^2 + \left(2\,e^{2h\zeta_1+ks} + 2\,e^{ks}\right) k\,\mu_{r1}\,\zeta_1 + \left(e^{2h\zeta_1+ks} - e^{ks}\right) k^2\,\mu_{r1}^2} \tag{4.49}$$

$$H(k) = \frac{k\,\mu_{r1}\,\zeta_1 - 2\,k^2\,\mu_{r1}^2}{\left(e^{2h\zeta_1+ks} - e^{ks}\right)\zeta_1^2 + \left(2e^{2h\zeta_1+ks} + 2\,e^{ks}\right) k\,\mu_{r1}\,\zeta_1 + \left(e^{2h\zeta_1+ks} - e^{ks}\right) k^2\,\mu_{r1}^2} \tag{4.50}$$

The complexity to find the current density from equation 4.46 derives from the integral overall k. We can again evaluate it with the Gauss-Laguerre quadrature formulae and we obtain:

$$\underline{J_1}(\rho, z) = -j\omega\sigma \sum_{i=1}^{n} w_i e^{x_i} \left[C_{11}(x_i)e^{\zeta_{1i} z} + C_{12}(x_i)e^{-\zeta_{1i} z}\right] J_1(x_i\rho) \tag{4.51}$$

where

$$\zeta_{1i} = \sqrt{x_i^2 + \frac{2j}{\delta_1^2}} \tag{4.52}$$

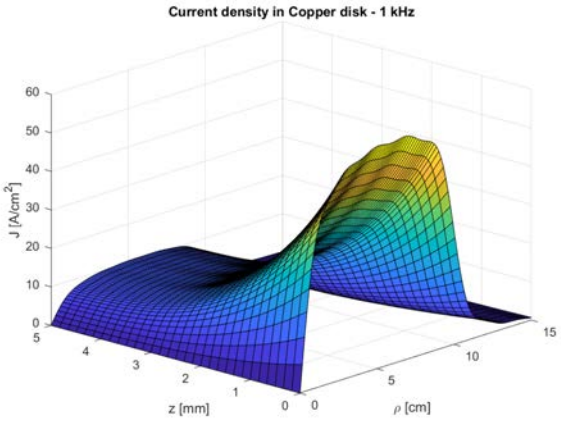

Figure 2.5: Current density distribution in copper disk with f = 1 kHz.

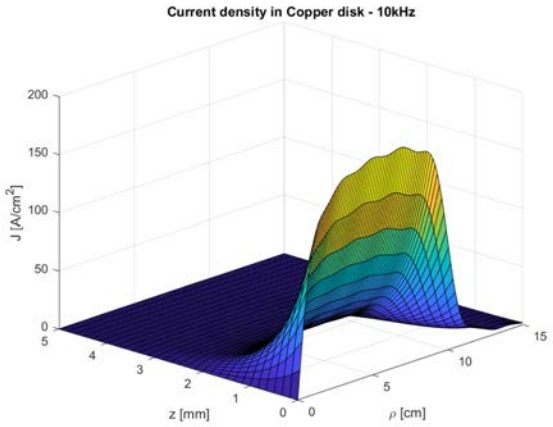

Figure 2.6: Current density distribution in copper disk with f = 10 kHz.

with the parameters described in table 2.1 for a copper disk of thickness 5 mm with $I = 10A$ we plot the current density at the frequency of 1 kHz and 10 kHz in the graphs 2.5 and 2.6 for different frequencies. The penetration depth is 2.1 mm at the frequency of 1 kHz and 670 μm at 10 kHz. We can see how for the higher frequency the current density is present mostly on the surface. The disposition of the current is well shown in figures 2.7 and 2.8 where is plotted the current density for different values of z. Figures 2.9 and 2.10 show the current density for different relative values of z for NiCr metal (σ = 950 kS/m, $\mu_r = 1$) at 10 kHz ($d.o.p.$ = 5.1 mm) and 70 kHz ($d.o.p.$ = 1.95 mm).

We can note that chose of the frequency depends basically by the material type (conductivity and permeability) and by required treatment, hardening or core heating.
We can now proceed to evaluate the power transmitted in the billet by using the method of the integral of the square current density overall the volume described by equation 4.44 and with the equivalent resistance seen by the inductor by using equation 3.42.

Material	f	R	X	RI^2_{eff}	$\int_V \frac{J^2}{\sigma} dV$	$err_{\%}(P)$
Copper	1 kHz	7.04 $m\Omega$	47.1 $m\Omega$	352 mW	332 mW	6.1%
$\sigma = 5.7MS/m$	5 kHz	16.7 $m\Omega$	214 $m\Omega$	836 mW	784 mW	6.6%
$\mu_r = 1$	10 kHz	23.9 $m\Omega$	417 $m\Omega$	1.19 W	1.12 W	6.7%
NiCr	10 kHz	189 $m\Omega$	538 $m\Omega$	9.43 W	8.95 W	5.3%
$\sigma = 950kS/m$	70 kHz	464 $m\Omega$	3.26 Ω	23.2 W	21.8 W	6.2%
$\mu_r = 1$	150 kHz	701 $m\Omega$	6.63 Ω	35.0 W	32.9 W	6.4%

Table 2.2: Comparison between the power transmitted in the metal disk for different materials at different frequencies ($I = 10A$).

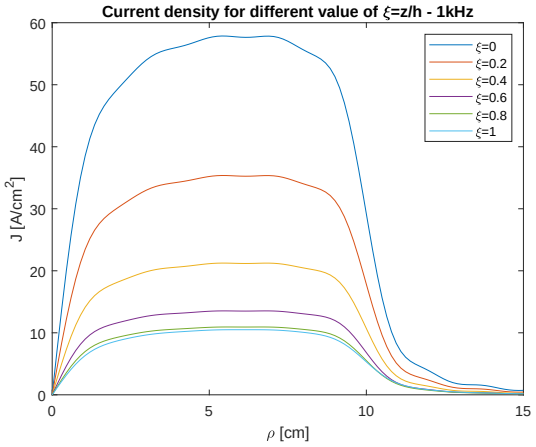

Figure 2.7: Current density distribution in copper disk with f = 1 kHz.

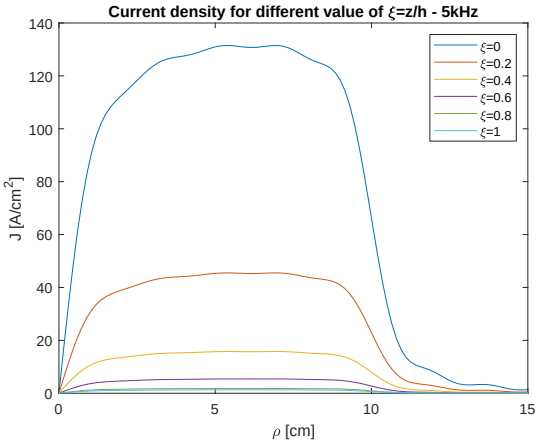

Figure 2.8: Current density distribution in copper disk with f = 5 kHz.

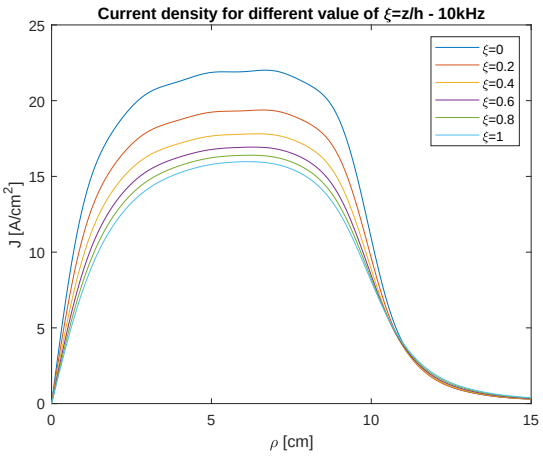

Figure 2.9: Current density distribution in NiCr disk with f = 10 kHz.

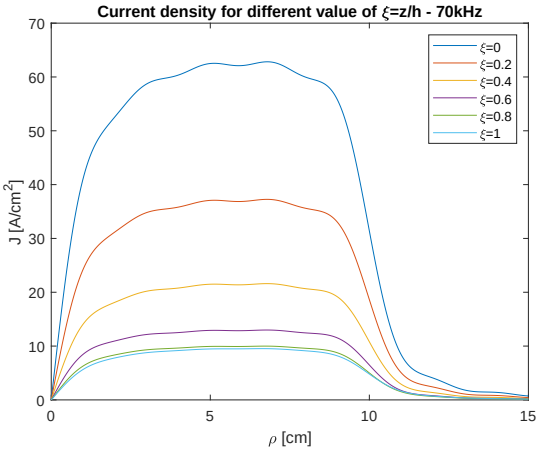

Figure 2.10: Current density distribution in NiCr disk with f = 70 kHz.

2.5 Electrical efficiency

The electrical efficiency is obtained as the ratio between power transformed into heat and the total active power absorbed by the inductor:

$$\eta_e = \frac{P_{heat}}{P_{tot}} = \frac{RI^2}{(R+R_{coil})I^2} = \frac{R}{R+R_{coil}} = \frac{1}{1+\frac{R_{coil}}{R}} \tag{5.53}$$

where R is the load resistance reported on the terminals of the inductor and R_{coil} is the resistance of the coil which we have to estimate.
We assume the inductor is made up Litz coil therefore the current is equally distributed along its section. We proceed to calculate the resistance of one turn R_{1t} with mean

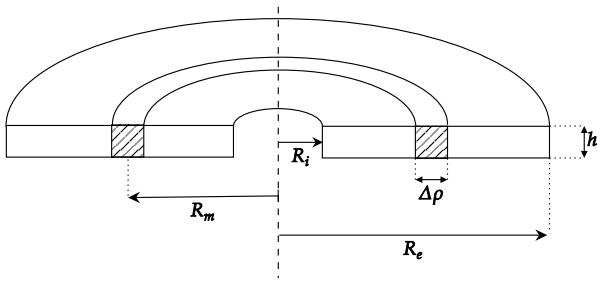

Figure 2.11

radius R_m as shown in figure 2.11 considering a coil with conductivity σ_c . the section of this turn is $\Delta\rho h_c$ where $\Delta\rho = (R_e - R_i)/N$ and $R_{1t}$is:

$$R_{1t} = \frac{1}{\sigma_c}\frac{2\pi R_m}{\Delta\rho h_c} \tag{5.54}$$

the mean radius is given by:

$$R_m = \int_{R_i}^{R_e} \frac{\rho}{R_e - R_i} d\rho = \frac{R_e^2 - R_i^2}{2(R_e - R_i)} \tag{5.55}$$

therefore the resistance of the coil R_{coil} made up N turns is:

$$R_{coil} = \frac{\pi N^2}{\sigma_c h_c}\frac{R_e^2 - R_i^2}{(R_e - R_i)^2} \tag{5.56}$$

We can calculate the electrical efficiency remembering that R is given by equation 3.41 and is the real part of $\Delta\dot{Z}$. The electrical efficiency is therefore:

$$\eta_e = \frac{1}{1 - \frac{1}{m_0 \frac{R_e - R_i}{R_e^2 - R_i^2} \mathrm{Im}\left\{\int_0^\infty [C_0(k)]^2 F(k) e^{-ks} dk\right\}}} \tag{5.57}$$

with:

$$m_0 = \omega\mu_0\sigma_c h_c \tag{5.58}$$

It's difficult to see from the equations 5.57 the dependences of the efficiency by the parameters. The graphs 2.12 and 2.13 show the behaviour of the efficiency in function of the ratio between disk thickness and penetration depth for copper and NiCr billets.

The efficiency depends obviously by the frequency and tends to one for high frequencies. For the more conductive material the efficiency grows slower with respect the other one. The air gap affects more for the copper disk which has the same conductivity of the coil. The electrical efficiency depends also by the ratio between conductivity of the coil and of the material and increases as the conductivity of the material decreases. It's more "easy" to heat a material with low conductivity in terms of efficiency because more is conductive the disk, more the coil heats itself with respect the load. Good conductive no-magnetic materials needs low current frequencies and the efficiency is low, these are the big problems for heating copper or aluminium. We can finally say that:

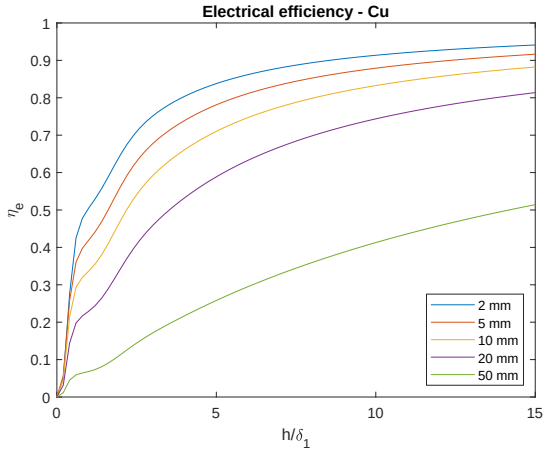

Figure 2.12: Electrical efficiency in function of the ratio between disk thickness and penetration depth for different air gap for copper.

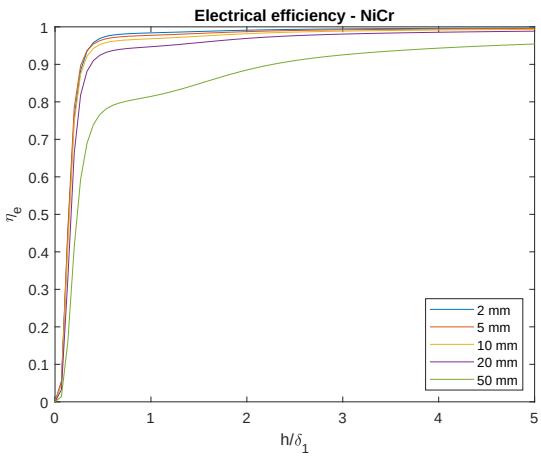

Figure 2.13: Electrical efficiency in function of the ratio between disk thickness and penetration depth for different air gap for NiCr.

- for $h/\delta_1 < 2$ the electrical efficiency is low even if the current is well distributed along the entire thickness of the disk.
- for $2 < h/\delta_1 < 5$ the heating occurs with satisfactory efficiency.
- fro $h/\delta_1 > 7$ the heating has a low thermal efficiency.

the electrical efficiency, for the effect of the material characteristics, could be very high (0.9) for material with low conductivity while it remains slow for material with high conductivity.

2.6 Quality factor and power factor

The quality factor Q is defined as the ratio between the reactive power and the active power absorbed by the inductor:

$$Q = \frac{X_{air} + \Delta X}{R_{coil} + R} \tag{6.59}$$

where we remember that ΔX is negative. Values of Q are reported in figures 2.14 and 2.15 in function of h/δ_1 respectively for copper and NiCr for different air gap thickness. The quality factor is an important quantity which can be used to calculate easily the cosϕ which is:

$$\cos\phi = \frac{R_{coil} + R}{\sqrt{(R_{coil} + R)^2 + (X_{air} + \Delta X)^2}} = \frac{1}{\sqrt{1 + Q^2}} \tag{6.60}$$

Always for non copper and NiCr with geometrical parameters described in table 2.1, the behaviour of the cosϕ is shown in figures As we can see the cosϕ is very low also for

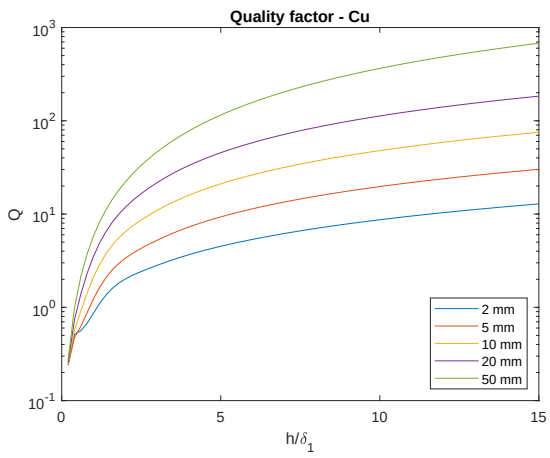

Figure 2.14: Quality factor in function of h/δ_1 for Cu.

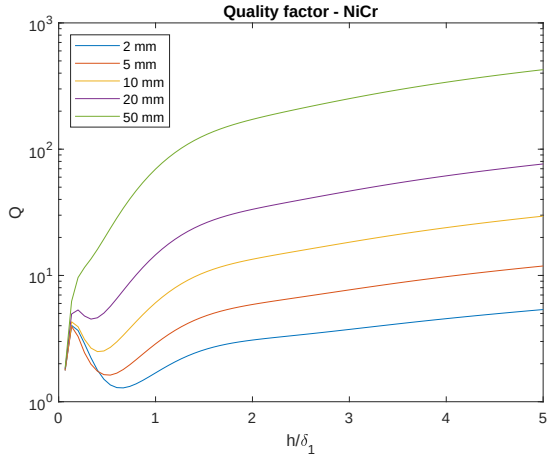

Figure 2.15: Quality factor in function of h/δ_1 for NiCr.

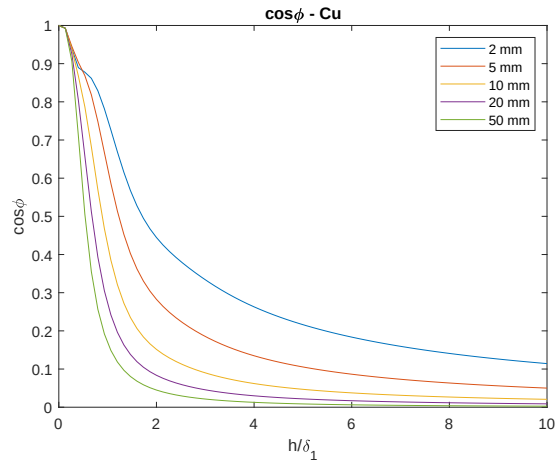

Figure 2.16: Cosϕ in function of h/δ_1 for Cu with different air gap thickness.

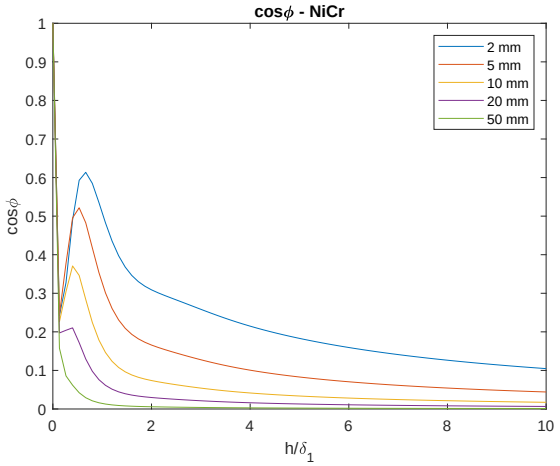

Figure 2.17: Cosϕ in function of h/δ_1 for NiCr with different air gap thickness.

reasonable value of h/δ_1, for this reason it's necessary the compensation of the inductive reactive power absorbed by the inductor with a capacitor connected in parallel. It's to note that in the line (cable) between power factor correction capacitor and the inductor, the current is strongly out of phase and the module of the current could assume high values.
The cosϕ is generally higher for copper with respect the NiCr. It depends strongly by the air gap thickness and has a different distribution in the case of NiCr i.e. there is a relative maximum at $h/\delta_1 \simeq 0.5$ which corresponds at the resonance frequency which is not present in the case of copper. At the resonant frequency (RF) the cos ϕ reaches the maximal value (with a good heating) and right at resonance frequency the pancake inductor has to be supplied. Even if the electrical efficiency is higher for higher

frequencies, setting the system at RF has the advantage to decrease the size of power factor correction capacitors and reduce the apparent power supplied from the inverter and moreover at low frequencies the heating is more uniform.

2.7 FEM

To compare the results obtained with the analytical model of pancake inductor with a FEM simulation by using COMSOL Multiphysics®. The model considers the conductive disk with infinite extension. For no-magnetic materials the induced current distribution along the radial coordinate ρ drops to zero for $\rho > R_e + 10\%R_e$ therefore the analytical model will fit with the FEM model if $R_b > 1.1R_e$. The analytical model doesn't take into account the variation of conductivity due by the temperature increase in the load and in the coil neither the magnetic saturation. In fact the aim of this thesis is the heating transfer mechanism for no-magnetic conductors.

The analytical model considers one dimensional coil therefore with no thickness while in the FEM simulation, but also in the reality, the coil has thickness h_c. In order to doesn't error we have to set the air gap in the analytical model:

$$s \longrightarrow s + \frac{h_c}{2}$$

In figure 2.18 is shown the distribution of the current along a 2D axisymmetric section of the disk with parameters in table 2.19.

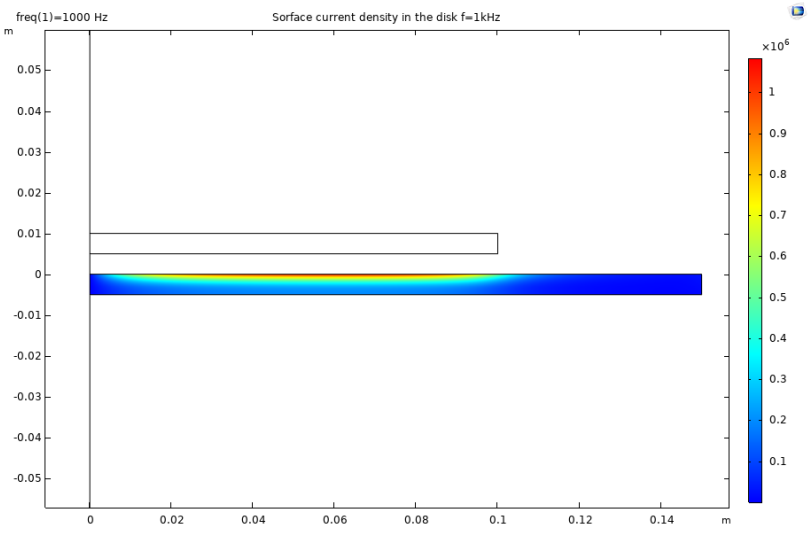

Figure 2.18: Current density distribution $[A/m^2]$ in the copper study.

Symbol	Value
f	1 kHz
I	10 A
R_e	100 mm
R_i	0 mm
R_b	150 mm
N	20
s	5 mm
h_c	5 mm
σ	57 MS
σ_{coil}	57 MS
μ_{r1}	1

Figure 2.19: Parameters of the FEM case of disk at f=1kHz with FEM simulation.

In order to compare the results of the FEM with the analytical model in figure 2.20 is plotted the surface current density (at z=0) along the radius ρ. We can see how the two curves of the current density distribution well fit.

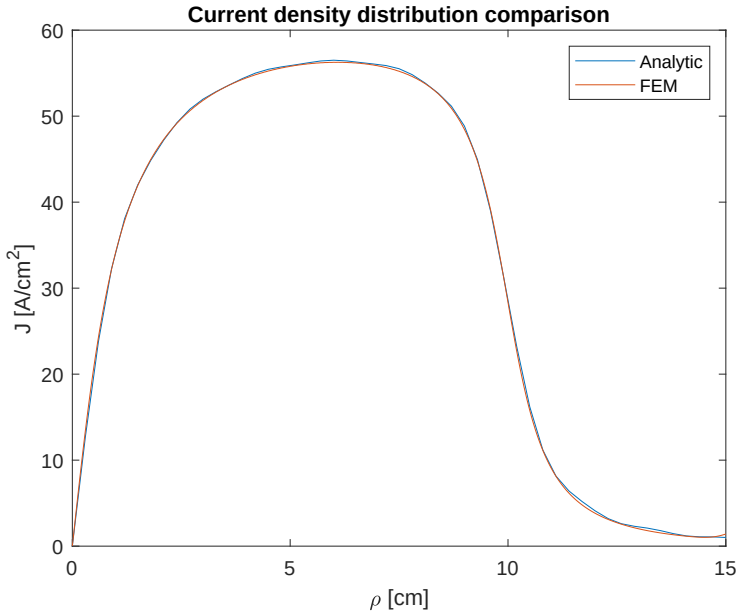

Figure 2.20: Current density comparison at z=0 in function of the radius.

To make a more effective comparison between the two models we wanna compare also the electrical parameters of the system as equivalent resistance R, the equivalent reactance X and the total power transmitted into the disk by using the integration of the current density inside the disk. In order to test the analytical model, we'll change the geometrical parameters with respect the previous examples. The coil is made up copper and the resistance of the coil has been computed with FEM and analytical model:

$$R_{coil,FEM} = 33.3\ m\Omega$$

$$R_{coil,AN} = 32.9\ m\Omega$$

The study is done for three material type: aluminium, steel and iron with a geometrical dimension similar to a bottom of a pot. The results and the parameters of the system is shown in table 2.3. As we can see the analytical model make good forecast in presence of no-magnetic materials, while it is in misleading for the magnetic ones. This is due by the fact that for magnetic materials the permeability depends by the magnetic flux density intensity as well as the temperature. For this reason choosing a value of μ_r at the final temperature of the disk is not enough. It's necessary to consider an average value of the permeability along the entire hysteresis cycle. Always taking in consideration the case of study, the steel keep up well its magnetic proprieties and indeed the discrepancy between FEM and analytical model is tolerable while for iron no. In fact for iron the μ_r strongly depends by the magnetic flux density strength and a correction is necessary. We have to pot therefore an average value of the permeability which can be calculated through:

$$\mu_{r,eq} = \frac{1}{B_i - B_f} \int_{B_i}^{B_f} \mu_r(B) dB \tag{7.61}$$

Geometrical parameterss	Material properties	Analytical	FEM	Err
$R_i = 25\ mm$	Aluminium	$R = 138\ m\Omega$	$R = 141\ m\Omega$	2.1%
$R_e = 80\ mm$	$\sigma = 37.7\ MS/m$	$X = 2.35\ \Omega$	$X = 2.18\ \Omega$	7.8%
s = 4 mm	$\mu_r = 1$	$P = 47.2\ W$	$P = 46.9\ W$	0.6%
$f = 20\ kHz$	AISI steel 430	$R = 2.23\ \Omega$	$R = 2.02\ \Omega$	10%
$I = 30\ A$	$\sigma = 1.5\ MS/m$	$X = 6.50\ \Omega$	$X = 15.43\ \Omega$	58%
N=25	$\mu_r = 100$	$P = 941\ W$	$P = 895\ W$	5.1%
$h = 3\ mm$, $h_{coil} = 2\ mm$	Iron	$R = 2.17\ \Omega$	$R = 1.38\ \Omega$	57%
$R_b = 90\ mm$	$\sigma = 9MS/m$	$X = 6.22\ \Omega$	$X = 50.8\ \Omega$	88%
$\sigma_{coil} = 57MS/m$	$\mu_r = 500$	$P = 957\ W$	$P = 605\ W$	58%

Table 2.3: Parameters of the case of study and comparison between FEM and analytical model.

where $\mu_{r,i}$ is the initial value and $\mu_{r,f}$ is the final value of the relative permeability which is:

$$\mu_r = \frac{1}{\mu_0}\frac{dB}{dH} \tag{7.62}$$

With this assumption correcting the permeability with its equivalent one we obtain the final values in table 2.4. We can note that even with the correction to the permeability,

Material properties	Analytical	FEM	Err
AISI steel 430	$R = 2.11\ \Omega$	$R = 2.02\ \Omega$	4.4%
$\sigma = 1.5\ MS/m$	$X = 5.95\ \Omega$	$X = 15.43\ \Omega$	61%
$\mu_{r,eq} = 69$	$P = 945\ W$	$P = 909\ W$	3.9%
Iron	$R = 1.39\ \Omega$	$R = 1.38\ \Omega$	0.7%
$\sigma = 9\ MS/m$	$X = 4.09\ \Omega$	$X = 50.8\ \Omega$	92%
$\mu_{r,eq} = 80$	$P = 603\ W$	$P = 605\ W$	0.3%

Table 2.4: Parameters of the case of study and comparison between FEM and analytical model with equivalent permeability.

the error of the reactance X in high. This error doesn't affect the value of the calculated power but affects strongly the forecast of the $\cos\phi$.

2.8 Soft magnetic yoke

If we insert a ferrite layer (soft magnetic yoke) up the coil we insulate magnetically the region above it and we increase the magnetic field magnitude in the metal disk. Figure 2.21 show the geometrical configuration, in particular the soft magnetic yoke is distant r from the coil and is a disk with infinite radius and supposing infinite permeability. The considerations done in the section 2.1 since the symmetry of the system are still valid, in particular the magnetic vector potential $\underline{\mathbf{A}}$ has only θ component and depends only by ρ and z in a cylindrical coordinate system (ρ,θ,z). As already done, we can

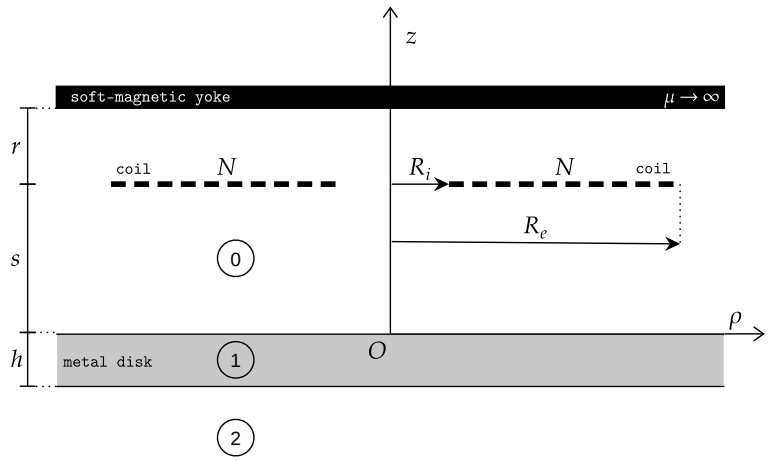

Figure 2.21: Schematic configuration of pancake inductor, load and soft magnetic yoke.

study the solutions in threimposing the continuity of magnetic vector potential if the two border regionse regions:

- Region 0, $(0 < z < s + r)$:
  Here the solution has two terms, one descending exponential term and growing one:

$$\begin{aligned} A_{\theta 0} &= A_{0e} + A_{0r} \\ &= \frac{\mu_0 NI}{2(R_e - R_i)} \int_0^\infty C_0(k)\left[e^{-k|s-z|}dk + C_{01}(k)e^{kz} + C_{02}(k)e^{-kz}\right]J_1(k\rho)dk \end{aligned} \tag{8.63}$$

  where:

$$C_0(k) = \int_{R_i}^{R_e} \rho J_1(k\rho)d\rho \tag{8.64}$$

- Region 1, $(-h < z < 0)$:

$$A_{\theta 1} = \int_0^\infty \left[C_{11}(k)e^{\zeta_1 z} + C_{12}(k)e^{-\zeta_1 z}\right]J_1(k\rho)dk \tag{8.65}$$

  where $\zeta_1^2 = k^2 + j\omega\sigma_1\mu_1$.

- Region 2, $(z < -h)$:

$$A_{\theta 2} = \int_0^\infty C_2(k)e^{kz}J_1(k\rho)dk \tag{8.66}$$

2.8.1 Boundary conditions

We will study the problem only for $-h \le z \le r + s$ and this leads to the following boundary conditions:

- z=r+s: imposing the orthogonality of magnetic field (cause the infinite permeability) respect the soft magnetic yoke which leads:

$$\frac{\partial A_{\theta 0}}{\partial z} = 0 \tag{8.67}$$

- z=0: imposing the continuity of magnetic vector potential in the two border regions and since the conservation of the radial component of the magnetic field we obtain:

$$\begin{aligned} A_{\theta 0} &= A_{\theta 1} \\ \frac{\partial A_{\theta 0}}{\partial z} &= \frac{1}{\mu_{r1}} \frac{\partial A_{\theta 1}}{\partial z} \end{aligned} \tag{8.68}$$

- z=-h: since the continuity of the magnetic vector potential:

$$A_{\theta 1} = A_{\theta 2} \tag{8.69}$$

This procedure leads to a system of equations in number equal to the number of the unknown coefficients C_{ij} which can be written in the matrix form[16]:

$$\begin{bmatrix} 1 & 1 & -1 & -1 & 0 \\ -k & k & \frac{\zeta_1}{\mu_{r1}} & -\frac{\zeta_1}{\mu_{r1}} & 0 \\ 0 & 0 & e^{-\zeta_1 h} & e^{\zeta_1 h} & -e^{-kh} \\ 0 & 0 & \frac{\zeta_1}{\mu_{r1}} e^{-\zeta_1 h} & -\frac{\zeta_1}{\mu_{r1}} e^{\zeta_1 h} & -\frac{k}{\mu_{r1}} e^{-kh} \\ -ke^{k(s+r)} & ke^{-k(s+r)} & 0 & 0 & 0 \end{bmatrix} \cdot \begin{bmatrix} C_{01} \\ C_{02} \\ C_{11} \\ C_{12} \\ C_2 \end{bmatrix} = \begin{bmatrix} -e^{-ks} \\ ke^{-ks} \\ 0 \\ 0 \\ -ke^{-kr} \end{bmatrix} \tag{8.70}$$

In the same way as done in section 2.3 we can derive the equivalent impedance of the system which is:

$$\dot{Z} = j \frac{\pi \omega \mu_0 N^2}{(R_e - R_i)^2} \int_0^\infty C_0(k)^2 \left[1 + C_{01}(k) e^{ks} + C_{02}(k) e^{-ks} \right] dk \tag{8.71}$$

with the load the variation of impedance is:

$$\Delta \dot{Z} = j \frac{\pi \omega \mu_0 N^2}{(R_e - R_i)^2} \int_0^\infty C_0(k)^2 \left[C_{01}(k) e^{ks} + C_{02}(k) e^{-ks} \right] dk \tag{8.72}$$

by using the Gauss-Laguerre quadrature formulae for simplify the expression, in order to implement it in the computational code equation 8.72 becomes:

$$\Delta \dot{Z} = R + j\Delta X = j \frac{\pi \omega \mu_0 N^2}{(R_e - R_i)^2} \sum_{i=1}^{n} \frac{1}{s} w_i C_0 \left(\frac{x_i}{s} \right)^2 \left[C_{01} \left(\frac{x_i}{s} \right) e^{2x_i} + C_{02} \left(\frac{x_i}{s} \right) \right] \tag{8.73}$$

In table 2.5 shows the variation of the equivalent resistance measured at the terminals of the coil due to the load and compared with the results found previously. We can see how for both the case of studies we have an increment of equivalent resistance adding a soft

Material	With yoke			Without yoke		
	Analytical	FEM	Err.	Analytical	FEM	Err.
Aluminium $\sigma = 37.7\ MS/m$ $\mu_r = 1$	R=174 mΩ	R=167 mΩ	4%	R=138 mΩ	R=141 mΩ	3%
Steel AISI 430 $\sigma = 1.5\ MS/m$ $\mu_r = 100$	R=5.26 Ω	R=5.48 Ω	4%	R=2.23 Ω	R=2.02 Ω	10%

Table 2.5: Variation of equivalent resistance with soft magnetic yoke.

magnetic yoke due to a greater concentration of the magnetic field on the workpiece. The analytical model outcomes are in according with the FEM simulation where the soft magnetic yoke had null electrical conductivity and $\mu_r = 4000$, like the common ferrite on the market. The heating with 10 A of current in the coil for aluminium is only 17 W despite the ferrite layer. In the case of steel the increase of resistance is double than without ferrite with consequentially the same increment of the power heating.
The magnetic flux density lines for pancake inductors with and without yoke are shown in the figures 2.22 and 2.23 for an aluminium workpiece. We can note how with the

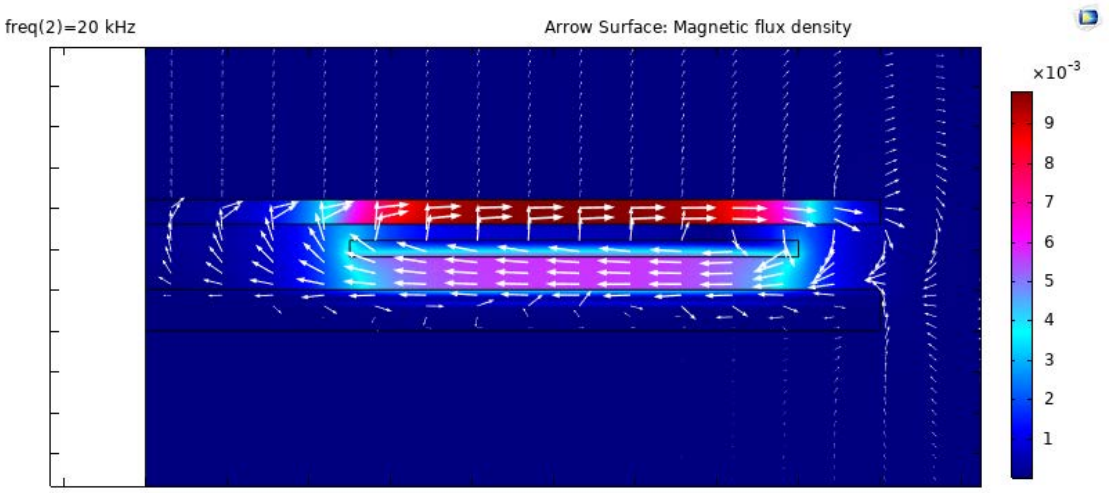

Figure 2.22: Magnetic flux density distribution with soft magnetic yoke.

ferrite layer above the pancake the magnetic field is less dispersed and for this reason the heating is grater.

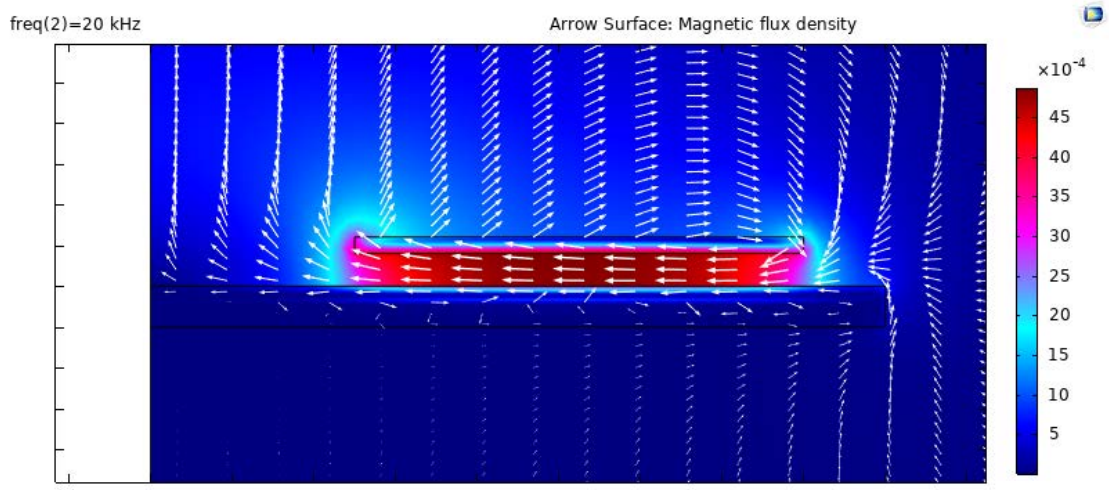

Figure 2.23: Magnetic flux density distribution without soft magnetic yoke.

2.9 Considerations

The analytical model which describes the pancake inductor heating system simulates with a good approximation the equivalent resistance R measured ad the terminals of the coil and compared with the FEM results. The error is below 5% for non magnetic materials while for magnetic materials as steel 430 or iron the error grows even above 50%. As we already said this issue can be solved by considering the mean value of the permittivity along the hysteresis cycle. Even with the correction by using the equivalent permeability the reactance X of the system is definitely underestimated and can't be token into account.
The analytical model therefore make good forecast when the load is made up non-magnetic material.
The analytical model moreover doesn't consider the hysteresis losses P_{hys} and the power transmitted is underestimated, it's necessary to add the following term:

$$P_{hys} = \eta B_{max}^{n} f V \tag{9.74}$$

where η is the Steinmetz hysteresis coefficient (depending on material $[J/m^3]$), B_{max} is the maximal value of the flux density, n is the Steinmetz exponent (range from 1.5 to 2.5 depending on material), f the frequency and V the volume of magnetic material.
We have to say that the magnetic flux density is not constant inside the material therefore it's necessary to take an average value.
In the last section we have seen how adding a soft magnetic yoke the resistance increases on equal characteristics, according with the FEM simulation. In conclusion the analytical model makes good forecast for non magnetic material. We have to remember that this model supports a huge range of frequency and therefore is useful to do preliminary estimates. The downside is that we are not interested to heat non-magnetic materials cause the poor electrical efficiency.

Chapter 3

Permanent magnets induction heating

3.1 Introduction

As already said in order to generate eddy currents into the workpiece it's necessary varies the magnetic flux inside itself. This operation can be done varying the magnetic field with respect the time as done for the pancake case or by varying the magnetic field in the space. In this chapter we will consider the last case.
The working principle is simple: the variation of magnetic flux is due by using permanent magnets which are in relative motion with respect the workpiece. The most simple configuration to implement and to study is when the permanent magnets are placed on a rotating disk closed to the metal piece to heat. Figure 3.1 shows the configuration of the system: there are two coaxial disks (metal disk and permanent magnets disk) along the **z** direction separate by a air layer of thickness s. The upper disk has radius R_3,

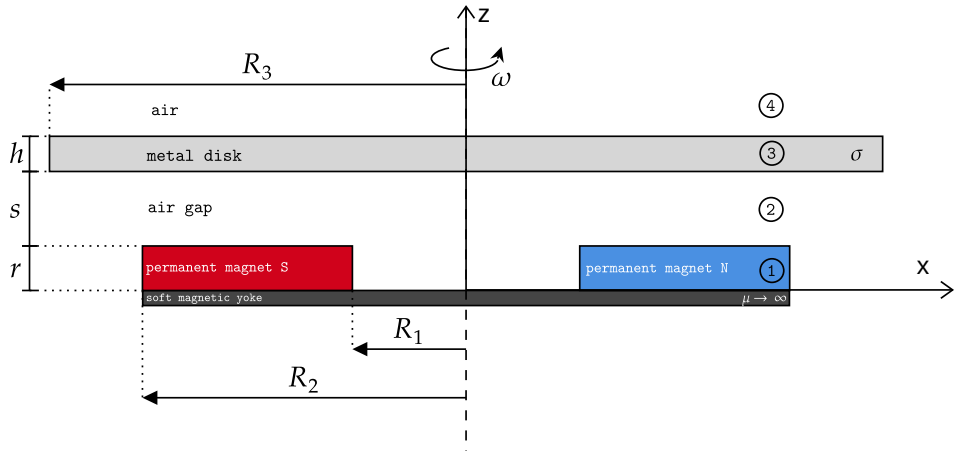

Figure 3.1: Geometrical parameters of the permanent magnets disk - metal disk.

thickness h and it is made up by a non magnetic conductor with electrical conductivity σ for example copper or aluminium and it's make round with angular speed ω. The velocity of a generic point belonging the conductive disk ad the distance ρ from the axes of rotation has velocity $\mathbf{v}$ in magnitude proportional to:

$$v = \omega\rho \tag{1.1}$$

and the direction is tangent. The other disk is fixed and it's constituted of no magnetic material with equally spaced permanent magnets (PM) bonded on top of it.

Figure 3.2 shows the geometrical proprieties of the permanent magnets disk.

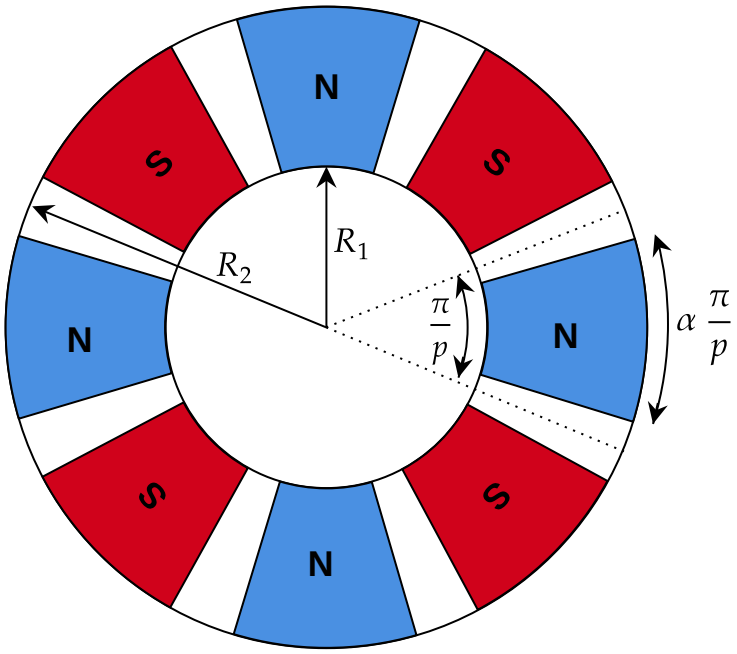

Figure 3.2: Geometrical parameters of the permanent magnets disk.

The magnets are disposed alternatively with North pole (N) and South pole (S) with a regular angular spacing π/p where p is the number of dipoles which constitute the system. Basically the angular spacing between two magnets with the same polarity is $2\pi/p$. The magnets have circular crown arch shape with R_1 and R_2 respectively the internal and external radius and the angle is $\alpha\pi/p$ with $0 < \alpha \leq 1$ to avoid the overlap of the two opposite poles.

The problem shows an elegant cylindrical symmetry, the natural way to study the system is using cylindrical coordinates (ρ, ϑ, z) even if this choice will complicate the partial differential equations carried by Laplacian, curl and the divergence. Our goal is to find an analytical solution of the current density $\mathbf{J}$ inside the billet. It's necessary to separate the solutions in four regions:

- ① : permanent magnets region ($r < z < 0$);

- ② : air gap region ($r \leq z < r + s$);
- ③ : conductive region ($r + s \leq z < r + s + h$);
- ④ : air infinite region* ($r + s + h \leq z$);

in order to solve the three-dimensional boundary value problem, we have to find the boundary conditions in the four regions. The region number four will be discussed later because neds particular precautions.

3.2 Magneto-dynamic formulation

In this section we will show the physical behaviour of a charged particle into a magnetic field, in particular we'll study the dynamics of single particle focussing to microscopical quantities. This will allow us to have not only a simple mathematical model but also a more general physical comprehension.

Let us consider the system in figure 3.1, the billet is rotating around z-direction with angular velocity ω. The cylindrical billet is made of non magnetic metal (aluminium or copper) with high electrical conductivity σ. Similarly to Drude model we can assume charges free to move inside the conductor. Considering the figure 3.3 a free charge into the billet in position $P(x, y)$ supposing positively charged (+q) is moving with respect a system of reference attached to the magnetic disk, the charge q is moving with velocity **v**.

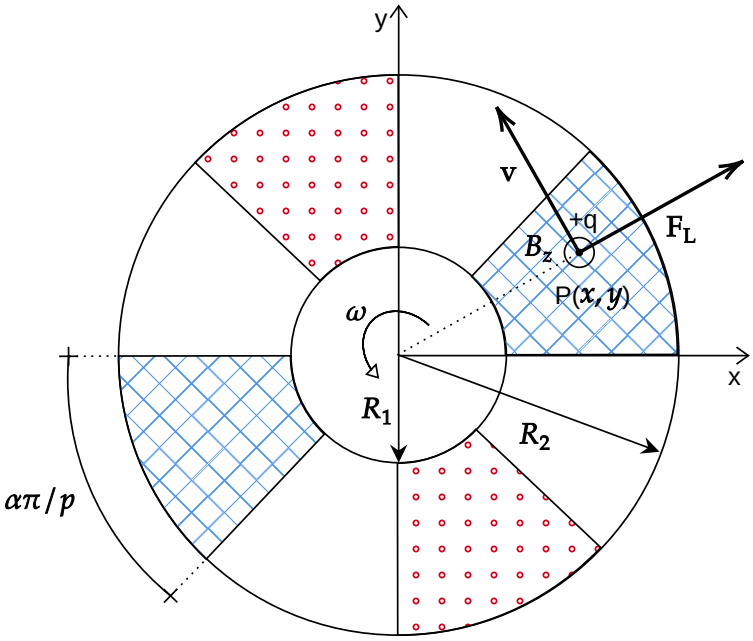

Figure 3.3: Lorentz force on a charged particle in magnetic field portion.

Inside the blue zone exist a magnetic field **B** supposing constant and only along positive z-direction. In the red zone the magnetic field is along negative z-direction while in the white zone no magnetic field is present. Where magnetic field is not zero, the Lorentz's force F_L acts on the charge with the relation:

$$\mathbf{F}_L = q\mathbf{v} \times \mathbf{B} \tag{2.2}$$

applying the dynamics to the charge taking into account the system's geometry we obtain the acceleration **a** of the charge:

$$\begin{pmatrix} a_x \\ a_y \\ a_z \end{pmatrix} = \frac{q}{m} \begin{pmatrix} v_x \\ v_y \\ v_z \end{pmatrix} \times \begin{pmatrix} 0 \\ 0 \\ B_z \end{pmatrix} = \frac{q}{m} \begin{pmatrix} v_y B_z \\ -v_x B_z \\ 0 \end{pmatrix} \tag{2.3}$$

where m is the particle mass, the equation 2.3 tell us that is zero the acceleration along z-direction thus there is the conservation of the velocity along the **B** direction; we suppose that in steady state conditions $v_z \equiv 0$. This three-dimensional problem is simplified in two-dimensional problem in (x,y). Reminding that the acceleration is the derivate with respect the time of the velocity ($\mathbf{a} = \dot{\mathbf{v}}$), we can write:

$$\begin{pmatrix} \dot{v}_x \\ \dot{v}_y \end{pmatrix} = \frac{qB_z}{m} \begin{pmatrix} v_y \\ -v_x \end{pmatrix} \tag{2.4}$$

where qB_z/m is the gyrofrequency and henceforth will be indicated as ω_c. Supposing to have the earth's average magnetic flux density field (B=35 μT) and considering electron as charges (q= -1.60·10^{-19} C, m= 9.11·10^{-31} Kg) ω_c is about 6.15 ·10^6 $rad \cdot s^{-1}$ value quite bigger with the angular velocity of the rotation ω. Equation 2.4 is a linear differential equations system that can be rewritten in terms of matrix:

$$\dot{\mathbf{v}} = \mathbf{A} \cdot \mathbf{v} \tag{2.5}$$

where **A** is the matrix

$$\mathbf{A} = \begin{pmatrix} 0 & \omega_c \\ -\omega_c & 0 \end{pmatrix} \tag{2.6}$$

the problem is resolvable with the method of matrix exponential and the solution has the following form:

$$\mathbf{v}(t) = e^{\mathbf{A}t} C \quad , \quad C \in \mathbb{R}^2 \tag{2.7}$$

the step now is to calculate the exponential of the matrix **A**, to do this it's necessary to diagonalize itself in the way that $\mathbf{A} = \mathbf{P} \cdot \mathbf{B} \cdot \mathbf{P}^{-1}$, where **B** is a diagonal matrix which it's easy to compute its exponential:

$$e^{\mathbf{A}t} = \mathbf{P} \cdot e^{\mathbf{B}t} \tag{2.8}$$

To find **B** it's necessary to find eigenvalues and eigenvectors of **A** which are $\lambda_1 = j\omega_c$ and $\lambda_2 = -j\omega_c$ with respective eigenvectors $w_1 = \begin{pmatrix} -j \\ 1 \end{pmatrix}$ and $w_2 = \begin{pmatrix} j \\ 1 \end{pmatrix}$ and we obtain:

$$\mathbf{v}(t) = \begin{pmatrix} -j & j \\ 1 & 1 \end{pmatrix} \cdot \begin{pmatrix} e^{j\omega_c t} & 0 \\ 0 & e^{-j\omega_c t} \end{pmatrix} \cdot \begin{pmatrix} c_1 \\ c_2 \end{pmatrix} \tag{2.9}$$

which becomes:

$$\begin{pmatrix} v_x(t) \\ v_y(t) \end{pmatrix} = \begin{pmatrix} -jc_1 e^{j\omega_c t} + jc_2 e^{-j\omega_c t} \\ c_1 e^{j\omega_c t} + c_2 e^{-j\omega_c t} \end{pmatrix} \tag{2.10}$$

now, in order to solve the differential equation system we have to impose the initially conditions. At time t=0 the charge is moving with the billet at distance r from the rotation axis with tangential velocity ωr therefore at the initial instant we have:

$$\begin{pmatrix} v_x(0) \\ v_y(0) \end{pmatrix} = \begin{pmatrix} 0 \\ \omega r \end{pmatrix} \tag{2.11}$$

with these conditions it's easy to see that the constants become $c_1 = c_2 = \omega r/2$, remembering the Euler's formula it can be written:

$$\begin{cases} v_x(t) = \omega r \sin(\omega_c t) \\ v_y(t) = \omega r \cos(\omega_c t) \end{cases} \tag{2.12}$$

with respect the supportive reference system to disk billet, the velocity of the charges are:

$$\begin{cases} v_x(t) = \omega r \sin(\omega_c t) \\ v_y(t) = \omega r (\cos(\omega_c t) - 1) \end{cases} \tag{2.13}$$

In order to have the chargee's trajectory we have to find the position integrating the velocities, supposing that for t=0 $x = r$ and $y = 0$ we obtain:

$$\begin{cases} x(t) = r + r\frac{\omega}{\omega_c}(1 - cos(\omega_c t)) \\ y(t) = r\frac{\omega}{\omega_c}(sin(\omega_c t) - \omega_c t) \end{cases} \tag{2.14}$$

The parametric plot of the equations 2.14 considering $\omega_c = 4\omega$ and radius r is showed in figure 3.4.

It's interesting to note that the x-position varies from r to $r + \delta r$ while the y-position tends globally to increment with the time (thanks to the initial velocity of the particle) but some times there is reduction of y i.e. the charge "turn back". In the system we studied, $\omega_c >> \omega$ therefore the y-pitch $\delta y = r\omega/\omega_c$ is very small as is small $\delta r = 2r\omega/\omega_c$. This model is not applicable to other studies, its aim is just to have a comprehension of the physical system. In fact for example a particle at the border of the magnetic region (blue and red region in figure 3.3) could be deflected in the non magnetic zone and no be more governed by the Lorenz's law. What do we expect is that boundary regions have a not well predictable behaviour with this magneto-dynamic formulation. A big lack of this model is the non consideration of the other charges which interact with each other. Considering the presence of other charges is a quantum-statistic problem, but we can say that in the middle of the magnet region there is the coexistence of charges spinning in opposite directions leading to very low values of current density. The last consideration is that the velocity is proportional to the angular velocity ω. According with the Drude's model, the current density $\mathbf{J}$ is proportional to the velocity. The electrical power losses due by the eddy currents is proportional to J^2 therefore what we do expect is:

$$P_{el} \propto \omega^2 \tag{2.15}$$

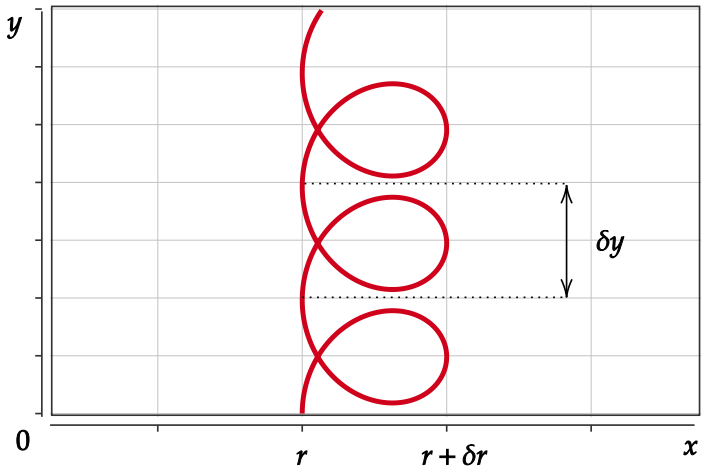

Figure 3.4: Trajectory of a particle in a magnetic flux density ($\omega_c = 4\omega$) with respect the billet reference system.

We'll discuss after the FEM model results.
At the end the magneto-dynamic formulation at the is not appropriated to study this case of study cause it doesn't takes into account the behaviour of all the charges inside the load to heat. We need a to study the system with a electromagnetic formulation based on the Maxwell's equations.

3.3 Linearisation of the system

The system presents an elegant cylindrical symmetries which leads us to think that the easier way to study the problem is with cylindrical coordinates. Even if this approach could simplify the geometrical definitions, it will carry out to a very complex differential equations deriving from the Maxwell's formulation of the fields, specifically with the "nabla" operator. An other important consideration is that the cross product between two vectors is defined only in cartesian coordinate system and not in the cylindrical one. Study the cylindrical system in cartesian coordinates is complex therefore there is an other approach to solve the problem i.e. the linearisation of the system. In this way we transform rotational motion into a linear motion. Figure 3.5 shows the linearised system; the geometrical quantities have been fitted starting from the system in Figure 3.1. The opposite permanent magnets are posed at distance τ from each other and have length $\alpha\tau$ and width L. The air gap from permanent magnets and conductive plate (thickness h and width D) is always s. In this system with respect the cylindrical the x-direction represents the azimuthal direction, the y-direction the radial one while the z-direction is the axial one. The relative speed v between conductive plate and permanent magnets is along x-direction with magnitude ωR_m. The system is supposed infinitely extended in both direction along the x-axis with a periodicity of 2τ with two pole pitch. As we can see from figure 3.6, the problem has three solution domains of

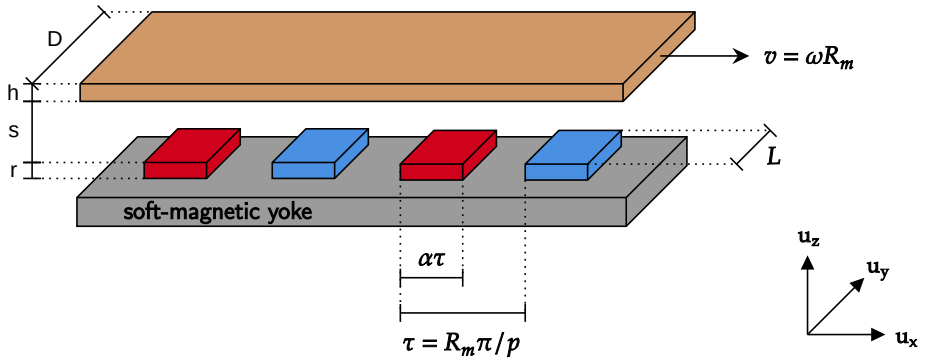

Figure 3.5: Three-dimensional representation of the linear eddy-current coupling.

the magnetic field: the permanent magnet region, the air gap region and the conductive one respectively region 1,2 and 3. In order to solve the eddy current problem it's nec-

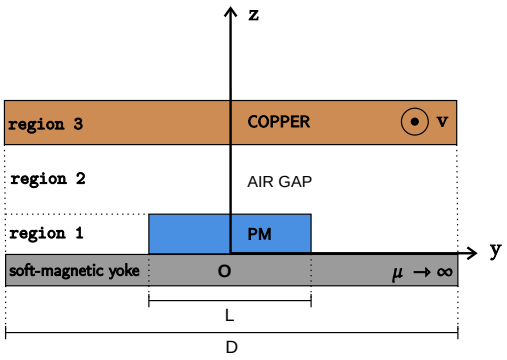

Figure 3.6: Transversal y-z section of the linearised system.

essary to find boundary conditions in x and y directions and interface conditions along the z-directions. As the origin of reference system we set the point O in the geometrical centre of permanent magnet between its layer and the soft-magnetic yoke layer.

3.3.1 Boundary conditions

Due to alternate polarity of the permanent magnets there is a periodicity of the system along the x-direction. This has repercussion also in the solution therefore it can be considered x only in the range $-\tau/2 \leq x \leq \tau/2$ and with the boundary condition:

$$\mathbf{H}_i(-\tau/2, y, z) = -\mathbf{H}_i(\tau/2, y, z) \quad \text{with } i = 1,2,3 \tag{3.16}$$

where $\mathbf{H}_i$ is the magnetic field in all the three regions. The minus sign is because we consider the single pole pitch and not the dipole pitch. Due to the soft-magnetic yoke with

a supposing infinite magnetic permeability the magnetic field has are only z-component at z=0:

$$\mathbf{H}_1(x,y,0)\times\hat{\mathbf{u}}_z = 0 \tag{3.17}$$

The study in the y-direction is limited by the geometrical dimension of the conductive plate therefore the domain is $-D/2 \leq y \leq D/2$. In this case we impose an artificial boundary condition: the perfect magnetic boundary condition (Dirichelet):

$$\mathbf{H}_i(x,\pm D/2,z)\times\hat{\mathbf{u}}_y = 0 \quad \text{with } i = 1,2,3 \tag{3.18}$$

this artificial condition obviously compromises the solution's accuracy but this impact is limited if D>L, which corresponds to a well designed eddy current coupling [17, 18].

An other important general boundary conditions is the continuity of magnetic field and magnetic flux density across a surface. Considering the figure 3.7 when the magnetic flux density across a from a material with permittivity μ_1 to a second material with μ_2, the normal component B_{N1} of the magnetic flux density near the boundary, immediately inside material 1 is equal to the normal component B_{N2} immediately inside the second material. There is therefore the conservation of the normal component

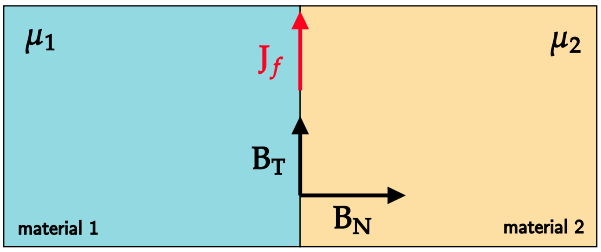

Figure 3.7: Normal and tangential components across two material's surface of the magnetic flux density.

of the magnetic flux density across a surface:

$$\mathbf{B}_{N1} = \mathbf{B}_{N2} \tag{3.19}$$

And since **B** and **H** are related by the permeability, we know how the normal component of the magnetic field H_N changes across the boundary:

$$\mu_1\mathbf{H}_{N1} = \mu_2\mathbf{H}_{N2} \tag{3.20}$$

If in the boundary exist a surface free current density $\mathbf{J}_f$ directed along the outline, we will have the magnetic field discontinuous by the exact amount of surface current density:

$$\mathbf{H}_{T1} - \mathbf{H}_{T2} = \mathbf{J}_f \times \hat{\mathbf{u}}_N \tag{3.21}$$

where $\hat{\mathbf{u}}_N$ is the unit normal points in the direction from medium 2 to medium 1 [19].

For our considerations the magnetic permittivity is always μ_0 therefore there is the continuity of the normal component of the magnetic flux density and the magnetic field. In our system no free current are presents therefore there is also the continuity of the tangential component of the magnetic field. Overall both magnetic flux density and magnetic field are preserved.

3.3.2 General solution in the non conductive regions

In the region 1 and 2 are present non conductive materials therefore no current flows inside these regions, Maxwell's equation can be written in the following form:

$$\begin{matrix} \nabla \cdot \mathbf{B}_i = 0 \\ \nabla \times \mathbf{H}_i = 0 \end{matrix} \qquad \text{with } i = 1,2 \tag{3.22}$$

this is a magneto-static problem, $\mathbf{H}$ is irrotational and can be express in terms of a magnetic scalar potential:

$$\mathbf{H}_i = -\nabla \Phi_i \quad \text{with } i = 1,2 \tag{3.23}$$

Solving a differential equation starting from Maxwell's equations with the scalar potential is easier with respect $\mathbf{H}$ or $\mathbf{B}$ which are 3-dimensional vectors i.e. we have to find only one solution instead of three. In the PM region there is a residual magnetization term $\mathbf{M}$ to takes into account, therefore the magnetic flux density is:

$$\mathbf{B}_i = \mu_0 \mu_{ri} \mathbf{H}_i + \mu_0 \mathbf{M}_i \tag{3.24}$$

where $\mu_0 = 4\pi \cdot 10^{-7} H \cdot m^{-1}$ is the permeability constant and μ_{ri} is the relative permeability. Combining equation 3.22, 3.23 and 3.24 we obtain:

$$\nabla^2 \Phi_i = \nabla \cdot \mathbf{M}_i \quad \text{with } i = 1,2 \tag{3.25}$$

PM are magnetized only the z-direction and the residual magnetization doesn't depend by z thus we can write:

$$\mathbf{M}_i = M_z(x,y)\hat{\mathbf{u}}_z \quad \text{with } i = 1,2 \tag{3.26}$$

The magnetization distribution has the $M(x,y)$ has a behaviour shown in figure 3.8 and 3.9. To express the magnetization if an analytic way it's we use the double Fourier series therefore the expression of $M(x,y)$ becomes:

$$M_z(x,y) = \frac{B_r}{\mu_0} \xi_x(x) \xi_y(y) \tag{3.27}$$

where B_r is the remanence flux density in the PMs, $\xi_x(x)$ and $\xi_y(y)$ are dimensionless functions of the only variables x and y respectively and have the following expression:

$$\xi_x(x) = \sum_{m=1,3,5,\ldots}^{\infty} \xi_{xm} \cos\left(m \frac{\pi}{\tau} x\right) \tag{3.28}$$

and

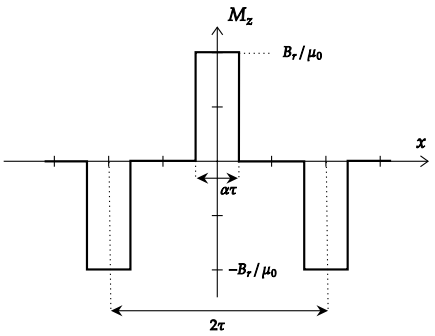

Figure 3.8: Magnetization distribution along x-direction.

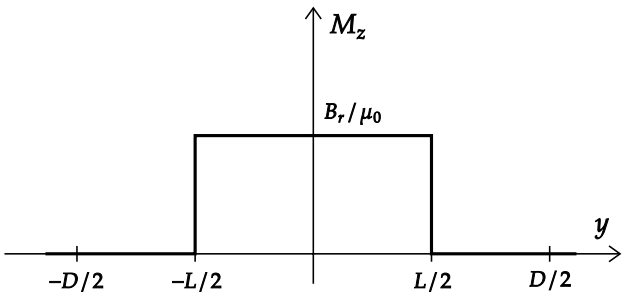

Figure 3.9: Magnetization distribution along y-direction.

$$\xi_y(y) = \sum_{n=1,3,5,\ldots}^{\infty} \xi_{yn} \cos\left(n\frac{\pi}{D}y\right) \tag{3.29}$$

with

$$\xi_{xm} = \frac{4}{m\pi}\sin\left(\frac{m\pi\alpha}{2}\right) \tag{3.30}$$

and

$$\xi_{yn} = \frac{4}{n\pi}\sin\left(\frac{n\pi L}{2D}\right) \tag{3.31}$$

We can now rewrite the equation 3.27 using the equations 3.28 and 3.29 therefore:

$$M_z(x,y) = \sum_{n=1,3,5,\ldots}^{\infty}\sum_{m=1,3,5,\ldots}^{\infty} M_{nm}\cos\left(m\frac{\pi}{\tau}x\right)\cos\left(n\frac{\pi}{H}y\right) \tag{3.32}$$

where

$$M_{nm} = \frac{16B_r}{\mu_0\pi^2 nm}\sin\left(\frac{m\alpha\pi}{2}\right)\sin\left(\frac{n\pi L}{2D}\right) \tag{3.33}$$

Because of the simplification of the future calculations it's useful to express the equation 3.32 in the following form:

$$M_z(x,y) = \Re\mathfrak{e}\left\{\sum_{n=1,3,5,\ldots}^{\infty}\sum_{m=1,3,5,\ldots}^{\infty} M_{nm}\cos\left(n\frac{\pi}{D}y\right)e^{jm\frac{\pi}{\tau}x}\right\} \tag{3.34}$$

The figure 3.10 shows the behaviour of the normalized function $M_z(x,y)$ in the three-dimensional space. If $M_z(x,y)$ doesn't depend by z, it's easy to see that $\nabla\cdot\mathbf{M}_i = 0$ therefore we obtain a second order partial differential equation valid in the two regions:

$$\frac{\partial^2\Phi_i}{\partial x^2} + \frac{\partial^2\Phi_i}{\partial y^2} + \frac{\partial^2\Phi_i}{\partial z^2} = 0 \quad \text{with } i = 1,2 \tag{3.35}$$

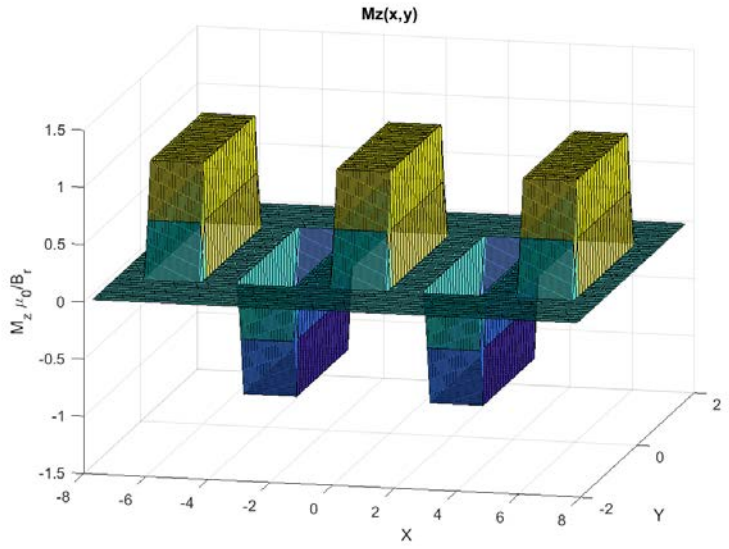

Figure 3.10: Tridimensional rapresentation of the magnetization $M_z(x,y)$.

The boundary conditions 3.16 and 3.18 (valid for boot the regions) are transmitted to the magnetic scalar potential:

$$\begin{aligned} \Phi_i(-\tau/2,y,z) &= -\Phi(\tau/2,y,z) \\ \Phi_i(x,-D/2,z) &= \Phi(x,D/2,z) \end{aligned} \qquad \text{with } i = 1,2 \tag{3.36}$$

According with the Fourier's series and the method of separation of variables, general solutions which satisfy boundary conditions 3.36 are:

$$\Phi_i(x,y,z) = \mathfrak{Re}\left\{ \sum_{n=1,3,5,..}^{\infty} \sum_{m=1,3,5,..}^{\infty} \bar{\Phi}_i(z) \cos\left(n\frac{\pi}{D}y\right) e^{jm\frac{\pi}{\tau}x} \right\} \quad \text{with } i = 1,2 \tag{3.37}$$

where n and m are odd integer numbers. Substituting the solution 3.37 into the equation 3.35 and making the derivates and simplifying we obtain:

$$\frac{d^2\bar{\Phi}_i(z)}{dz^2} = \left\{ \left(\frac{n\pi}{D}\right)^2 + \left(\frac{m\pi}{\tau}\right)^2 \right\} \bar{\Phi}_i(z) \tag{3.38}$$

which has solution:

$$\bar{\Phi}_i(z) = \bar{A}_i e^{\alpha_{nm} z} + \bar{B}_i e^{-\alpha_{nm} z} \tag{3.39}$$

where α_{nm} doesn't depend by the region and its value is:

$$\alpha_{nm} = \sqrt{\left(\frac{n\pi}{D}\right)^2 + \left(\frac{k\pi}{\tau}\right)^2} \tag{3.40}$$

therefore the solution in the two regions are given by the equation 3.37 with Φ_i equal to:

$$\bar{\Phi}_1(z) = \bar{A}_{nm} e^{\alpha_{nm} z} + \bar{B}_{nm} e^{-\alpha_{nm} z} \tag{3.41}$$

$$\bar{\Phi}_2(z) = \bar{C}_{nm} e^{\alpha_{nm} z} + \bar{D}_{nm} e^{-\alpha_{nm} z} \tag{3.42}$$

where the constants $\bar{A}_{nm}$, $\bar{B}_{nm}$, $\bar{C}_{nm}$ and $\bar{D}_{nm}$ are in general complex numbers to be determined using the interface boundary conditions [20].

3.3.3 General solution in the conductive region

Maxwell's equations in the billet region (region 3) have to considerate the presence of current density therefore can be written as follows:

$$\nabla \times \mathbf{E}_3 = -\frac{\partial \mathbf{B}}{\partial t} \quad , \quad \nabla \times \mathbf{H}_3 = \mathbf{J}_3 \quad , \quad \nabla \cdot \mathbf{B}_3 = 0 \tag{3.43}$$

where $\mathbf{E}_3$ in the electric field and $\mathbf{J}_3$ the induced current density in region 3. The Ohm's law for a moving conductor with velocity $\mathbf{v}$ with respect a stationary magnetic field is expressed by:

$$\mathbf{J}_3 = \sigma(\mathbf{E}_3 + \mathbf{v} \times \mathbf{B}_3) \qquad \text{with } \mathbf{v} = v\hat{\mathbf{u}}_x \tag{3.44}$$

The reference system we consider is supportive of the magnets disk and in steady state conditions the magnetic source is static therefore:

$$\frac{\partial \mathbf{B}}{\partial t} = 0 \tag{3.45}$$

and the eddy current problem reduces to a magneto-static problem. Without any simplification, combining the equations 3.43 and 3.44, with some algebraic passages we obtain:

$$\nabla \times \mathbf{H}_3 = \sigma(\mathbf{v} \times \mathbf{B}_3) \tag{3.46}$$

making the curl to both the terms and remembering that $\nabla \times (\nabla \times \mathbf{H}) = \nabla(\nabla \cdot \mathbf{H}) - \nabla^2 \mathbf{H}$, considering from the equation 3.45 $\nabla \cdot \mathbf{H} = 0$ we obtain:

$$\nabla^2 \mathbf{H} = -\sigma \mu_0 \nabla \times (\mathbf{v} \times \mathbf{H}_3) \tag{3.47}$$

the product vector between $\mathbf{v}$ and $\mathbf{H}_3$ thanks to the choice of the cartesian coordinates system becomes:

$$\mathbf{v} \times \mathbf{H}_3 = \begin{pmatrix} v \\ 0 \\ 0 \end{pmatrix} \times \begin{pmatrix} H_x \\ H_y \\ H_z \end{pmatrix} = \begin{pmatrix} 0 \\ -vH_z \\ vH_y \end{pmatrix} \tag{3.48}$$

in order to lighten the notation from now on the subscript 3 will be removed even if the solution is always intended in the region 3. We can now make the curl to the resultant vector in the equation 3.48 which becomes:

$$\nabla \times (\mathbf{v} \times \mathbf{H}) = \begin{pmatrix} v(\frac{\partial H_y}{\partial y} + \frac{\partial H_z}{\partial z}) \\ -v\frac{\partial H_y}{\partial x} \\ -v\frac{\partial H_z}{\partial x} \end{pmatrix} = -v \begin{pmatrix} \frac{\partial H_x}{\partial x} \\ \frac{\partial H_y}{\partial x} \\ \frac{\partial H_z}{\partial x} \end{pmatrix} \tag{3.49}$$

using the relation ($\nabla \cdot \mathbf{H} = 0$). Now we can write the three partial differential equations:

$$\begin{cases} \frac{\partial^2 H_x}{\partial x^2} + \frac{\partial^2 H_y}{\partial y^2} + \frac{\partial^2 H_z}{\partial z^2} = \sigma \mu_0 v \frac{\partial H_x}{\partial x} \\ \frac{\partial^2 H_x}{\partial x^2} + \frac{\partial^2 H_y}{\partial y^2} + \frac{\partial^2 H_z}{\partial z^2} = \sigma \mu_0 v \frac{\partial H_y}{\partial x} \\ \frac{\partial^2 H_x}{\partial x^2} + \frac{\partial^2 H_y}{\partial y^2} + \frac{\partial^2 H_z}{\partial z^2} = \sigma \mu_0 v \frac{\partial H_z}{\partial x} \end{cases} \tag{3.50}$$

Now, in order to solve this PDE we proceed with the method of the variable separation with the boundary conditions 3.16 and 3.18, we suppose the solutions have the following structure:

$$\begin{aligned} H_x(x,y,z) &= \mathfrak{Re}\left\{ \sum_{n=1,3,5,\dots}^{\infty} \sum_{m=1,3,5,\dots}^{\infty} \bar{H}_{x,nm}(z) \cos\left(n\tfrac{\pi}{D} y\right) e^{jm\frac{\pi}{\tau}x} \right\} \\ H_z(x,y,z) &= \mathfrak{Re}\left\{ \sum_{n=1,3,5,\dots}^{\infty} \sum_{m=1,3,5,\dots}^{\infty} \bar{H}_{z,nm}(z) \cos\left(n\tfrac{\pi}{D} y\right) e^{jm\frac{\pi}{\tau}x} \right\} \end{aligned} \tag{3.51}$$

where $\bar{H}_{nmx}(z)$ and $\bar{H}_{nmz}(z)$ are functions of the only z variable. Similarly what we've done in the previous section:

$$\begin{aligned} \bar{H}_{x,nm} &= \bar{E} e^{\gamma_{nm} z} + \bar{F} e^{-\gamma_{nm} z} \\ \bar{H}_{z,nm} &= \bar{G} e^{\gamma_{nm} z} + \bar{H} e^{-\gamma_{nm} z} \end{aligned} \tag{3.52}$$

where $\bar{E}$, $\bar{F}$, $\bar{G}$ and $\bar{H}$ are constants to be determined by the boundary conditions while:

$$\gamma_{nm} = \sqrt{\left(\frac{n\pi}{D}\right)^2 + \left(\frac{m\pi}{\tau}\right)^2 + jm\sigma\mu_0 v \frac{\pi}{\tau}} \tag{3.53}$$

The term $H_y(x,y,z)$ is given by $\nabla \cdot \mathbf{H} = 0$ therefore is directly obtainable from $H_x(x,y,z)$ and $H_z(x,y,z)$:

$$H_y(x,y,z) = -\int \left(\frac{\partial H_x}{\partial x} + \frac{\partial H_z}{\partial z} \right) dy \tag{3.54}$$

Using equations 3.51, 3.52 we can rewrite 3.54 as follows:

$$H_y(x,y,z) = \mathfrak{Re}\left\{ \sum_{n=1,3,5,\dots}^{\infty} \sum_{m=1,3,5,\dots}^{\infty} \bar{H}_{y,nm}(z) \sin\left(n\frac{\pi}{D} y\right) e^{jm\frac{\pi}{\tau}x} \right\} \tag{3.55}$$

where

$$\bar{H}_y(z) = -\frac{D}{n\pi}\left(jm\frac{\pi}{\tau}\bar{H}_x(z) + \frac{d\bar{H}_z(z)}{dz} \right) \tag{3.56}$$

3.3.4 Composition of the solutions

Now that we have found the general solutions in all the three regions we can proceed to find the particular solutions imposing the boundary conditions. We introduce now a fourth region which is the space over the billet, is made up air and is supposed infinitive

extended. We already know the solution in the region 4 because is the same of the 1 and 2 and is:

$$\Phi_4(x,y,z) = \mathfrak{Re}\left\{ \sum_{n=1,3,5,..}^{\infty} \sum_{m=1,3,5,..}^{\infty} \bar{\Phi}_4(z) \cos\left(n\frac{\pi}{D}y\right) e^{jm\frac{\pi}{\tau}x} \right\} \tag{3.57}$$

with:

$$\bar{\Phi}_4(z) = \bar{J}_{nm} e^{\alpha_{nm} z} + \bar{I}_{nm} e^{-\alpha_{nm} z} \tag{3.58}$$

where, again, $\bar{J}_{nm}$ and $\bar{I}_{nm}$ are constant to be determined by the boundary conditions. We also know that α_{nm} is a real positive number. The solution for $z \to +\infty$ must be zero therefore must be zero also $\bar{J}_{nm}$. We have now nine unknown coefficients to determine, we need therefore nine independent linear equations. From the equation 3.17 we obtain:

$$\Phi_1(x,y,0) = 0 \tag{3.59}$$

From the conservation of all the components of the magnetic field between region 1 and 2 (z=r) we have:

$$\begin{aligned} &\Phi_1(x,y,r) = \Phi_2(x,y,r) \\ &\frac{\partial \Phi_1(x,y,r)}{\partial z} = \frac{\partial \Phi_2(x,y,r)}{\partial z} - M_z(x,y) \end{aligned} \tag{3.60}$$

From the conservation of all the components of the magnetic field between region 2 and 3 (z=r+s) we have:

$$\begin{aligned} \frac{\partial \Phi_2(x,y,r+s)}{\partial x} &= -H_{3x}(x,y,r+s) \\ \frac{\partial \Phi_2(x,y,r+s)}{\partial y} &= -H_{3y}(x,y,r+s) \\ \frac{\partial \Phi_2(x,y,r+s)}{\partial z} &= -H_{3z}(x,y,r+s) \end{aligned} \tag{3.61}$$

And from the conservation of all the components of the magnetic field between region 3 and 4 (z=r+s+h) we have:

$$\begin{aligned} \frac{\partial \Phi_4(x,y,r+s+h)}{\partial x} &= -H_{3x}(x,y,r+s+h) \\ \frac{\partial \Phi_4(x,y,r+s+h)}{\partial y} &= -H_{3y}(x,y,r+s+h) \\ \frac{\partial \Phi_4(x,y,r+s+h)}{\partial z} &= -H_{3z}(x,y,r+s+h) \end{aligned} \tag{3.62}$$

The system can be written in matrix form:

$$[\mathbf{A}]_{nm} \cdot [\mathbf{Y}]_{nm} = [\mathbf{B}]_{nm} \tag{3.63}$$

where the matrix $[\mathbf{A}]_{nm}$ is:

$$\begin{bmatrix}
1 & 1 & 0 & 0 & 0 & 0 & 0 & 0 & 0 \\
e^{\alpha_{nm}r} & e^{-\alpha_{nm}r} & -e^{\alpha_{nm}r} & -e^{-\alpha_{nm}r} & 0 & 0 & 0 & 0 & 0 \\
e^{\alpha_{nm}r} & -e^{-\alpha_{nm}r} & -e^{\alpha_{nm}r} & e^{-\alpha_{nm}r} & 0 & 0 & 0 & 0 & 0 \\
0 & 0 & \frac{e^{\alpha_{nm}z_h}}{\frac{\tau}{jm\pi}} & \frac{e^{-\alpha_{nm}z_h}}{\frac{\tau}{jm\pi}} & e^{\gamma_{nm}z_h} & e^{-\gamma_{nm}z_h} & 0 & 0 & 0 \\
0 & 0 & \frac{e^{\alpha_{nm}z_h}}{\left(\frac{D}{n\pi}\right)^2} & \frac{e^{-\alpha_{nm}z_h}}{\left(\frac{D}{n\pi}\right)^2} & \frac{e^{\gamma_{nm}z_h}}{\frac{\tau}{jm\pi}} & \frac{e^{-\gamma_{nm}z_h}}{\frac{\tau}{jm\pi}} & \gamma_{nm}e^{\gamma_{nm}z_h} & -\gamma_{nm}e^{-\gamma_{nm}z_h} & 0 \\
0 & 0 & \alpha_{nm}e^{\alpha_{nm}z_h} & -\alpha_{nm}e^{-\alpha_{nm}z_h} & 0 & 0 & e^{\gamma_{nm}z_h} & e^{-\gamma_{nm}z_h} & 0 \\
0 & 0 & 0 & 0 & e^{\gamma_{nm}z_t} & e^{-\gamma_{nm}z_t} & 0 & 0 & \frac{e^{\alpha_{nm}z_t}}{\frac{\tau}{jm\pi}} \\
0 & 0 & 0 & 0 & \frac{e^{\gamma_{nm}z_t}}{\frac{\tau}{jm\pi}} & \frac{e^{-\gamma_{nm}z_t}}{\frac{\tau}{jm\pi}} & \gamma_{nm}e^{\gamma_{nm}z_t} & -\gamma_{nm}e^{-\gamma_{nm}z_t} & \frac{e^{\alpha_{nm}z_t}}{\left(\frac{D}{n\pi}\right)^2} \\
0 & 0 & 0 & 0 & 0 & 0 & e^{\gamma_{nm}z_t} & e^{-\gamma_{nm}z_t} & \alpha_{nm}e^{\alpha_{nm}z_t}
\end{bmatrix} \tag{3.64}$$

where $z_h = r + s$ and $z_t = r + s + h$ and:

$$[\mathbf{Y}]_{nm} = \begin{bmatrix} \bar{A} \\ \bar{B} \\ \bar{C} \\ \bar{D} \\ \bar{E} \\ \bar{F} \\ \bar{G} \\ \bar{H} \\ \bar{I} \end{bmatrix} \quad \text{and} \quad [\mathbf{B}]_{nm} = \begin{bmatrix} 0 \\ 0 \\ -\frac{M_{nm}}{\alpha_{nm}} \\ 0 \\ 0 \\ 0 \\ 0 \\ 0 \\ 0 \end{bmatrix} \tag{3.65}$$

The unknown vector is easy to determinate and is:

$$[\mathbf{Y}]_{nm} = [\mathbf{A}]_{nm}^{-1} \cdot [\mathbf{B}]_{nm} \tag{3.66}$$

the inversion of the matrix $[\mathbf{A}]_{nm}$ is implemented in the computational codex by using MATLAB®therefore an analytical expression of the unknown coefficients is not shown because of its length. The current density inside the metal is calculable from the equation:

$$\mathbf{J}_3 = \nabla \times \mathbf{H}_3 \tag{3.67}$$

which becomes:

$$J_{3x} = \sum_{n,m=1,3,5,\ldots}^{\infty} \frac{D\, e^{\frac{j m \pi x}{\tau}} \sin\left(\frac{n\pi y}{D}\right)\left(\frac{j m \pi \left(\bar{E}\,\gamma_{nm}\, e^{z\gamma_{nm}} - \bar{F}\,\gamma_{nm}\, e^{-z\gamma_{nm}}\right)}{\tau} + \bar{G}\,\gamma_{nm}^2\, e^{z\gamma_{nm}} + \bar{H}\,\gamma_{nm}^2\, e^{-z\gamma_{nm}}\right)}{n\pi} - \\ - \frac{e^{\frac{j m \pi x}{\tau}}\left(\bar{G}\, e^{z\gamma_{nm}} + \frac{\bar{H}}{e^{z\gamma_{nm}}}\right) n\pi \sin\left(\frac{n\pi y}{D}\right)}{D} \tag{3.68}$$

$$J_{3y} = \sum_{n,m=1,3,5,\ldots}^{\infty} e^{\frac{j m \pi x}{\tau}} \cos\left(\frac{n\pi y}{D}\right)\left(\bar{E}\, e^{z\gamma_{nm}}\,\gamma_{nm} - \bar{F}\,\gamma_{nm}\, e^{-z\gamma_{nm}}\right) - \\ - \frac{e^{\frac{j m \pi x}{\tau}} \cos\left(\frac{n\pi y}{D}\right)\left(\bar{G}\, e^{z\gamma_{nm}} + \frac{\bar{H}}{e^{z\gamma_{nm}}}\right) j\,\pi}{\tau} \tag{3.69}$$

The z-component of the current density J_{3z} has an analytical form but the computational results (once computed the unknown coefficients $\bar{A}$,..., $\bar{I}$) show that J_{3z} is zero with an approximation of 10^{-31} i.e. the induced current flows only in the x-y plane (laminar eddy current). Figures 3.11, 3.12 and 3.13 show the behaviour of the induced current into the magnetic disk in $z = r + s + h/2$ with the parameters shown in table 3.1.

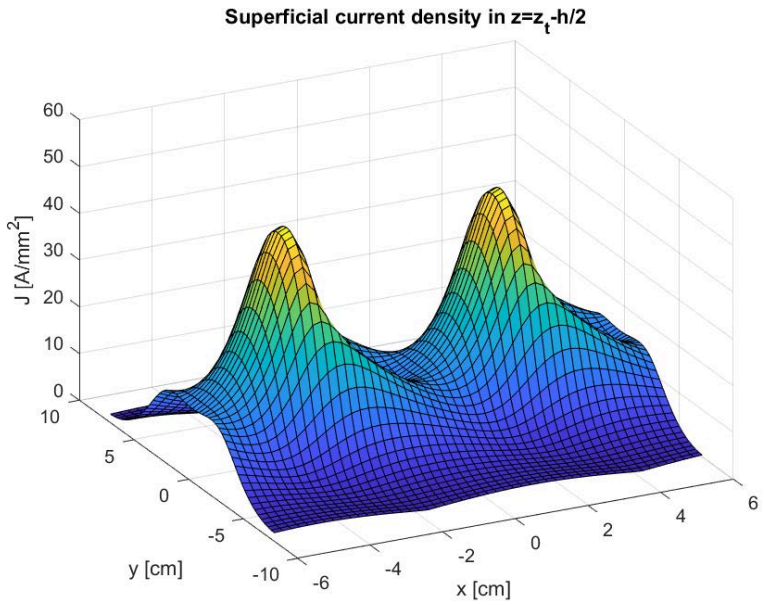

Figure 3.11: Current density magnitude distribution for the linearised system.

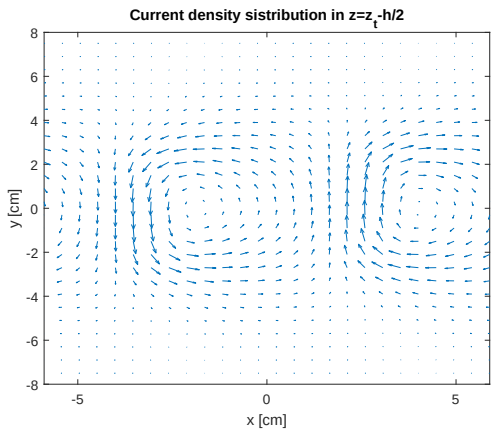

Figure 3.12: Induced current density distribution for the linearised system.

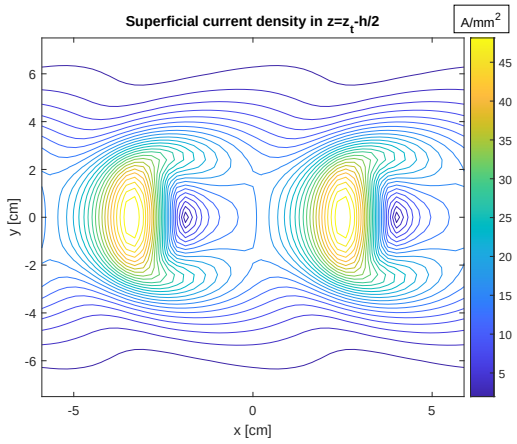

Figure 3.13: Induced current density magnitude for the linearised system - isolines.

Symbol	Description	Value
R_1	Inner radius of the magnets	50 mm
R_2	Outer radius of the magnets	100 mm
R_3	Radius of the conductive disk	150 mm
r	Magnet thickness	5 mm
s	Air-gap length	5 mm
h	Conductive plate thickness	5 mm
α	PMs pole-arch to pole-pitch ratio	0.9
p	Pole-pairs number	4
B_r	Remanence of PMs	1 T
σ	Conductivity of the metal	57 MS/m
ω	Angular velocity	1000 rpm
N	Number of harmonic terms in x-direction	20
M	Number of harmonic in y-direction	20

Table 3.1: Parameters of the case of study.

3.4 Power transmitted into the disk and electromagnetic torque

The power generated for Joule effect due by the eddy currents is calculable with the integral over the volume of the disk of the square of the eddy currents divided the electrical conductivity. We've seen how the current density from equations 3.68 and 3.69 has sum for n and m for each the components; when we compute the square, the final expression becomes complicated. It's not possible to have a simple analytical expression of the power losses in the billet. We can however estimate the losses by using the sum instead of the integral:

$$P = \int_V \frac{J^2}{\sigma} dxdydz \sim \sum_{\{x_i,y_i,z_i\}\in V} \frac{J^2(x_i,y_i,z_i)}{\sigma} \Delta x \Delta y \Delta z \tag{4.70}$$

In order to have an analytical expression, we suggest to compute the power losses with the electromagnetic torque which have a more simple expression. Once found the torque, assuming the system with no other losses, the power is the torque multiplying by ω i.e.:

$$P = T_e \omega \tag{4.71}$$

The electromagnetic torque is obtained using Maxwell stress tensor[1] which, in presence of only magnetic fields, leads to the total electromagnetic force along the speed direction by means of the formula[21]:

$$F_e = \frac{1}{\mu_0} \int_S B_x B_z dS \tag{4.72}$$

[1] More details about the Maxwell stress tensor will be addressed in the chapter 4.

where S is a generic surface perpendicular to the z axis. We chose, in order to have a simple expression of the magnetic flux density, to set the surface S in the border between region 1 and region 2, as shown in figure 3.14. Multiplying equation 4.72 for R_m we

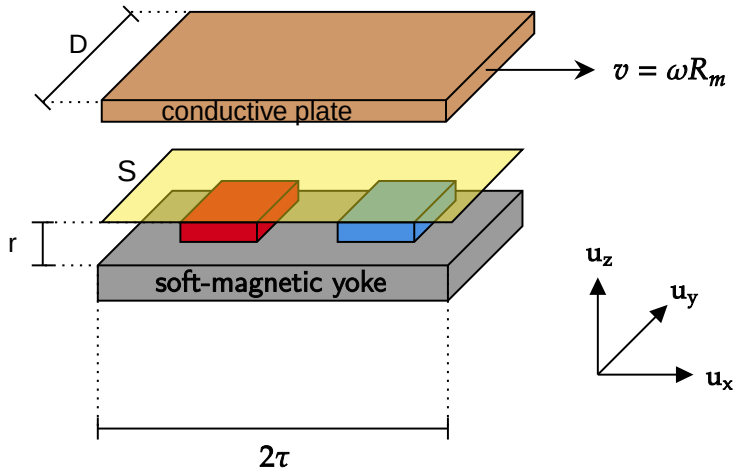

Figure 3.14: Surface chosen to calculate the electromagnetic torque.

obtain the torque given by a single pole-pair therefore. The integral over the surface S is for $-\tau < x < \tau$ and $-D/2 < y < D/2$. For p pole-pairs and remembering that $\mathbf{B}_2 = \mu_0 \mathbf{H}_2$, the electromagnetic torque T_e is:

$$T_e = pR_m\mu_0 \int_{-\tau}^{\tau}\int_{-D/2}^{D/2} H_{2x}(x,y,r)H_{2z}(x,y,r)dydx \tag{4.73}$$

In region 2 the magnetic field is expressed by the equation 3.23 and is for the two components:

$$H_{2x}(x,y,r) = -\frac{\partial \Phi_2}{\partial x} = -\Re\mathfrak{e}\left\{\sum_{n=1,3,5,\ldots}^{\infty}\sum_{m=1,3,5,\ldots}^{\infty} jm\frac{\pi}{\tau}[Ce^{\alpha_{nm}r} + De^{-\alpha_{nm}r}]\cos\left(\frac{n\pi}{D}y\right)e^{jm\frac{\pi}{\tau}x}\right\} \tag{4.74}$$

$$H_{2z}(x,y,r) = -\frac{\partial \Phi_2}{\partial z} = -\Re\mathfrak{e}\left\{\sum_{n=1,3,5,\ldots}^{\infty}\sum_{m=1,3,5,\ldots}^{\infty} \alpha_{nm}[Ce^{\alpha_{nm}r} - De^{-\alpha_{nm}r}]\cos\left(\frac{n\pi}{D}y\right)e^{jm\frac{\pi}{\tau}x}\right\} \tag{4.75}$$

We can note how the electromagnetic torque depends directly on the physical and geometrical parameters. We have now two expressions to evaluate the power losses into the metallic disk as we have a two expression to evaluate the electromagnetic torque which acts on the metal disk. Figure 3.15 shows the torque in function of the slip speed ω by using the two methods (equations 4.71 and 4.73) with parameter in table 3.1. We can see how the torque calculated by using the electromagnetic stress tensor is a bit lower ($\sim$ 5%) with respect the other method. Beyond the numerical values the two curves follow the same trend i.e. the torque has a maximum about at 800 rpm.
This is a good result because this is the validation of the two methods which have completely different and independents formulations.

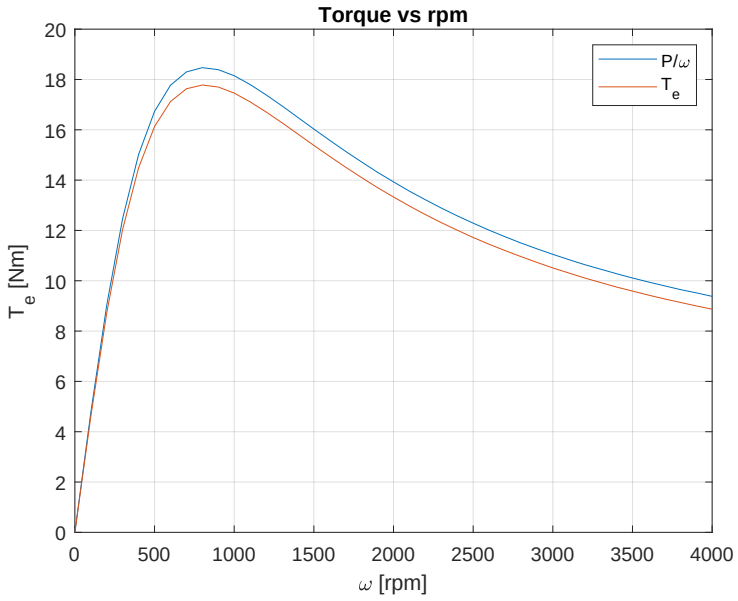

Figure 3.15: Torque comparison between two independent methods of calculation.

3.5 Axial force

The eddy currents into the metallic disk generate a magnetic field which interacts with the magnetic field of the permanent magnets thus a force is born. In general the force can be computed as the opposite to the gradient of the potential energy E_p i.e.:

$$\mathbf{F} = -\nabla E_p \tag{5.76}$$

If we assume that the metal disk is bigger enough with respect the external radius of the PMs disk in order to avoid the eddy current in the edge of the disk, we can say that a variation of the position of the disk in x and y-direction doesn't change the potential energy therefore F_x and F_y are both zero. We can therefore, neglecting the gravitational potential, say that the only force acting on the disk is along z.
In the analytical model we developed the outcome is the power generated, therefore we have to use the power and not the potential energy. The instantaneous force along z is:

$$F_z(t) = -\frac{\partial E_p}{\partial z} \tag{5.77}$$

in a time laps δt a quantity of energy $E_p = P\delta t$ is transmitted to the rotation od the PMs to the billet and converted into heat and this continues for the next δt. The choose of δt is not arbitrary, δt has to be chosen low enough that the variation of power in the time laps δt is negligible with the variation of power along z. This is the quasi static condition, we can therefore say that the average force in the time laps δt is:

$$< F_z >_{\delta t} = \frac{1}{\delta t}\int_0^{\delta t} F_z(t)dt = -\frac{\partial P}{\partial z}\delta t \tag{5.78}$$

In our problem the condition of quasi stationary is verified and we assumed δt= 1s. Figure 3.16 shows the axial force in function of the air gap thickness by assuming as case of study parameters in table 3.1. We can note how the force is positive o.r. repulsive and

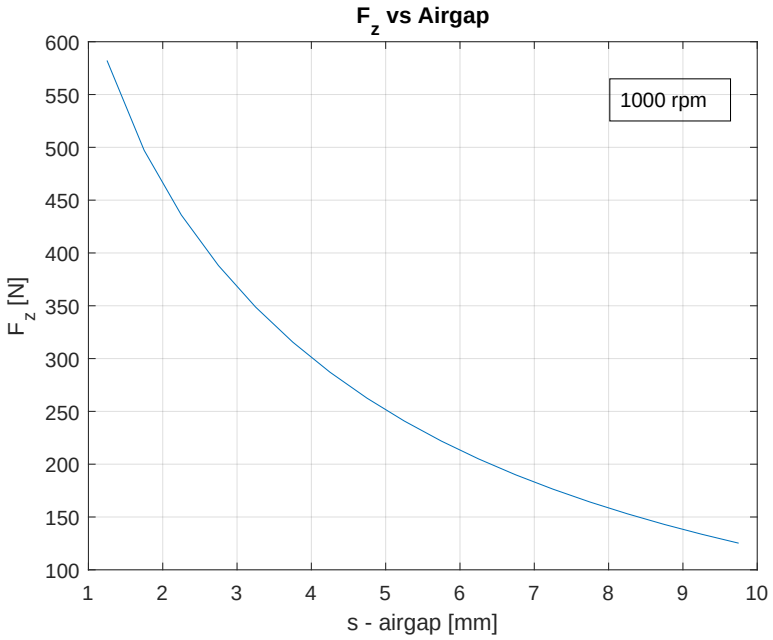

Figure 3.16: Axial force in function of the air gap thickness at 1000 rpm.

assumes higher values with respect the weight of the metallic disk and decrease with the increasing air gap thickness.
This method of calculation of the axial force is powerful but neds to compute the derivate of the power, therefore at least two values of power i.e. two computing sessions. We can therefore use an other approach to the axial force calculation this time direct: taking into account the Maxwell stress tensor with the surface S already used for the calculation of the electromagnetic torque, the force is [22]:

$$F_z = p\mu_0 \int_{-D/2}^{D/2} \int_{-\tau}^{\tau} \frac{H_{2z}^2(x,y,r) - H_{2x}^2(x,y,r) - H_{2y}^2(x,y,r)}{2} dxdy \tag{5.79}$$

Figure 3.17 shows the behaviour of the axial force in function of the slip speed for different air gap thickness (3, 5 and 7 mm). We can see how the force is null for velocity equal to zero as we expected since copper is not magnetic material and grows for higher velocities.

With the method described by the equation 5.76 for air gap thickness equal to 5 mm we computed an axial force of 251 N while with the Maxwell stress tensor method 280 N. The two methods give outcomes with 10% of errors. From now on we will use the second method because needs less computational power and will be compared with the FEM results.
The physical explanation of the phenomena is that every system evolves to the state at

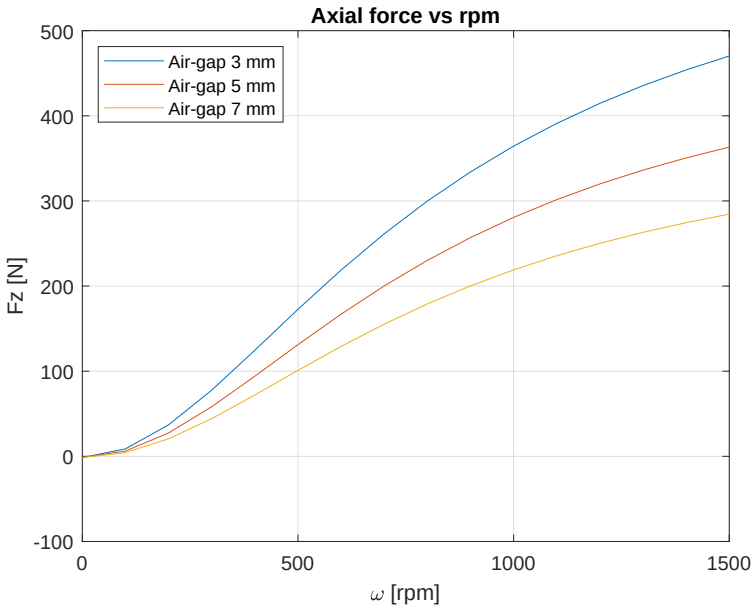

Figure 3.17: Axial force in function of the slip speed for different air gap thickness by using the Maxwell stress tensor.

lower energy. The eddy currents in the metallic disk generate a magnetic field which tends to oppose to the external magnetic field due by the magnets. The generated magnetic field is directed in the opposite way of the external one and this generates a repulsive force and as the system is configured this force will be always repulsive, because the system would reach the state of minimal energy which is the state without currents in the disk therefore for $z \to \infty$.

In the same way the state with lower energy is the state where the slip speed is null and this is also the reason of the electromagnetic torque.

3.6 FEM Model

In order to check the results derived from the analytical model we use a 3D finite element model (FEM) by using COMSOL Multiphysics®. The analytical model gave us results from a linearised system therefore, to compare the results with the FEM method, we have to reconvert to the cylindrical system. In particular the expression of the power for the linearised system is:

$$P_{lin} = \int_{z_t-h}^{z_t} \int_{-D/2}^{D/2} \int_{-\tau}^{\tau} w_i(x,y,z) dx dy dz \tag{6.80}$$

where $w_i = J^2/\sigma$ is the specific volume power. If find the expression over a disk we have to take in mind that the total volume of integration has to be the volume of the disk equal to $\pi R_3^2 h$ while the equation 6.80 gives a volume equal to $2\tau Dh = 2R_m \pi Dh/p$.

The expression of D has to take into account a symmetrical distribution of the current density, therefore if $R_m = R_3/2$, $D = R_3$ otherwise a more general expression is:

$$D = 2(R_3 - R_2) + R_2 - R_1 \tag{6.81}$$

which take into account only the region of the disk with current described by the linearised system. The final expression of the power in the disk of p pole-pairs number is:

$$P_{disk} = p\frac{R_3^2}{2R_m D}P_{lin} \tag{6.82}$$

The FEM model is shown in figure 3.18 with parameters in table 3.19 where the light blue volume is the conductive disk and the permanent magnets disk has 4 pole-pairs numbers.

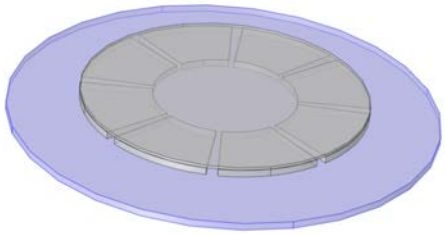

Figure 3.18: Geometrical 3D FEM model of the system.

Symbol	Description	Value
R_1	Inner radius of the magnets	50 mm
R_2	Outer radius of the magnets	100 mm
R_3	Radius of the conductive disk	150 mm
r	Magnet thickness	5 mm
s	Air-gap length	5 mm
h	Conductive plate thickness	5 mm
α	PMs pole-pitch ratio	0.9
p	Pole-pairs number	4
B_r	Remanence of PMs	1 T
σ	Conductivity of the metal	57 MS/m
ω	Angular velocity	1000 rpm
y	Yoke thickness	2 mm
μ_{ry}	Yoke relative permeability	4000

Figure 3.19: Parameters of the FEM model.

The same model has been modified also for 1, 2, 6, 7, 8 and 10 pole-pairs numbers. The simulation ran for about 40 seconds at 1000 rpm but, for higher values of speed, it ned even more one hour to converge to the solution while the analytical model Matlab®'s implementation only 4 seconds independently by the rpm value. The results of the simulation have been shown in figure 3.20 for the current density magnitude where the top of the disk is the z-coordinates equal to r+s and the white arrows indicate the current density direction. We can note how the current distribution follows in steady state the geometrical conformation of the PMs disk. There are regions of the disk indicates with blue colour where a very low current flows. In order to increase the power losses in the disk it's necessary to remove as possible the blue zones increasing R_2 and decreasing R_1 i.e. rising the PM's surface. An other parameter to consider is the pole-pairs number, in figures 3.21 and 3.22 is shown the current disposition in the disk in the bottom side and in the top side respectively. It easy to note that the current density is lower in the top layer with respect the upper one because of the bigger distance from the magnets.

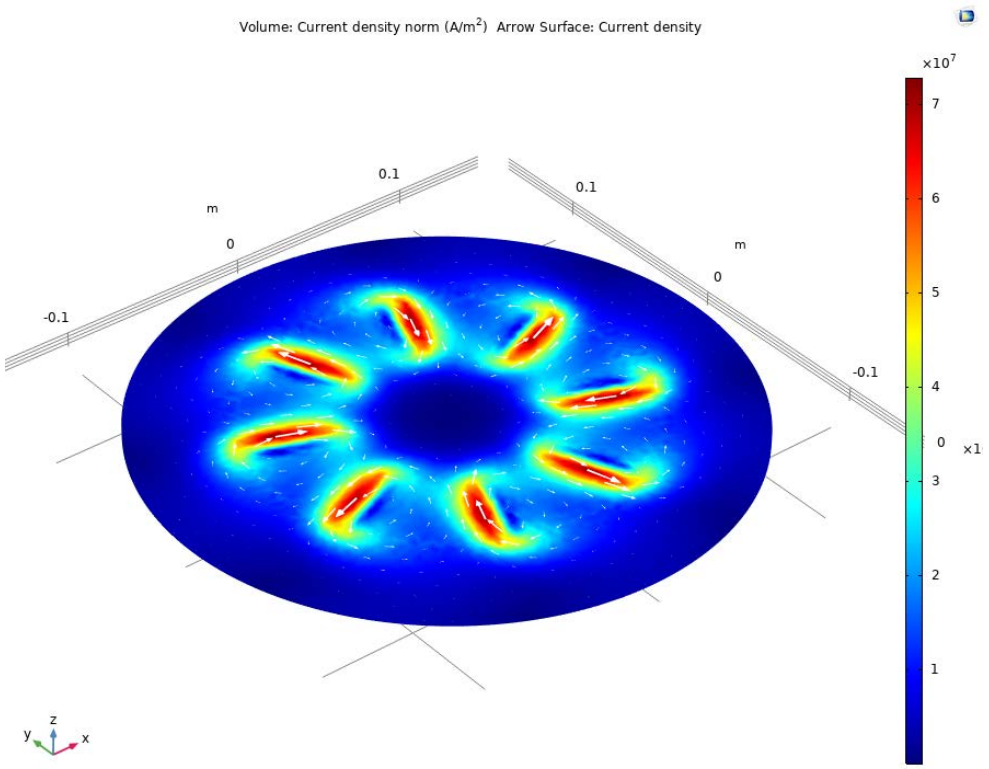

Figure 3.20: Results of current density distribution for FEM simulation on an axonometric view.

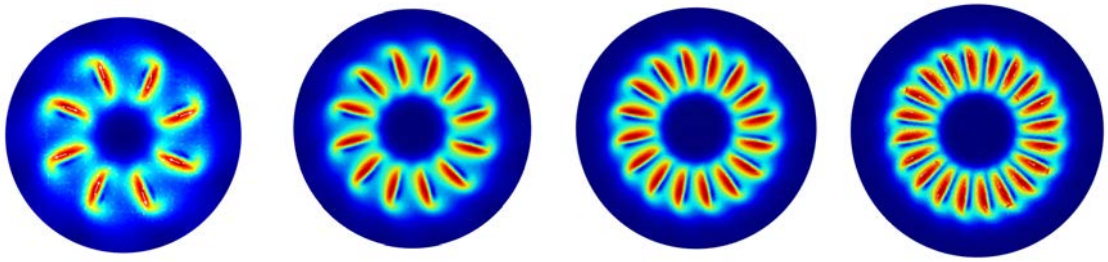

(a) p=4 (b) p=6 (c) p=8 (d) p=10

Figure 3.21: Current density distribution for different pole-pairs number - bottom.

3.7 FEM comparison

In this section we will talk about the comparison between analytical model and FEM model. In particular we will discuss about the power supplied to the disk in function of the slip speed, number of pole-pairs and α. Al the studies are done considering parameters in tables 3.1 and 3.19.

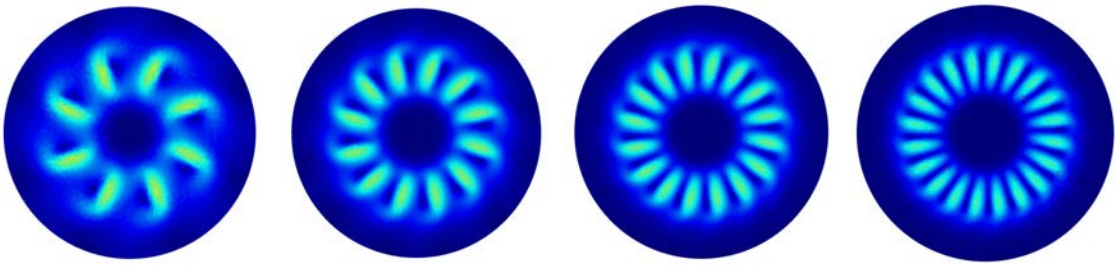

(a) p=4 (b) p=6 (c) p=8 (d) p=10

Figure 3.22: Current density distribution for different pole-pairs number - top.

- **Slip speed:** the distribution of the power in function of the slip speed is shown in figure 3.23. We can note how the analytical model well forecasts the behaviour of the power transmitted into the billet especially for low angular velocity. For higher velocity the error between the two models grows, this is due by the error of the discrete integration of the current density in the volume disk, which can be decrease arbitrarily by using lower steps, and the intrinsic error for the analytical model due by the linearisation of a rotating system. We can also note that at about 600 rpm is present a inflection point i.e. the increase of the power's derivate is positive before this point and after negative. The power for low slip speed depends by the square of the velocity while for high slip speed depends linearly. We'll investigate later because, as already said, the computational time for FEM model at slip speed bigger than 1500 rpm is huge. For this reason the comparison is limited to this slip speed.

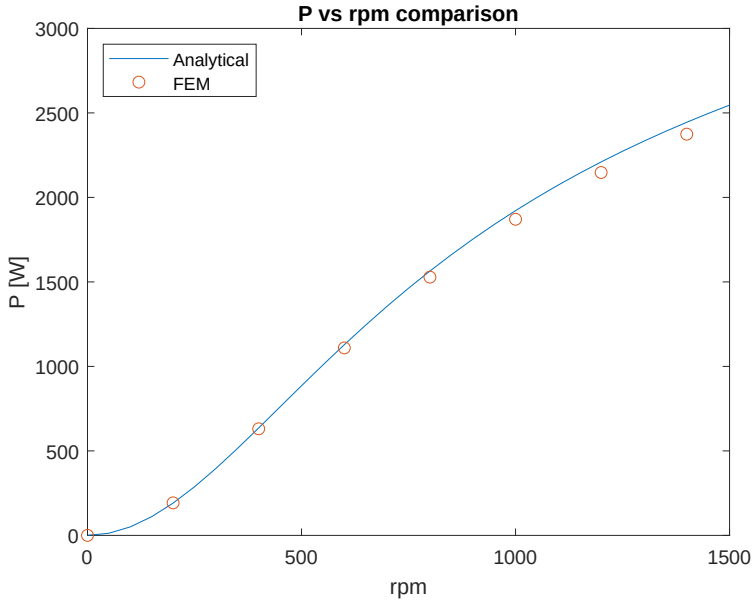

Figure 3.23: Power versus slip speed.

- **Number of pole-pairs:** the distribution of the power in function of the pole-pairs number is shown in figure 3.24. We can see how again the analytical model well fits with the FEM results. In particular the power has a maximum bot for the analytical model and for FEM at p=8. The power has a similar value also for p=7 and p=9. This peak is present because increasing the pole-pairs number increase too the magnitude of the eddy current and the number of peak zone but decrease also the thickness of the these zones. The optimal value is reach for p=8 at 1000 rpm.

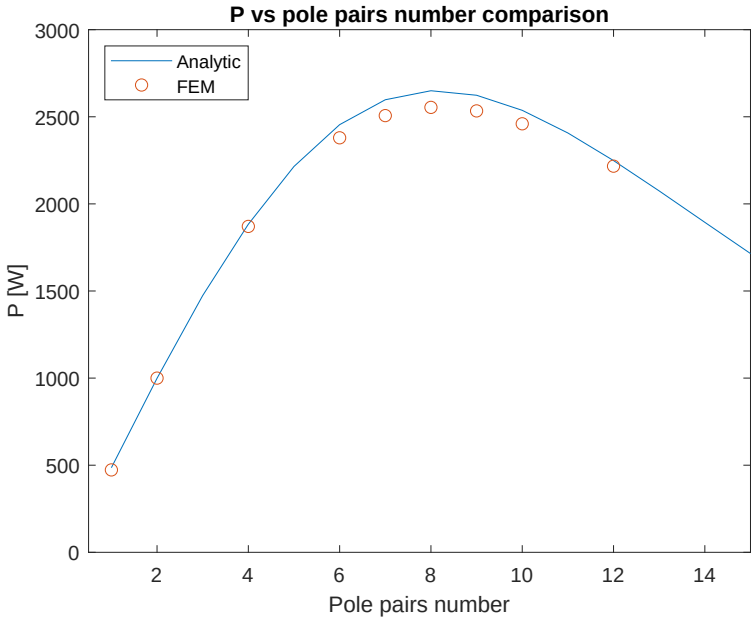

Figure 3.24: Power versus pole-pairs number at 1000 rpm.

- **Permanent magnets pole-arc to pole-pitch ratio (α):** the distribution of the power in function of the parameter α is shown in figure 3.25. We can see how the analytical model well fits with the FEM results. The growth of the power in function of α is about linear. In order to reach high values of power we have to choose α as high as possible. Ideally α can reach the unit value.

It could been interesting also to compare the eddy current density distribution in the disk but this is misleading because the linear analytical model considers the mean effect of the eddy current and locally the current density distribution could be in mismatching.

Others quantities to compare with the FEM model are the torque and the axial force. The torque, as previously seen, can be computed starting from the power losses into the metallic disk which well fits with the FEM outcomes. The axial force has instead to be compared because comes from an other formulation. Figure 3.26 shows the comparison for the two quantities in function of the slip speed. The FEM model shows that for ω=0 F_z is lower than zero while is about zero since the analytical model. In general the

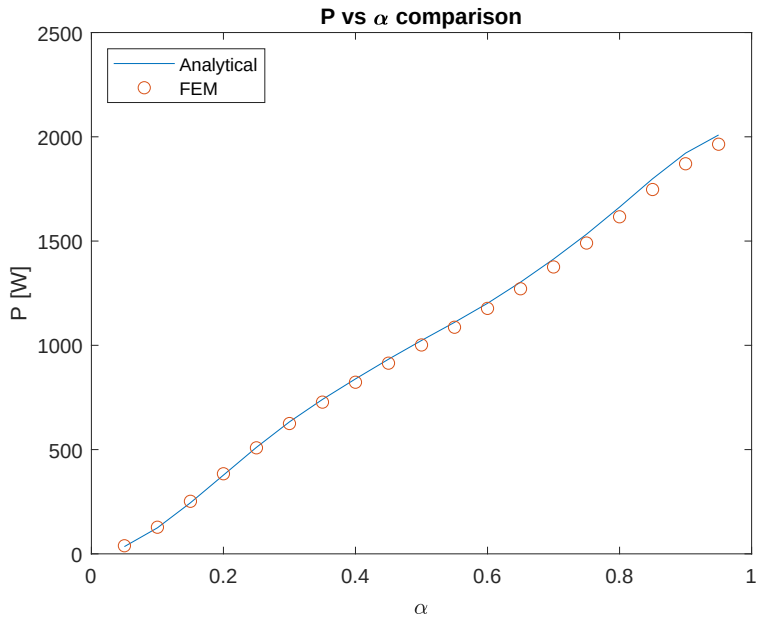

Figure 3.25: Power versus permanent magnets pole-arch to pole-pitch ratio at 1000 rpm.

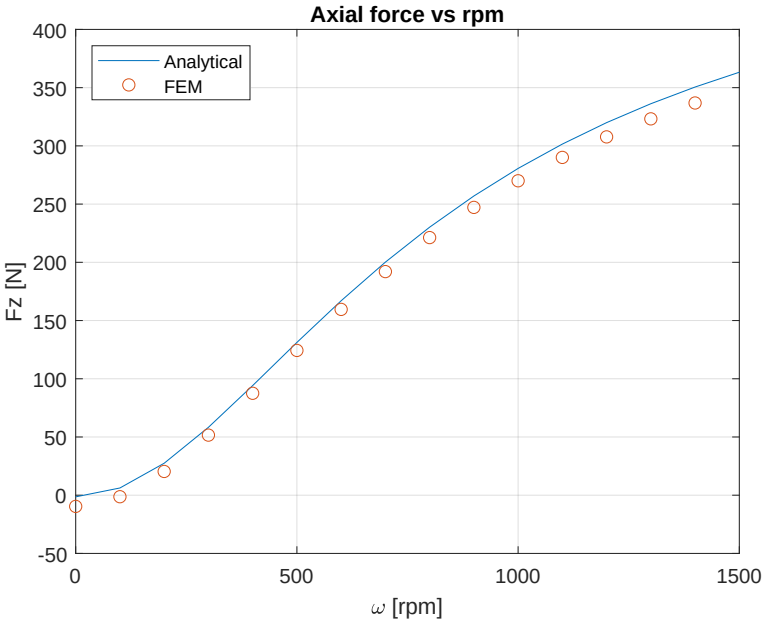

Figure 3.26: Axial force comparison in function of the slip speed.

FEM outcomes are in agree with the results of the analytical forecast especially for the behaviour of the curves with respect the numerical values. Again the FEM's outcomes

are a bit lower with respect the analytical ones.

3.8 Influence of parameters on power

The goal of heating a metal by using permanent magnets is increment as high as possible the power therefore in this section we will study the parameters which influence the power, how depends by they in order to have a efficient heating system. As we've seen in the previous section, the analytical model is in agree with the FEM results, therefore we will use the first one. As already done we will use the parameters shown in table 3.1.

The power can be controlled by the permanent magnet characteristics or by the configuration of the mechanical system type. The PMs characteristics are:

- **Permanent magnet pole-arc to pole pitch ratio (α):** this parameter as already said, affects the power about linearly therefore it has to be selected as near to 1 as possible because for the Faraday-Neumann's Law the variation of magnetic flux is maximal at α=1 while for the other values the variation is not from N to S instantaneously but soft. Figure 3.27 shows the power in function of α for different values of pole-pairs number p. We can see how the choice of p affect also the growth of the curve: for $\alpha < 0.3$ p=4 maximize the power otherwise p=8. Others geometrical parameters of the PMs are the external and internal radius R_1 and $R-2$ that have to be chosen is such a way that the magnet would by as bigger as possible i.e. $R_1 \to R_3$ and $R_2 \to 0$ in order to cover as high as possible the metal disk's area.

- **Magnetic flux density remanence (B_r) of PMs:** the remanence of the PMs affects strongly the power supplied, as shown in figure 3.28 the power depends exponentially by the remanence. Once again we have the power peak reached weakly for p = 8.

- **PMs thickness (r):** this parameter is affects the power transmission linearly as shown in figure 3.29, this time is plotted only for p=4 because is mostly linear independently by the value of p. The thickness of the magnets is a good parameter for adjust the power supplied in the planning phase, the downside is that the PMs disk will have bigger moment of inertia.

The mechanical and geometrical configuration of the system can control the power transfer to the disk. These parameters are:

- **Slip speed:** this is the main contributor to the power supplied to the disk and the movement of the magnets with respect the metal disk convert the mechanical power into the thermal power.we can see from figure 3.30 the behaviour of the power in function of the velocity. We can see how the curves have a higher angular coefficient for low rpm which decreases for higher velocity until stabilized. We can observe how low speed the optimal number of pole-pairs is 8 and for speed higher than 1750 rpm, the optimal p is 10. Probably this trend continues for p=12 an so on.

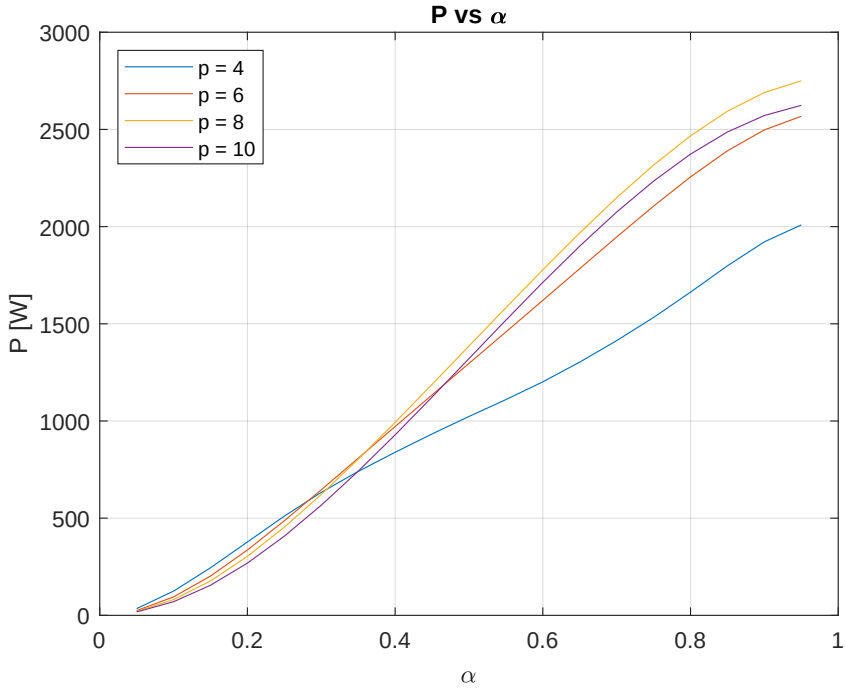

Figure 3.27: Power in function of the parameter α at 100rpm.

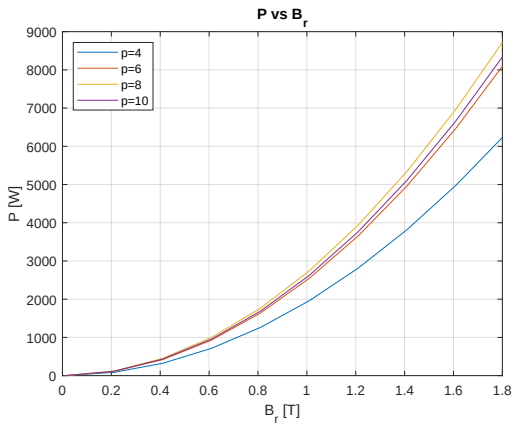

Figure 3.28: Power in function of magnet remanence.

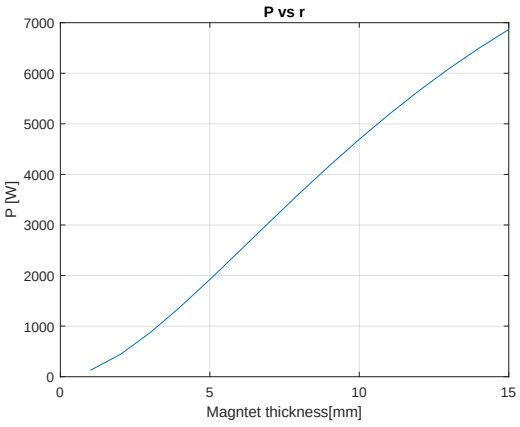

Figure 3.29: Power in function of the magnet thickness.

- **Air gap thickness (s):** the distance between permanent magnets and metal disk is a crucial parameter. In order to convert mechanical power in heat s has to be as low as possible. As shown is figure 3.31 the dependence of the power to the air gap thickness decreases exponentially. With s equal to 5 mm the total power is 2 kW while if s is equal to 2 mm we obtain an increase of power more of the 50%.

Summarizing the power can be controlled by controlling the magnetic field with α, B_r or permanent magnets thickness but the main parameter is the slip speed between

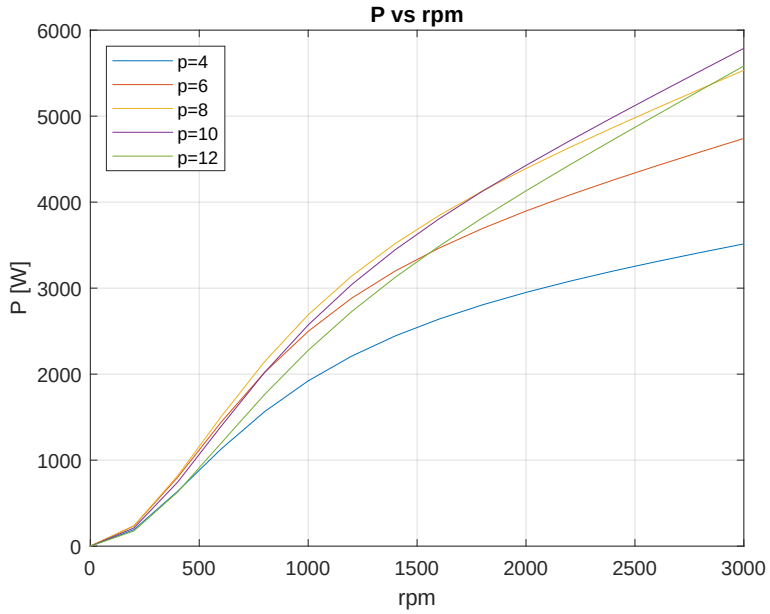

Figure 3.30: Power in function of the slip speed for different pole-pairs number.

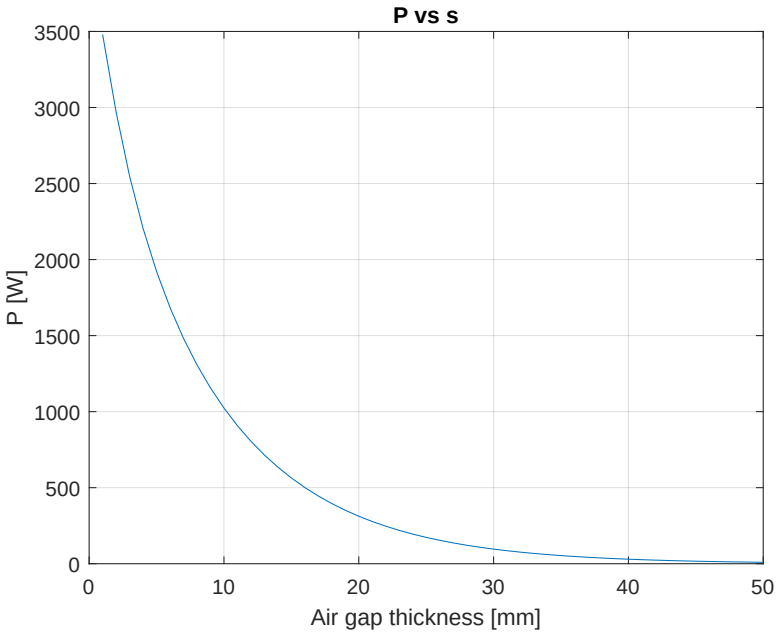

Figure 3.31: Power in function of the air gap thickness.

PMs and disk. The air gap has to be as low as possible for maximum magnetic field transmission.
We have to take into account that the metal disk is an active part to the system and the

power transmitted depends by the electrical properties of the metal i.e. the conductivity σ. In figure 3.32 is shown the power in function of the conductivity of the disk, it's easy to see how the power is low, with equal conditions, for low material conductivity: the permanent magnets works well only for good conductors. We can therefore said that in

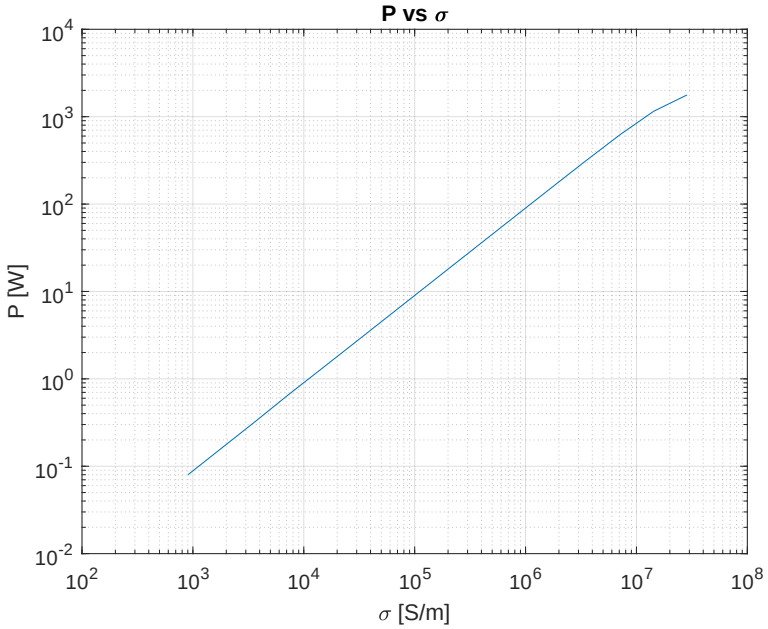

Figure 3.32: Dependence of the power by the conductivity of the metal disk.

first approximation is valid the relation:

$$\frac{\log P_{mat_1}}{\log P_{mat_2}} = \frac{\log \sigma_{mat_1}}{\log \sigma_{mat_2}} \tag{8.83}$$

where σ_{mat_1} is the conductivity of the material 1 while σ_{mat_2} of the material 2. The relation is valid also for the torque because there is proportionality between power and torque:

$$\frac{\log T_{mat_1}}{\log T_{mat_2}} = \frac{\log \sigma_{mat_1}}{\log \sigma_{mat_2}} \tag{8.84}$$

These two equation give an order of magnitude and are valid if the two materials have a big range of difference.

3.9 Magnetic materials

If we suppose the disk is made up magnetic material with relative permeability μ_r the mathematical model changes in the boundary conditions and in the term γ_{nm} defined in 3.53 becomes:

$$\gamma_{nm} = \sqrt{\left(\frac{n\pi}{D}\right)^2 + \left(\frac{m\pi}{\tau}\right)^2 + jm\sigma\mu_0\mu_r v\frac{\pi}{\tau}} \tag{9.85}$$

while the boundary conditions expressed in equations 3.59 and 3.60 remain the same while change 3.61 and 3.62 taking into account the conservation of the normal component of the magnetic flux density and the conservation of the tangential component of the magnetic field on the boundary described by equation 3.20, we obtain:

$$\begin{aligned}\frac{\partial\Phi_2(x,y,r+s)}{\partial x} &= -H_{3x}(x,y,r+s)\\ \frac{\partial\Phi_2(x,y,r+s)}{\partial y} &= -H_{3y}(x,y,r+s)\\ \frac{\partial\Phi_2(x,y,r+s)}{\partial z} &= -\mu_r H_{3z}(x,y,r+s)\end{aligned} \tag{9.86}$$

and

$$\begin{aligned}\frac{\partial\Phi_4(x,y,r+s+h)}{\partial x} &= -H_{3x}(x,y,r+s+h)\\ \frac{\partial\Phi_4(x,y,r+s+h)}{\partial y} &= -H_{3y}(x,y,r+s+h)\\ \frac{\partial\Phi_4(x,y,r+s+h)}{\partial z} &= -\mu_r H_{3z}(x,y,r+s+h)\end{aligned} \tag{9.87}$$

and the matrix $[\mathbf{A}]_{nm}$ defined in 3.64 becomes:

$$\begin{bmatrix}
1 & 1 & 0 & 0 & 0 & 0 & 0 & 0 & 0\\
e^{\alpha r} & e^{-\alpha r} & -e^{\alpha r} & -e^{-\alpha r} & 0 & 0 & 0 & 0 & 0\\
e^{\alpha r} & -e^{-\alpha r} & -e^{\alpha r} & e^{-\alpha r} & 0 & 0 & 0 & 0 & 0\\
0 & 0 & \frac{e^{\alpha z_h}}{\frac{\tau}{jm\pi}} & \frac{e^{-\alpha z_h}}{\frac{\tau}{jm\pi}} & e^{\gamma z_h} & e^{-\gamma z_h} & 0 & 0 & 0\\
0 & 0 & \frac{e^{\alpha z_h}}{\left(\frac{D}{n\pi}\right)^2} & \frac{e^{-\alpha z_h}}{\left(\frac{D}{n\pi}\right)^2} & \frac{e^{\gamma z_h}}{\frac{\tau}{jm\pi}} & \frac{e^{-\gamma z_h}}{\frac{\tau}{jm\pi\mu_r}} & \gamma e^{\gamma z_h} & -\gamma e^{-\gamma z_h} & 0\\
0 & 0 & \alpha e^{\alpha z_h} & -\alpha e^{-\alpha z_h} & 0 & 0 & \mu_r e^{\gamma z_h} & \mu_r e^{-\gamma z_h} & 0\\
0 & 0 & 0 & 0 & e^{\gamma z_t} & e^{-\gamma z_t} & 0 & 0 & \frac{e^{\alpha z_t}}{\frac{\tau}{jm\pi}}\\
0 & 0 & 0 & 0 & \frac{e^{\gamma z_t}}{\frac{\tau}{jm\pi\mu_r}} & \frac{e^{-\gamma z_t}}{\frac{\tau}{jm\pi\mu_r}} & \gamma e^{\gamma z_t} & -\gamma e^{-\gamma z_t} & \frac{e^{\alpha z_t}}{\left(\frac{D}{n\pi}\right)^2}\\
0 & 0 & 0 & 0 & 0 & 0 & \mu_r e^{\gamma z_t} & \mu_r e^{-\gamma z_t} & \alpha e^{\alpha z_t}
\end{bmatrix}_{nm} \tag{9.88}$$

the quantities α and γ replace, for a lighter notation, α_{nm} and γ_{nm} respectively. A magnetic material like iron influences the magnetic flux density inside the disk, in particular the magnetic field inside the body load is stronger and the eddy currents grown and the transmitted power is higher. The higher is the permeability the lower is the depth of penetration, this means that for high magnetic materials the current is superficial and the power decrease.
Figure 3.33 shows the behaviour of the power losses into a iron disk ($\sigma = 10\ MS/m$) supposing we can change the permeability μ_r. The parameters of the geometry are always the same, shown in table 3.1 but for 8 pole-pair numbers.
The outcomes of the analytical model are then compared with the FEM results just until the permeability $\mu_r = 10$ cause the grown of computational time with μ_r. We have

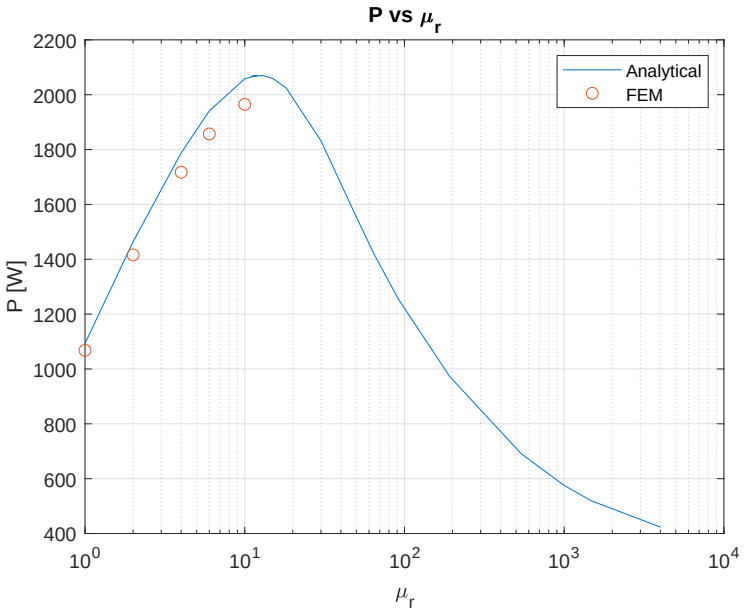

Figure 3.33: Power in function of the relative permeability of the disk (1000 rpm, $\sigma = 10\ MS/m$, p=8).

to remember that the analytical model doesn't take into account the losses due by hysteresis in ferromagnetic materials but anyway we can say that for magnetic materials the eddy currents losses have a bigger contribute to the power the non magnetic material. We observe the power peak at $\mu_r = 12$ and the power is double than at $\mu_r = 1$, above the peak the power decreases drastically. The real iron permeability is certainly higher than 1000, therefore we can say that heating magnetic materials with permanent magnets is not effective. Moreover magnetic loads generate an attractive force for low rotation speed and a repulsive one for higher speed, there is therefore a particular rpm value where the axial force is zero.

3.10 Considerations

Contrary to what has been done for the pancake inductor analytical model, in the case of permanent magnet analytical model, the power transferred to the load is computer by integrating the current density inside the volume of the metallic disk. This heating system well works for good no magnetic conductors and soft magnetic however the materials to heat have generally high permittivity therefore we can say that this process in ineffective.
The analytical model outcomes are in a very good agreement with the FEM ones, because of the high computational time for high speed rotation and high permeability, a comparison couldn't be done. Since the rotational system hap been mapped into a linear translation, the limits of the model are correlated to this transformation, in particular the model forecast are precise until che $R_2 - R_1 < 50\% R_2$.

Chapter 4

Maxwell stress tensor

In this chapter we will compare the pancake induction heating and heating by permanent magnets, in particular we will discuss about the limitations of these two systems. In fact the main problem of the PMs heating is the axial force and the torque which affect the workpiece. The main question is: if both the two heating systems produce a time dependent magnetic field inside the load, why only the PMs heating system generates a torque and an axial force. In order to answer at this question we start with the concept of momentum of an electromagnetic field.

4.1 Momentum of an electromagnetic field

Let us consider figure 4.1, two charges q_1 and q_2 both positive, are moving along the two axes with velocity $\mathbf{v}_1$ and $\mathbf{v}_2$. The charge q_1 is in motion with respect q_2 with veloc-

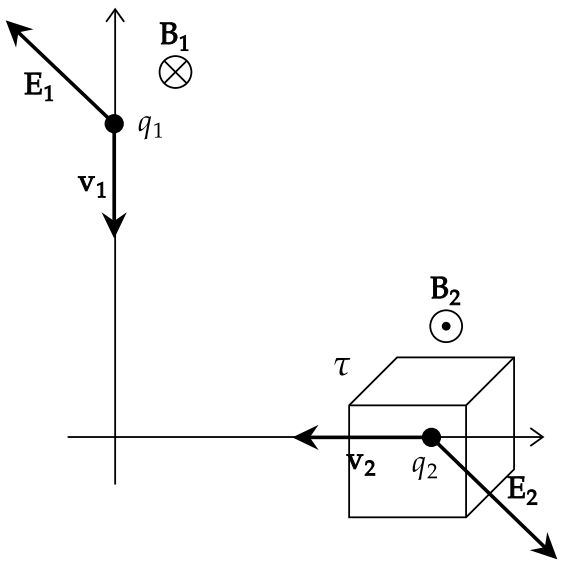

Figure 4.1: Electromagnetic interaction of two charges.

ity $\mathbf{v} = \mathbf{v}_1 - \mathbf{v}_2$ generates a magnetic flux density $\mathbf{B}_2$ in q_2 and a non-coulombian electric field as well. Both the charges are affected by a Lorentz's force which is the variation of momentum. If we consider only the system of q_2 we observe a variation of momentum $\mathbf{p}$ for a mechanical isolated system. Put like that, it would seem that an isolated system violates the conservation of momentum. In reality, we must also consider the contribution of the electromagnetic field: it carries momentum.
In order to understand the momentum of the electromagnetic field always considering figure 4.1, let us take the infinitesimal volume τ and let calculate the force on the particle q_2:

$$\mathbf{F} = \int (\mathbf{E} + \mathbf{v} \times \mathbf{B}) dq_2 \tag{1.1}$$

we can extend the concept to a local distribution of charge density ρ and remembering that $\mathbf{J} = \rho\mathbf{v}$ equation 1.1 becomes:

$$\mathbf{F} = \int_\tau (\mathbf{E} + \mathbf{v} \times \mathbf{B}) \rho d\tau = \int_\tau (\rho\mathbf{E} + \mathbf{J} \times \mathbf{B}) \rho d\tau \tag{1.2}$$

Now, remembering the Maxwell's equations:

$$\begin{aligned} \nabla \cdot \mathbf{D} &= \rho \\ \mathbf{J} &= \nabla \times \mathbf{H} - \tfrac{\partial \mathbf{D}}{\partial t} \end{aligned} \tag{1.3}$$

we obtain:

$$\mathbf{F} = \int_\tau \left[\mathbf{E}(\nabla \cdot \mathbf{D}) - \mathbf{B} \times (\nabla \times \mathbf{H}) - \frac{\partial \mathbf{D}}{\partial t} \times \mathbf{B} \right] d\tau \tag{1.4}$$

expressing:

$$\begin{aligned} \frac{\partial}{\partial t}(\mathbf{D} \times \mathbf{B}) = \frac{\partial \mathbf{D}}{\partial t} \times \mathbf{B} + \mathbf{D} \times \frac{\partial \mathbf{B}}{\partial t} \Rightarrow \frac{\partial \mathbf{D}}{\partial t} \times \mathbf{B} = \\ = \frac{\partial}{\partial t}(\mathbf{D} \times \mathbf{B}) - \mathbf{D} \times \frac{\partial \mathbf{B}}{\partial t} \\ = \frac{\partial}{\partial t}(\mathbf{D} \times \mathbf{B}) + \mathbf{D} \times (\nabla \times \mathbf{H}) \end{aligned} \tag{1.5}$$

therefore equation 1.4 becomes:

$$\mathbf{F} = -\int_\tau \frac{\partial}{\partial t}(\mathbf{D} \times \mathbf{B}) d\tau + \int_\tau \left[\mathbf{E}(\nabla \cdot \mathbf{D}) - \mathbf{D} \times (\nabla \times \mathbf{E}) - \mathbf{B} \times (\nabla \times \mathbf{H}) \right] d\tau \tag{1.6}$$

now we can insert in the expression 1.6 the term $\mathbf{H}(\nabla \cdot \mathbf{B})$ which is identically null in order to obtain a symmetrical expression for the electric and magnetic fields:

$$\mathbf{F} + \int_\tau \frac{\partial}{\partial t}(\mathbf{D} \times \mathbf{B}) d\tau = \int_\tau \left[\mathbf{E}(\nabla \cdot \mathbf{D}) - \mathbf{D} \times (\nabla \times \mathbf{E}) + \mathbf{H}(\nabla \cdot \mathbf{B}) - \mathbf{B} \times (\nabla \times \mathbf{H}) \right] d\tau \tag{1.7}$$

the force $\mathbf{F}$ is the variation of mechanical momentum $\mathbf{p}$ i.e. $\mathbf{F} = \frac{d\mathbf{p}}{dt}$ and $\int_\tau (\mathbf{D} \times \mathbf{B}) d\tau$ has the size of momentum. We can therefore define the *momentum volume density of the electromagnetic field*:

$$\mathbf{g} = \mathbf{D} \times \mathbf{B} \tag{1.8}$$

The quantity $\mathbf{E}(\nabla\cdot\mathbf{D})-\mathbf{D}\times(\nabla\times\mathbf{E})+\mathbf{H}(\nabla\cdot\mathbf{B})-\mathbf{B}\times(\nabla\times\mathbf{H})$ can be expressed as a 3×3 tensor $\tilde{\mathbf{T}}$ whose components after a few algebraic steps are:

$$T_{ij}=\epsilon_0\left\{E_iE_j+c^2B_iB_j-\frac{1}{2}\delta_{ij}(E^2+c^2B^2)\right\} \tag{1.9}$$

where c is the speed of light and δ_{ij} is the Kronecker delta. If we define $\mathbf{G}=\int_\tau \mathbf{g}d\tau$, the force expression becomes:

$$\mathbf{F}=\frac{\partial}{\partial t}(\mathbf{p}+\mathbf{G})=\int_{\partial\tau}\tilde{\mathbf{T}}\cdot dS \tag{1.10}$$

If the material doesn't absorb momentum i.e. we are in void, the tensor $\tilde{\mathbf{T}}$ is null therefore if we consider the total tridimensional space where are limited all the fields, the integral over the border on τ is equal to zero i.e.:

$$\frac{\partial}{\partial t}(\mathbf{p}+\mathbf{G})=0\rightarrow\mathbf{p}+\mathbf{G}=\text{constant} \tag{1.11}$$

We have obtained the momentum conservation for body and electromagnetic fields.

4.1.1 Conservation of angular momentum

If the electromagnetic field carries momentum, what we expect is that carries the angular momentum as well. We can then define, by analogy with the momentum volume density, the *angular momentum volume density* $\mathbf{l}$:

$$\mathbf{l}=\mathbf{r}\times\mathbf{g}=\mathbf{r}\times(\mathbf{D}\times\mathbf{B}) \tag{1.12}$$

since equation 1.12 we can define the transferred angular momentum to a material volume τ as:

$$\mathbf{L}=\int_\tau \mathbf{l}d\tau \tag{1.13}$$

If magnetic fields are presents and if $\mathbf{D}\times\mathbf{B}\neq 0$ then there will be present an angular momentum associated at the electromagnetic field. Since equation 1.13 we can obtain the torque $\mathbf{M}$:

$$\mathbf{M}=\frac{d\mathbf{L}}{dt} \tag{1.14}$$

4.2 Pancake inductors angular momentum

As already told in the chapter 2 the magnetic flux density $\mathbf{B}$ produced by the pancake inductor due the symmetry of the system has only radial and axial component. Since the same symmetry the electric displacement field $\mathbf{D}$ has only tangential component, $\mathbf{D}$ and $\mathbf{B}$ are shown in figures 4.3 and 4.4 for a z-ρ section by using a FEM simulation.
If we consider a generic point inside the metal workpiece identified with the position vector $\mathbf{r}$ with respect the point O in the middle of the disk as shown in figure 4.2. The

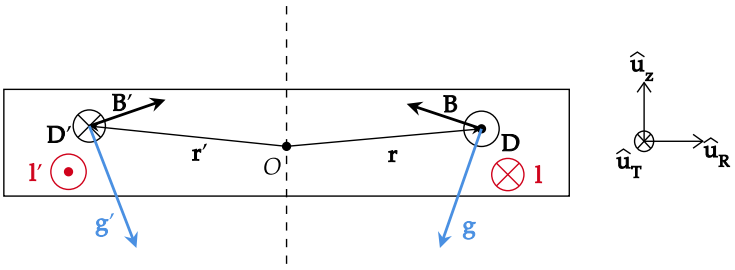

Figure 4.2: Angular momentum volume density in the workpiece.

momentum volume density **g** becomes:

$$\mathbf{g} = \begin{pmatrix} 0 \\ D_T \\ 0 \end{pmatrix} \times \begin{pmatrix} B_R \\ 0 \\ B_z \end{pmatrix} = \begin{pmatrix} D_T B_z \\ 0 \\ -D_T B_R \end{pmatrix} \tag{2.15}$$

now by using equation 1.12 we can calculate the angular momentum volume density **l**, taking into account that **r** has radial and axial component, we obtain:

$$\mathbf{l} = \mathbf{r} \times \mathbf{g} = \begin{pmatrix} r_R \\ 0 \\ r_z \end{pmatrix} \times \begin{pmatrix} D_T B_z \\ 0 \\ -D_T B_R \end{pmatrix} = \begin{pmatrix} 0 \\ r_R D_T B_R + r_z D_R B_T \\ 0 \end{pmatrix} \tag{2.16}$$

we found that in this particular configuration **l** has only tangential component. In the same way we can calculate **l**′ for the symmetrical point described by the position vector **r**′ such that:

$$\mathbf{r} = \begin{pmatrix} x \\ y \\ z \end{pmatrix} \Rightarrow \mathbf{r}' = \begin{pmatrix} -x \\ -y \\ z \end{pmatrix} \tag{2.17}$$

then, as also shown graphically:

$$\mathbf{l}' = -\mathbf{l} \tag{2.18}$$

Now we proceed to calculate the angular momentum **L** for the electromagnetic field as the integral over all the volume of the workpiece by using the equation 1.13. The angular momentum d**L** for a infinitesimal volume dτ centred in the point described by **r** is:

$$d\mathbf{L} = \mathbf{l} d\tau \tag{2.19}$$

similarly the angular momentum d**L'** for a infinitesimal volume dτ' centred in the point described by **r'** is:

$$d\mathbf{L'} = \mathbf{l'} d\tau' = -\mathbf{l} d\tau \tag{2.20}$$

the infinitesimal volumes for uniformity are the same dτ=dτ'. If we calculate the integral over the metallic disk with cylindrical coordinates (ρ,θ,z) and we split it in two sides we obtain:

$$\mathbf{L} = \int_\tau \mathbf{l} d\tau = \int_0^\pi \rho d\theta \int_0^R d\rho \int_{-h/2}^{h/2} dz \mathbf{l} + \int_\pi^{2\pi} \rho d\theta \int_0^R d\rho \int_{-h/2}^{h/2} dz \mathbf{l'} = 0 \tag{2.21}$$

where R is the radius of metal disk and h is its thickness. The two integral are opposite therefore their sum is zero. If the angular momentum is constantly zero, also the total torque on the workpiece is zero. This condition of null torque is given thanks the cylindrical symmetry the system presents which affects the disposition of **B** and **D**.

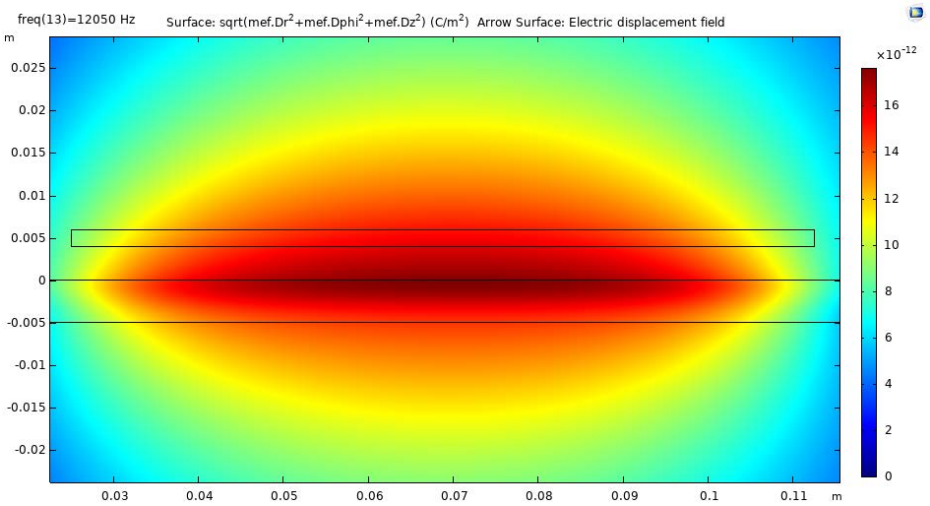

Figure 4.3: Electric displacement value for pancake inductor system (only azimuthal component).

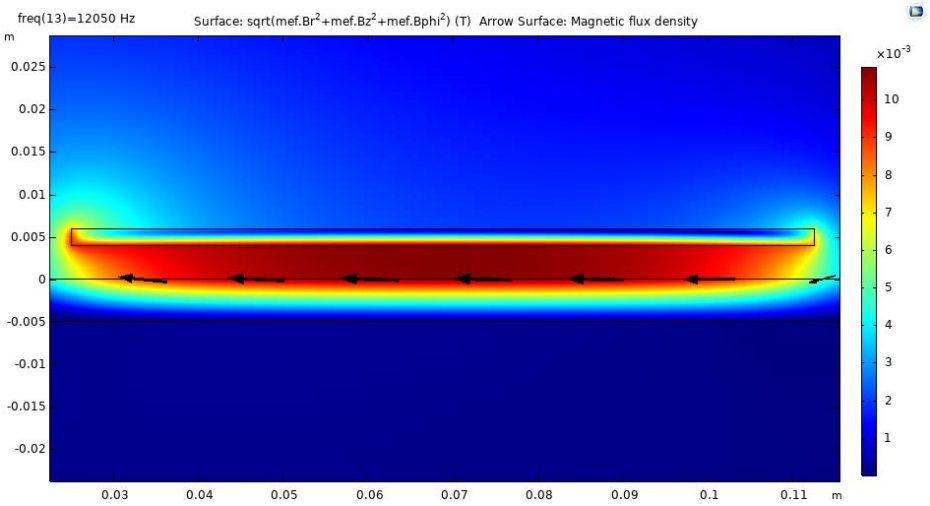

Figure 4.4: Magnetic flux density value for pancake inductor system (no azimuthal component).

4.3 PMs angular momentum

Similarly to the pancake calculation, let us consider a generic point described by a position vector **r** as shown in figure 4.5. Let's take a second point described by the vector

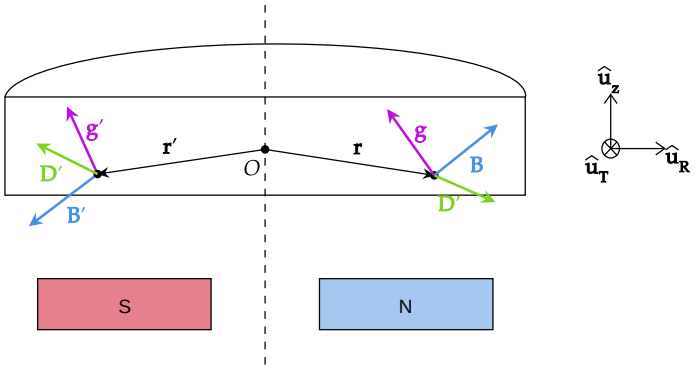

Figure 4.5: **B** and **D** in two magnetic-symmetrical points inside the metal disk for PMs heating system.

position **r'** shifted of one pole-pole pitch along the azimuthal angle i.e. in cylindrical coordinates:

$$\mathbf{r} = \begin{pmatrix} \rho \\ \theta \\ z \end{pmatrix} \Rightarrow \mathbf{r'} = \begin{pmatrix} \rho \\ \theta + \frac{\pi}{p} \\ z \end{pmatrix} \tag{3.22}$$

Both the magnetic flux density **B** and the electric displacement **D** in the point **r** into the metallic disk are, in general, oriented in all the three directions (see figure 4.7 and 4.8) i.e. have radial, tangential and axial component:

$$\mathbf{B}(\mathbf{r}) = \begin{pmatrix} B_R \\ B_T \\ B_z \end{pmatrix} \quad \text{and} \quad \mathbf{D}(\mathbf{r}) = \begin{pmatrix} D_R \\ D_T \\ D_z \end{pmatrix} \tag{3.23}$$

in the point **r'** the two vectors are, since the symmetry of the system:

$$\mathbf{B'}(\mathbf{r'}) = \begin{pmatrix} -B_R \\ -B_T \\ -B_z \end{pmatrix} \quad \text{and} \quad \mathbf{D'}(\mathbf{r'}) = \begin{pmatrix} -D_R \\ -D_T \\ -D_z \end{pmatrix} \tag{3.24}$$

the vector **g** in **r** is:

$$\mathbf{g}(\mathbf{r}) = \begin{pmatrix} g_R \\ g_T \\ g_z \end{pmatrix} = \begin{pmatrix} D_R \\ D_T \\ D_z \end{pmatrix} \times \begin{pmatrix} B_R \\ B_T \\ B_z \end{pmatrix} = \begin{pmatrix} D_T B_z - D_z B_T \\ D_z B_R - D_R B_z \\ D_R B_T - D_T B_R \end{pmatrix} \tag{3.25}$$

while the vector the vector **g'** in **r'** is:

$$\mathbf{g'}(\mathbf{r'}) = \begin{pmatrix} g'_R \\ g'_T \\ g'_z \end{pmatrix} = -\begin{pmatrix} D_R \\ D_T \\ D_z \end{pmatrix} \times -\begin{pmatrix} B_R \\ B_T \\ B_z \end{pmatrix} = \begin{pmatrix} D_z B_T - D_T B_z \\ D_R B_z - D_z B_R \\ D_R B_T - D_T B_R \end{pmatrix} = \mathbf{g}(\mathbf{r}) \tag{3.26}$$

We demonstrated that the vector **g'** in **r'** has the same value of **g** in **r** considering the radial, tangential and axial component. If we calculate draw **g** in all the point with azimuthal pitch equal to π/p starting a generic point described bt **r** we obtain the graphic in figure 4.6. the angular momentum volume density **l** in **r** will have the same compo-

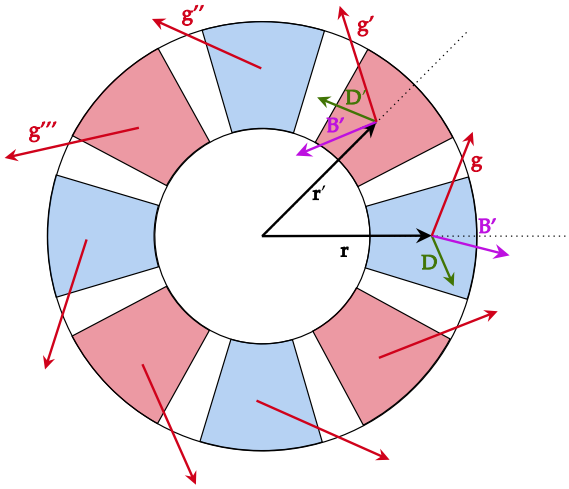

Figure 4.6: **B**, **D** and **g** in PMs disk in axonometric view.

nents in **r'**, **r"** and so on:

$$\mathbf{l}(\mathbf{r}) = \mathbf{r}\times\mathbf{g} = \mathbf{r'}\times\mathbf{g'} = \ldots = \mathbf{r}^{(2p)}\times\mathbf{g}^{(2p)} = \begin{pmatrix} l_R \\ l_T \\ l_z \end{pmatrix} \tag{3.27}$$

when we calculate the contribution of d**L** for all the $2p$ points in cartesian coordinates we obtain taking into account that, always for symmetries, the infinitesimal volume is equal for all the points:

$$\begin{pmatrix} dL_x \\ dL_y \\ dL_z \end{pmatrix} = \begin{pmatrix} l_x + l'_x + \ldots + l_x^{(2p)} d\tau \\ l_y + l'_y + \ldots + l_y^{(2p)} d\tau \\ l_z + l'_z + \ldots + l_z^{(2p)} d\tau \end{pmatrix} = \begin{pmatrix} 0 \\ 0 \\ 2p l_z d\tau \end{pmatrix} \tag{3.28}$$

the only contributor to the angular momentum is therefore along z-direction. And this is given by the geometrical symmetry of the system, which manifests itself in the fields. Take a point P in the disk, the magnetic and electric fields in P are alternating with respect the time. For example for the magnetic flux density is valid the relation:

$$\int_T \mathbf{B}(P,t)dt = 0 \quad \text{with} \quad T = \frac{2\pi}{\omega p} \tag{3.29}$$

always for symmetry also the electric displacement field is still alternating therefore:

$$\int_T \mathbf{D}(P,t)dt = 0 \quad \text{with} \quad T = \frac{2\pi}{\omega p} \tag{3.30}$$

The momentum volume density **g** and therefore **L** don't follow the same alternating law, in fact they are directed always in the same direction therefore the average value is different than zero:

$$\frac{2}{T}\int_{T/2}\mathbf{L}(t)dt \neq 0 \tag{3.31}$$

The period of **L**(t) is one half on the period of **B**(t) and **D**(t) cause the **L** varies from 0 to its maximal value. The torque present on the system is calculable since the equation 1.14 and, like **L**, has only the axial component as we expected.
In conclusion the difference between pancake and PMs which manifests presence of torque in the last mentioned system, lies in the symmetry of the geometry which leads the disposition of the field. In particular the *braking of the azimuthal symmetry* for system generates the axial torque. For example if the magnets wouldn't placed with equispaced angles an other symmetry would be broken and an other component on the torque would be generated. The same considerations can be done to explain the presence of the axial force in the case of permanent magnet induction heating.

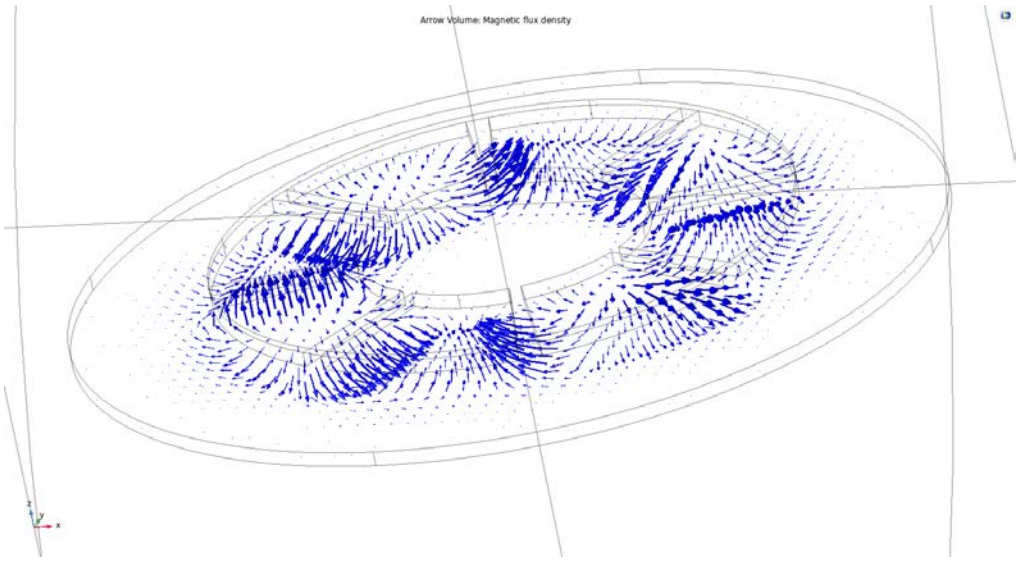

Figure 4.7: Magnetic flux density **B** inside the metallic disk.

Figure 4.8: Electric displacement field **D** inside the metallic disk.

Chapter 5

Applications

Practical applications of heating by using permanent magnets can be widely used in the industry for heat no-magnetic billets with an important primary energy saving with respect heating by frames or the classical induction heating.
The most critical point is the electromagnetic torque and the axial force applied to the billet, generated by the relative motion of the permanent magnets with respect the workpiece which therefore needs an attachment system for the billet. The need to operate with an attachment system limits considerably the possible applications, in particular the domestic ones. In fact the system as presented can't be use as hobs because the pot will start to rotate around itself and move upward making cooking impossible but above all, dangerous for the people. An other drawback is the presence on the hob of strong magnetic fields generated by the PMs which also exist with the system off and can interact with external devices.
A possible domestic application which can find diffusion in the eastern countries is a cooking plate heated by permanent magnets. This solution can be achivable because the plate is fixed to the cooking system structure therefore cooking is safe as long as you use non-metallic tools.

In the next sections are presented some possible solutions to avoid the electromagnetic torque applied to the workpiece but, as already mentioned, not the axial force.

Before of all we will show the actual technology to make possible the permanent magnets induction heating in particular the mechanism of rotation and the PMs, in order to have an order of magnitude of the parameters in the system.

5.1 Components of PMs induction heating

We've seen in the previous chapter how many parameters are presents in the PMs induction heating system and the influence of them on the power transfer. The goal obviously is to transmit power as high as possible and is necessary to have an order of magnitude of the achivable parameters in particular remanence of the magnets, velocity and torque of the motor.

- **Motors:** the electric motor is the device which convert the electrical power into mechanical one and is the only component which contributes at the heating. As

we have seen the power is proportional to the slip speed and therefore have to be as high as possible. The motors can be divided in two groups: AC motors and DC motors.
AC motors are characterized by efficiency from 85% for 1 kW of power to 96% for big high efficiency motors (P>100 kW) but depends also by torque and velocity i.e. the working conditions. Synchronous and asynchronous motors can be controlled in velocity but also in torque with an inverter which have efficiency from 88% for low power to 96% for output power grater than 40 kW[23]. Figure 5.1 shows the efficiency maps of synchronous and asynchronous motors. We can see that these

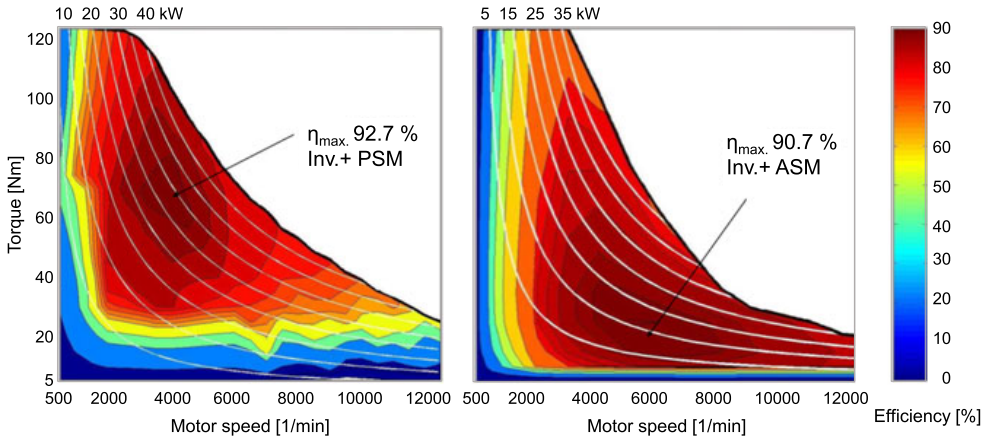

Figure 5.1: Typical efficiency maps of synchronous (PSM) and asynchronous motor(ASM)[24].

motors can reach 12000 rpm and the efficiency (inverter + motor) depends by the working point but is high for a big range of speed/torque points. AC motors have a simple design and a low relative low cost but need a speed controller (inverter) and are work bad for low speed.
DC motors present a simply design, have an easy torque and high speed control, in fact it's necessary to varying the voltage sent to the motor. Are characterized in general by slightly lower efficiency with respect AC motors. The speed for DC motors varies from 1000 to 5000 rpm.
An other type of motor is the *Electronically Commuted* (EC) characterized with permanent magnets on the rotor and use electronics to control the voltage and current applied to the motor. They have by a slightly higher efficiency with respect the others but the cost increases[25].

- **Permanent magnets (PMs):** are typically described by proprieties as remanence (B_r) and coercivity (H_c).
Remanence is the residual magnetization that remains when no magnetic field is applied to a magnetic material that was previously magnetized to saturation. It is often used interchangeably with the term remanent magnetization, or the residual magnetization when no magnetic field is applied, whether or not the material was

previously magnetized to saturation. Remanence is directly related to the amount of magnetic flux that can be generated with a permanent magnet.
Coercivity is the magnetic field required to reduce the magnetization of a material that is magnetized to saturation down to zero. It is a measure of the ability of a magnetic material to resist demagnetization, i.e., the permanency of a materials magnetization. The term coercivity is often used interchangeably with coercive field, the term for any magnetic field that reduces magnetization to zero whether or not the material was previously magnetized to saturation.Magnetic materials are classified as hard or soft based on coercivity. Hard magnetic materials such as permanent magnets have high coercivity, while soft magnetic materials such as electrical steel have low coercivity. Coercivity is a structure-sensitive extrinsic magnetic property, affected by temperature, crystal anisotropy, stress-state, and microstructural impurities[26].
For soft magnetic the saturation of magnetization (J_s) substitutes the remanence. These three parameters are shown in figure 5.2 for different magnet type. An

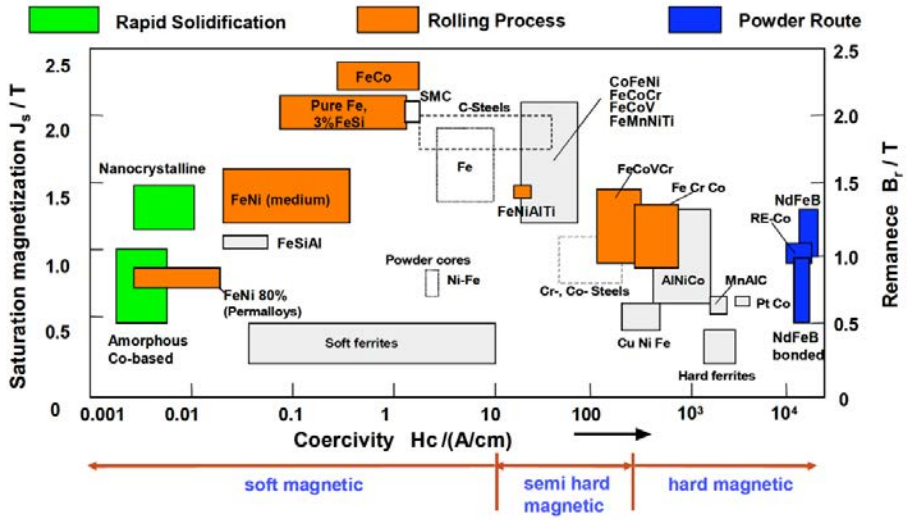

Figure 5.2: Coercivity, saturation magnetization, and remanence of various magnetic materials[27].

other important parameter is the working temperature and the Curie temperature T_c which are respectively the temperature range where the magnet maintains its proprieties and the maximal temperature where above T_c the magnet becomes paramagnetic.
There are many PMs some of the most important are AlNiCo which present high temperature stability and high remanence which make it widely used in measuring instruments. AlNiCo is characterized by high Curie temperature ($\backsim$800 °C) with working temperature up to 550 °C.
The ferrite can be used for high temperature up to 300 °C, is the most economical and presents high corrosion resistance but it has low mechanical strength and low remanence.

NdFeB is a rare-earth element characterized by remanence up to 1.5 T which make it the most powerful magnet on the market. Is has Curie temperature of 350 °C with working temperature up to 230 °C. Are characterized by very low corrosion resistance therefore is applied on the surface a protective layer. There are neodymium magnets of different degrees: the degree is a code that always starts with the letter N (abbreviation of Neodymium) and is followed by two digits (e.g. N27, N30, N33, N35, N38, N40, N42, N45, N48, N50). The higher numbers have higher energy and currently are commercialized until the degree N52 which guarantees B_r of 1.43-1.45 T. Figure 5.3 shows a commercial N52 arc segment strong permanent NdFeB neodymium magnet with axial magnetization, the magnets shape studied in the analytical model.

Figure 5.3: N52 Arc Segment Strong Permanent NdFeB Neodymium Magnet with axial magnetization (Guangzhou Zixiong Import and Export Co.).

5.2 Coaxial PMs disks

A possible solution to avoid the issue of the electromagnetic torque on the workpiece is to develop a system with two independent coaxial PMs disks rotating in opposite ways. The idea is to identify a configuration of velocities which cancel the total electromagnetic torque allowing to maintain the metal disk motionless.
Figure 5.4 shows the configuration of the system. The internal PMs disk rotates with angular velocity ω_1 while the external circular crown rotates with ω_2 in the opposite way. The PMs of the internal disk have a sector of circular crown shape with internal radius R_1 and external one R_2 and angle length $\alpha\pi/p$. In the same way the external PMs have internal radius R_3 and the external one R_4 and in the picture the magnets have the same angle length. For example purpose only the internal and the external PMs disks have the same pole-pairs number p which is 4 but obviously this is a grade of freedom for the design of a possible optimized system.
The theoretical ratio between the two velocities, in order to avoid the total torque, is basically given by the ratio between the two mean radius in order to have the same

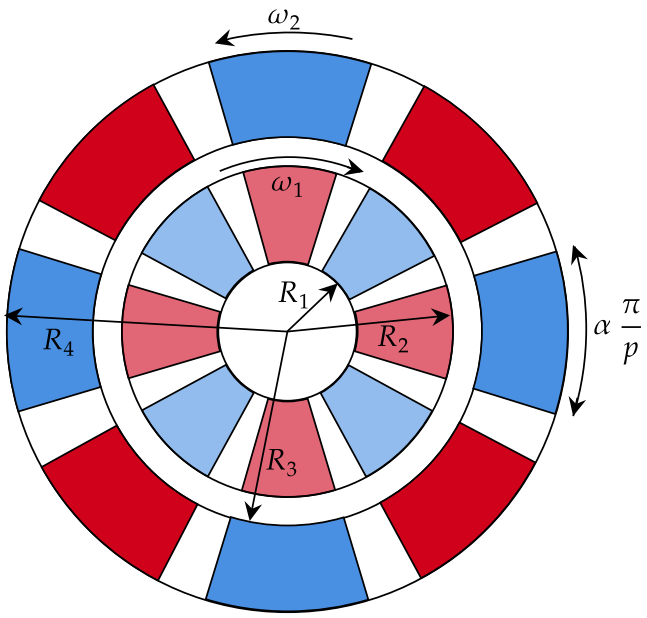

Figure 5.4: Coaxial PMs disk system geometrical configuration.

peripheral speed which satisfy the conservation of angular momentum law:

$$\left.\frac{\omega_1}{\omega_2}\right|_{T_e=0} = \frac{R_{m2}}{R_{m1}} = \frac{R_3 + R_4}{R_1 + R_2} \tag{2.1}$$

where ω_1 is obviously grater than ω_2. It's interesting to note that this assumption is independent by the characteristic of the load (metallic disk) depends only by the geometrical parameters of the configurations which are the internal and external radius.
A FEM simulation about this configuration has been made and compared with the analytical model. The FEM model was developed for the system with parameters shown in table 5.1 while figure 5.5 shows the geometrical configuration of the analysed system. The angular velocity of the two disks is not reported in the table because has been changed in order to achieve the condition of null torque which has be reached in the FEM model by attempts with an error of $10^{-}3\ Nm$. Setting the internal angular velocity ω_1 equal to 2500 rpm the condition of null torque has been reached with ω_2 equal to 748 rpm. Figure 5.6 shows the current density distribution in the metal disk, it's easy to note that the main contributor to the heating is the internal disk, we can therefore say that the external disk performs the torque cancellation function. In fact setting $\omega_1 = 0$ and $\omega_2 = 748$ rpm the system generates 616.55 W while, in opposite conditions $\omega_1 = 2500$ rpm and $\omega_2 = 0$ the power is 1733 W while for both rotating disks 2119.5 W. The last value is not the sum of the two powers because for is not valid the superposition principle. In order to optimize the system we suggest to make the external PMs as thin as possible and to obtain $\omega_1 \backsim \omega_2$.

Even if the analytical model considers only one rotating PMs disk, we can approach to the problem by using the superposition principle i.e. calculate the eddy current

Symbol	Description	Value
R_1	Internal radius of the inner magnets	20 mm
R_2	External radius of the inner magnets	65 mm
R_3	Internal radius of the outer magnets	70 mm
R_4	External radius of the outer magnets	90 mm
R_d	Radius of the conductive disk	100 mm
r	Magnet thickness	5 mm
s	Air-gap length	5 mm
h	Conductive plate thickness	3 mm
α	PMs pole-arch to pole-pitch ratio	0.9
p	Pole-pairs number	8
B_r	Remanence of PMs	1 T
σ	Conductivity of the metal (Cu)	57 MS/m
y	Yoke thickness	2 mm
μ_{ry}	Yoke relative permeability	4000

Table 5.1: Parameters of the case of study for coaxial PMs disks.

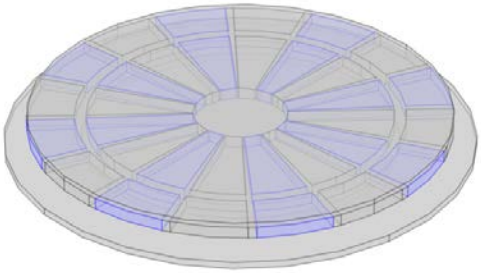

Figure 5.5: Geometry of the FEM for coaxial permanent magnet disks.

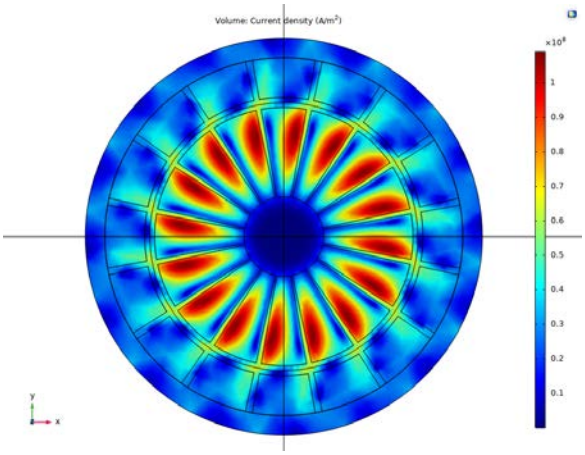

Figure 5.6: Current density distribution.

considering only the internal disk rotating and external one stopped. We can therefore calculate the currents with the internal PMs disk stopped and the other in rotating. The sum of the two currents is therefore the current of the system with both rotating disks. Also in this case to calculate ω_2 which satisfies the null torque condition we proceed by attempts; in figure 5.7 are shown the values of ω_2 in function of ω_1 in order to obtain null torque. We can see how at low velocity the basic relation 2.1 indicates with "Theoretical" is valid while for higher velocities (>500 rpm) ω_2 is lower with respect the theoretical forecast. With the parameters of the case of study the theoretical speed

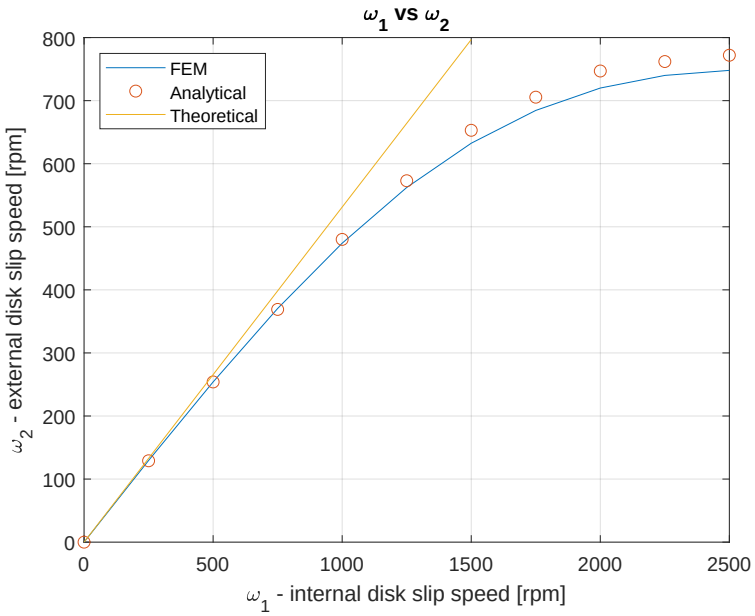

Figure 5.7: External velocity in function of the internal velocity with the condition of null torque.

relation is:

$$\omega_2^{TH} = \frac{R_{m,int}}{R_{m,ext}} = 0.531\omega_1 \tag{2.2}$$

Analytical model and FEM simulation again are in agree even if is still presence the positive difference between analytical and FEM outcomes.

5.2.1 Considerations

The system with two opposite rotating PMs disks obviously presents a more complexity due by the needed to have two independent rotating system to build but also to control. The issues related to this system are the following:

- It's needed a big accuracy to set ω_2 in function of ω_1 to avoid perfectly the torque. If the metal disks to heat is standardized ω_2 can be a default function of ω_1 but if the metal disk change in shape or in material it's necessary to develop a feedback system with sensor which measures the speed and the direction of the metal disk in order to accelerate the internal or the external disk. It must be said that isn't necessary which the electromagnetic torque is perfectly zero because on the disk act static friction forces anyway.
- The axial force is still present therefore a blocking system is required.
- It's necessary that the disk has been positioned perfectly with the centre in the rotation axes od the PMs or which the disk is bigger with respect the PMs in order

to avoid the x and y-direction force satisfied only with these conditions.

- The external velocity depends also by the material type, in fact for aluminium the null torque condition is different with the respect copper when is not satisfied the theoretical condition. By changing only the metal of the disk, table 5.2 shows the values of ω_2 which satisfy the null torque condition. We can note how for the

Material	ω_1	ω_2	T_e	F_z
Cu (57 MS/m)	2500 rpm	738 rpm	2.06E-5 Nm	191.2 N
Al (37.7 MS/m)	2500 rpm	1008 rpm	-1.90E-4 Nm	129.3 N

Table 5.2: Null torque conditions for copper and aluminium.

aluminium disk ω_2 tends to the theoretical value of 1328 rpm which, as already mentioned, depends only by the geometrical properties of the system.

5.3 Alternating PMs disk motion

An other approach to avoid the torque which affects the metallic disk is to apply an alternating rotation of the PMs disk in order to have the average torque equal to zero. The instantaneous torque is in general different to zero and therefore it's necessary to study the response of the mechanical system in order to control the resonance phenomena. At the instant t the disk is affect by the electromagnetic torque T_e which in sinusoidal steady state is described by the relation:

$$T_e(t) = T_{e,max}\sin(\omega t) \tag{3.3}$$

where the initial time has been chosen in order to have torque equal to zero. An other force applied on the disk is the friction which have torque T_f assumed constant. If the disk is still the friction is null while if the disk is in motion, the friction is in the opposite direction of T_e. We can therefore incorporate the friction in T_e. Applying the dynamic to the disk which have moment of inertia I we obtain the equation:

$$I\frac{d^2\theta(t)}{dt^2} = T_{e,max}\sin(\omega t) \tag{3.4}$$

The solution of this differential equation is the sum of the solution of the associated homogeneous equation plus the particular solution which are respectively:

$$\theta'(t) = A\frac{d\theta}{dt} + B\theta \tag{3.5}$$

$$\theta''(t) = \left(\frac{\omega_0}{\omega}\right)^2 \sin(\omega t - \pi) \tag{3.6}$$

where $\omega_0 = \sqrt{T_{e,max}/I}$ is the natural frequency. If we consider the disk with initial position and velocity equal to zero (A=0=B) the general solution is the equation 3.6 and the oscillation amplitude (which is in phase opposition) θ_{max} is therefore:

$$\theta_{max} = \left(\frac{\omega_0}{\omega}\right)^2 \tag{3.7}$$

The goal is to obtain an amplitude as low as possible therefore ω have to be as high as possible with respect ω_0. It's interesting to understand the values of ω_0 for a copper and aluminium disk. We suppose to operate with parameters of the example in chapter 3 shown in table 3.1 in particular the radius of the disk is 15 cm. At 1000 rpm we suppose that the torque is about the same for copper and aluminium of 14 Nm. We remember that the torque once reach the max value, decrease with increasing ω. Remembering that for a cylinder of radius R and mass M the moment of inertia is $\frac{1}{2}MR^2$ and remembering that $\rho_{Al} = 2.70\ kg/dm^3$ and $\rho_{Cu} = 8.92\ kg/dm^3$, the ratio between the two natural frequencies is:

$$\frac{\omega_0^{Cu}}{\omega_0^{Al}} = \sqrt{\frac{T_e^{Cu}}{T_e^{Al}}\frac{\rho_{Al}}{\rho_{Cu}}} \sim \sqrt{\frac{\rho_{Al}}{\rho_{Cu}}} = 0.55 \tag{3.8}$$

For this system of heating based on alternating motion of the permanent magnets it's easy to heat copper with respect aluminium because of its lower natural frequency which is:

$$\omega_0^{Cu} = \sqrt{\frac{T_e}{I}} \sim 19.80\ rad/s \equiv 189\ rpm \tag{3.9}$$

If we set therefore for example ω equal to 2000 rpm the amplitude of the oscillations is lower than 0.5° without considering the reduction of torque due by the higher velocity. Now we've understand what we have to choose a frequency bigger with respect the natural frequency, we can start to study the alternating PMs disk motion.
With the support of figure 5.8 we start to study the angular position φ of the PM with respect the metallic disk in function of the time. In sinusoidal steady state the angle for example have the following expression:

$$\varphi(t) = -\varphi_M \cos(\omega_{PM} t) \tag{3.10}$$

where ω_{PM} is the angular velocity of the PMs disk, imposed for example by an actuator and φ_M is the amplitude of oscillation which, in order to have a optimized system, has to be an integer multiple of the magnet pitch:

$$\varphi_M = k\frac{\pi}{p} \quad k \in \mathbb{N} \tag{3.11}$$

The instantaneous angular velocity ω is therefore:

$$\omega(t) = \dot{\varphi}(t) = \varphi_M \omega_{PM} \sin(\omega_{PM} t) \tag{3.12}$$

we can therefore say that ω has maximal value ω_M which is:

$$\omega_M = \varphi_M \omega_{PM} \tag{3.13}$$

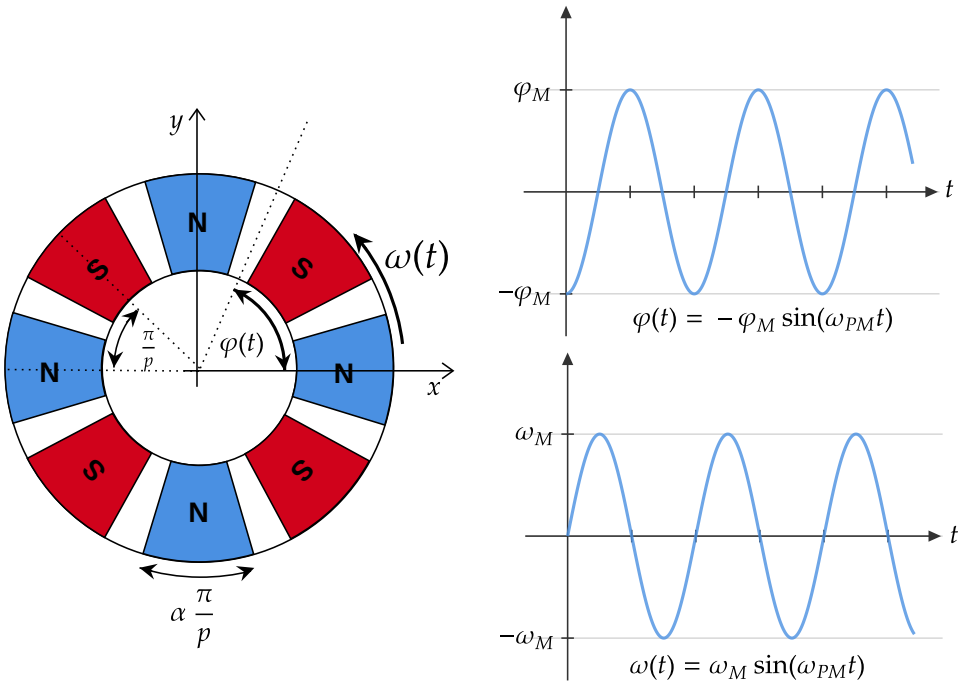

Figure 5.8: Alternating PMs disk system.

We can therefore apply this result to the analytical model: in fact we can study this system with quantities defined in sinusoidal steady state as a linear system by using the expressing with the RMS value. The RMS value of the angular velocity, which is the only parameter that interest us, is expressed by:

$$\omega_{RMS} = \frac{1}{\sqrt{2}} \varphi_M \omega_{PM} \tag{3.14}$$

which depends by the pitch of the PMs disk and by its frequency. In order to have a good value of power it's necessary to have a big pitch in fact, being φ_M expressed in radians, decrease the product with ω_{PM} if lower of 57.3°.
For this system, for the complexity of implementation in Comsol Multiphysics®, the FEM simulation will not be done also because the difficulty to create an alternating mechanical motion makes this system difficult to develop.

5.3.1 Considerations

The complexity of this configuration is the type of movement which can be make starting from a rotational motion to a alternating one with a connecting rod-crank mechanism or by stepper motors. The issues derived by this system are related to the inertia of the PMs disk which have to change the direction of rotation many times per second therefore if the PMs disk is no lighter enough the mechanical stress is huge.

Even if this method makes null the average torque doesn't cancel the axial force thus it's necessary to fix the metal disk. An other important issue is that this system has limited power because of the maximal parameters influence the transmitted power with its RMS value. An advantage is that for this system the centre of the metallic disk not necessarily has to be placed along the rotation axes, in fact is every position the average torque is always null. This gives opportunity to heat complex shape object.

5.4 Specular PMs disks

This configuration has been studied in order to eliminate both the torque and the axial force acting on the metallic disk. The idea is to put an other PMs disk above the metallic disk, specular with respect the bottom one. We have therefore two PMs disks which have to control the conditions of null torque and null axial force with its angular velocity. Anyway the goal is not to attain these two conditions but transmit controlled power! Therefore it's necessary to insert an'other degree of freedom which can be reached by adding an other disk. As shown in figure 5.9 the third PMs disk in inserted in the centre of the bottom disk, creating the coaxial PMs disk configuration already seen in section 5.2. We can therefore name 1 the PMs bigger bottom disk with internal radius R_{i1} and

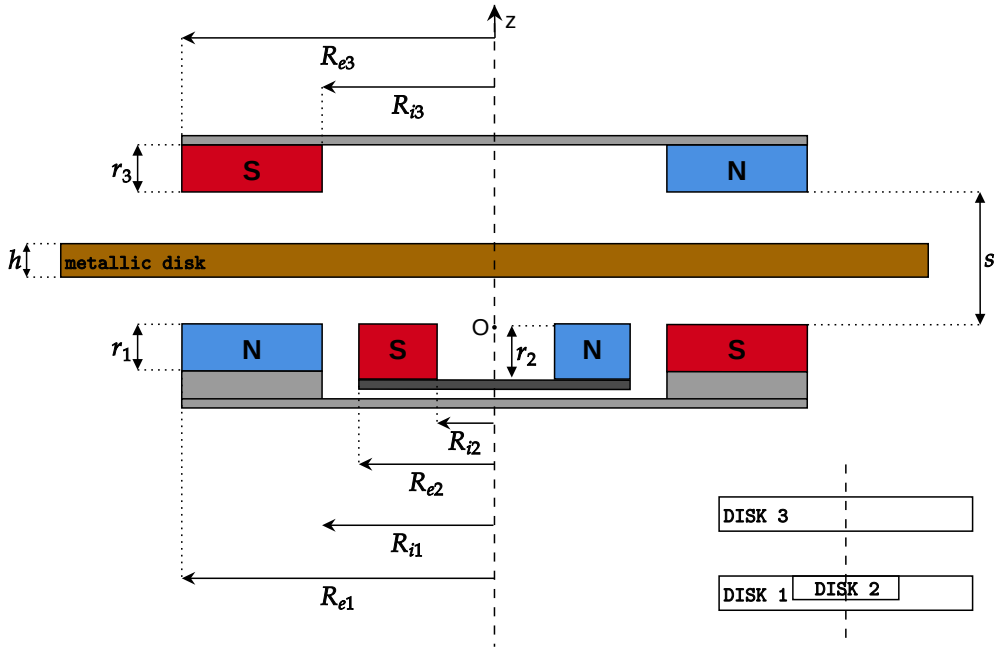

Figure 5.9: Schematic representation of specular PMs disk.

eternal R_{e1}, the bottom internal 2 with radii R_{i2} and R_{e2} while the upper would be the PMs disk 3 with R_{i3} and R_{e3}. We suppose that the PMs of the disks 1 and 2 are levelled at the same z-coordinate therefore s is the air gap thickness between the top and the

bottom disks. The system of equation to satisfy is therefore:

$$\begin{cases} P(\omega_1, \omega_2, \omega_3)\Big|_{z^*} = P^* \\ T_e(\omega_1, \omega_2, \omega_3)\Big|_{z^*} = 0 \\ F_z(\omega_1, \omega_2, \omega_3)\Big|_{z^*} = mg \end{cases} \tag{4.15}$$

where P^* is the power transmitted into the metallic disk which has mass m, g is the gravity (9.81 m/s^2) while z^* indicates the z-coordinate of equilibrium. It has to note that if the metallic disk would not subjected to the gravity force, the condition of $T_e = 0$ and $F_z = 0$ would be reached by using only the PMs disks 1 and 2 with the condition of opposite speed if the two disks are identical.
As an example we consider a specular PMs disks system with parameters shown in table 5.3. Due by the large number of degree of freedom of the system we decide to impose

Symbol	Description	Value
R_{e1}	External radius of disk 1	90 mm
R_{i1}	Internal radius of disk 1	70 mm
R_{e2}	External radius of disk 2	60 mm
R_{i2}	Internal radius of disk 2	40 mm
R_{e3}	External radius of disk 3	90 mm
R_{i3}	Internal radius of disk 3	70 mm
R_d	Radius of the conductive disk	120 mm
r	Magnet thickness	5 mm
s	Air-gap length	15 mm
h	Conductive plate thickness	5 mm
α	PMs pole-arch to pole-pitch ratio	0.9
p	Pole-pairs number	8
B_r	Remanence of PMs	1 T
σ	Conductivity of the metal (Cu)	57 MS/m
m	Mass of conductive metal	2.02 Kg
y	Yoke thickness	2 mm
μ_{ry}	Yoke relative permeability	4000

Table 5.3: Parameters of the case of study for specular PMs disks.

the disk 1's speed at ω_1 equal to 1000 rpm. This condition can been seen as the imposition of the transmitted power P^* i.e. ω_1 controls the power while ω_2 and ω_3 control the torque T_e and the axial force F_z null conditions. The 3D graphics in figures 5.10 and 5.11 show the behaviour of the axial force and the electromagnetic torque in function of the ratio ω_1/ω_3 and the vertical shift Δz of the centre of the metal disk from the midway point of the air gap. The red plan represents the two-dimensional ω_1/ω_3-Δz plane where the axial force is null and the torque as well. The intersection of the red plan with the surf is a line. If exist, the equilibrium condition is reached when the is a intersection point between the line of the force and the line of the torque. The two graphics don't take into account the speed of the disk 2 (ω_2=0). In fact the speed of

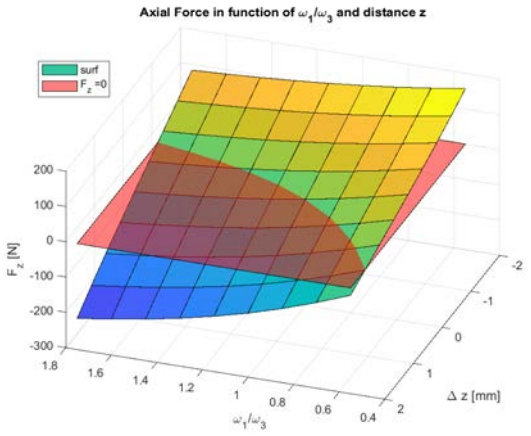

Figure 5.10: Axial force in function of ω_1/ω_3 and distance of the disk from the geometrical centre.

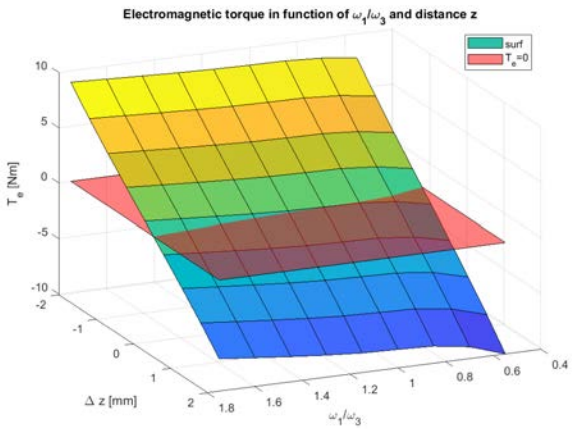

Figure 5.11: Electromagnetic torque in function of ω_1/ω_3 and distance of the disk from the geometrical centre.

the second disk is necessary if no intersection points are present between the lines. An other parameter to take in mind is the weight of the metal disk which can be considered by moving the axial force's red plan not for F_z=0 but for $F_z = mg$. This condition leads to a new equilibrium situation which is with a negative shift. The balance condition given by the intersection of the lines is well shown in the figure 5.12 where are plotted the torque and force lines on the (ω_1/ω_3,Δz) bidimensional space. As we expected,

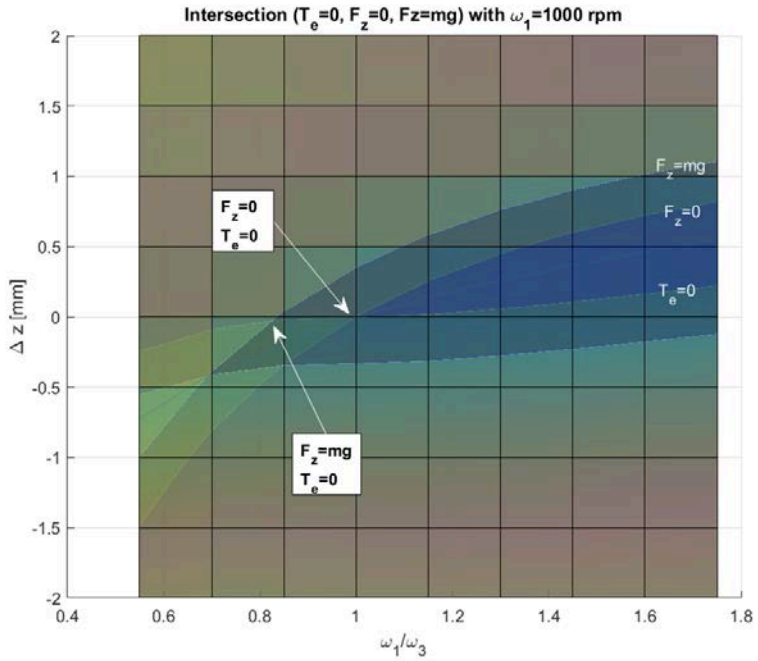

Figure 5.12: Balance conditions for torque and axial force.

without considering the weight of the workpiece the point of equilibrium is reached for ω_1=ω_3 with null shift while, taking into account the mass m of the metal, the new balance condition is reached with a negative shift in fact the metal disc would tend to fall down. The downward shift is extremely limited (<0.1 mm) cause the high electromagnetic force involved on the system. It's easy to see that the variation of torque with respect the distance z is limited than the variation of force and both curves increase with the speed increasing.
Another piece of information to derive is the stability of the equilibrium point: supposing that initially the work piece is put in the middle of the air gap and the PMs disks 1 and 3 are rotating with same opposite speed. Due to the weight force the workpiece starts to move down and this z variation makes rotating it in the direction of the disk 1's rotating speed. The relative slip speed with the PMs disk 3 increase and the repulsive force for the disk 3 as well while the relative. The slip between disk 1 and work piece has been decreased with a consequential reduction of the axial force. This situation could lead to an unstable condition but the variation of air gap between metal disk and PMs disk 1 increase drastically the axial force with a consequential increase of the axial force which affect the workpiece therefore we have a steady balance.
The transmitted power in function of $\omega_1/\omega/2$ and Δz is shown in figure 5.13. We can

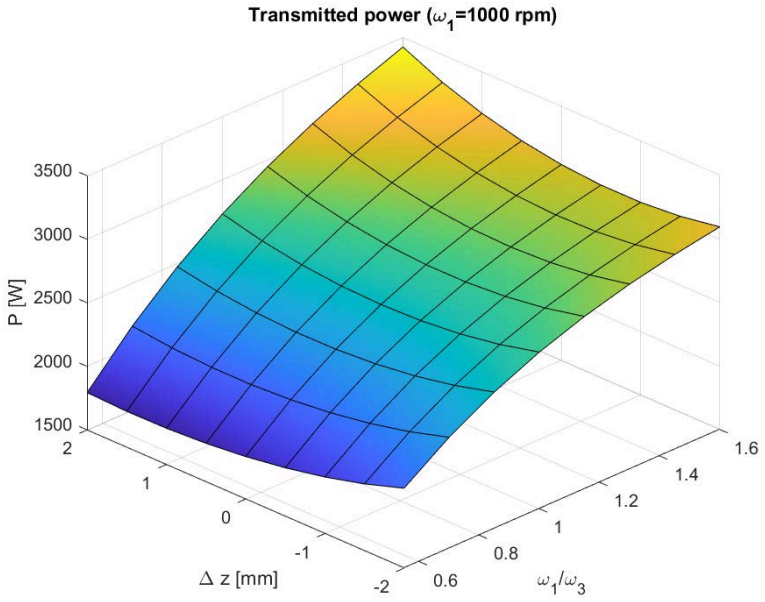

Figure 5.13: Power distribution in function of ω_1/ω_3 and Δz.

note that the balance conditions is achieved with the minimum of the power, once fixed the ratio of velocities. Figure 5.14 shows the transmitted power in function of ω_1 and ω_3 and if $\omega_1 = \omega_3 = 1000$ rpm the power is P = 2.50 kW while with only one disk in motion the power would be 670 W. This is the proof that we can't apply the superposition of the effects for the power, in fact we applied the superposition for the current. The power therefore is by using two specular disks, one on the top and one on the bottom

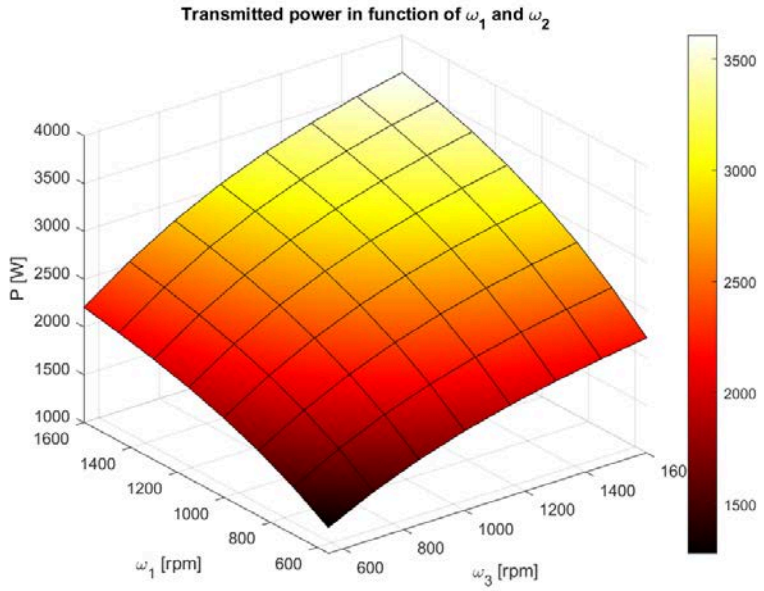

Figure 5.14: Power transmitted in function of ω_1 and ω_3 for Δz=0.

of the workpiece, is more than the double of the power transmitted for a single disk in rotation. That's due to the fact that the second PMs disk changes the magnetic field distribution in the core of the workpiece in particular we obtain a stronger the magnetic flux density time variation which generates for the Faraday's law a bigger electromotive force and induced current as well; this is a particularity of the specular PMs disks system.
These consideration are valid only disregarding the speed of the 2^{nd} disk cause the complication of the system and the difficulty to draw a graphic in function of ω_1, ω_2 and ω_3.

5.4.1 Considerations

This kind of system allows to avoid the torque and the axial force which affect the workpiece and it has the following advantages as well:

- High increase of the transmitted power on the workpiece.
- More uniform heating along the thickness of the workpiece and symmetry of the eddy current density on the both sides of it.
- The suspension of the workpiece in air reduces the heat conduction losses.
- Possibility to reduce the air gap thickness cause the workpiece tends to be arranged in the middle between the upper and the lower disks.

The complexity of this heating system is the main issue and gives the following drawbacks:

- Necessity to have a sensor which measures the slip speed of the metal disk.
- Necessity to have a control system on the basis of the workpiece slip speed which controls in feedback
- High mechanical complexity manufacturing for the system.
- Difficulty to manage a system with three PMs disks velocities ω_1, ω_2, ω_3.

5.5 Hybrid system

As we already told, induction heating system is customized on the basis of the material to heat, the shape of the workpiece, the type of heat treatment (core heating, hardening, preheating) in terms of inductor shape but mainly on frequency. It works better for magnetic metals conductors while the electrical efficiency to hear copper or aluminium is generally below 50%.
The permanent magnets system, on the other hand, works best for good conductive materials and the power is proportional to the round speed of the PM with respect the load and doesn't heat magnetic metals. In order to obtain a system which combine the characteristics of heating with sufficient efficiency for good conductors and magnetic poor conductor starting from copper to magnetic steels, we can join pancake inductor with PMs to obtain an hybrid system as shows in figure 5.15. The pancake inductor has

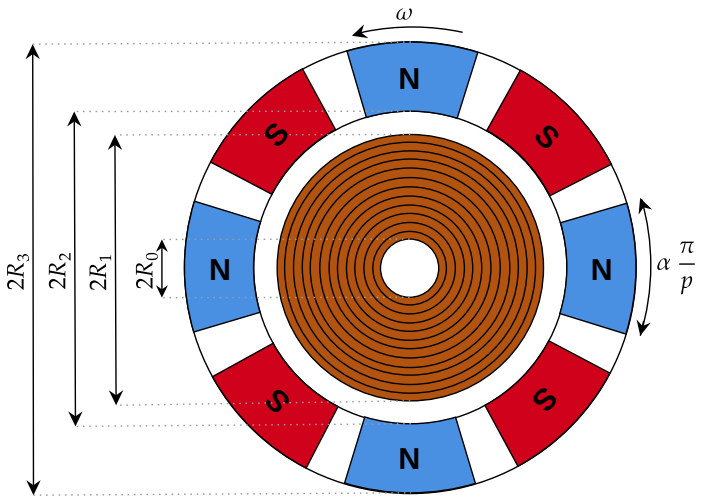

Figure 5.15: Hybrid system scheme.

internal radius R_0 and external R_1 while the PMs disk with four pole pairs number has internal radius R_2 and the external R_3. The idea is that in presence of a magnetic workpiece only the pancake inductor is power on while is off in presence of good conductor and the PMs disk rotates with angular velocity ω.
Obviously what we do expect is that axial force and torque are still present on the workpiece when PMs turns therefore it's necessary to fix it.

If R_2 is at least 10% grater than R_1 we can consider the two system separately because the induced currents don't mix and therefore in this condition the total transmitted power can is the sum of the power for each contributor. Considering an hybrid system with characteristic in table 5.4 we wanna to show the possibility to heat a metallic disk made up copper and AISI steel 430. The main contributor to heating copper is the PM

Quantity	Value	Description
R_0	25 mm	Internal radius inductor
R_1	80 mm	External radius inductor
R_2	100 mm	Internal radius PM disk
R_3	130 mm	External radius PM disk
R_d	150 mm	Metallic disk radius

Table 5.4: Parameter of the case of study.

disk which with a speed of 1550 rpm generates into the disk with thickness 5 mm with an airgap 5 mm is 2.18 kW. While a pancake coil with 25 turns and 30 A only 38 W with a very poor efficiency so it's not convenient to switch it on. The choice to place the PMs disk externally derives that the heating produced is very higher if would be placed internally. Figures 5.16 and 5.17 show the graph of the current density J in function of the radial coordinate of the disk ρ and the depth z for the hybrid system into the metallic disk made of copper and steel respectively. How we expected, in the copper

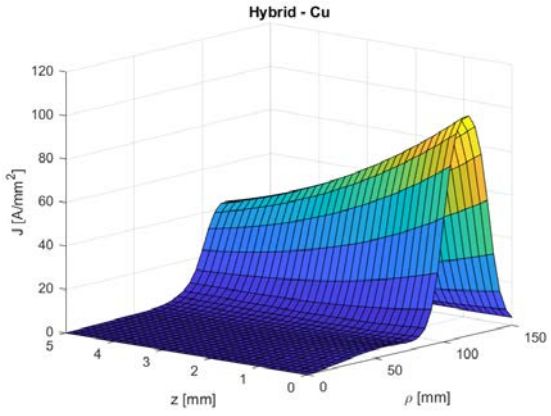

Figure 5.16: Surface current density in copper disk for hybrid system - 1 kHz - 1500 rpm.

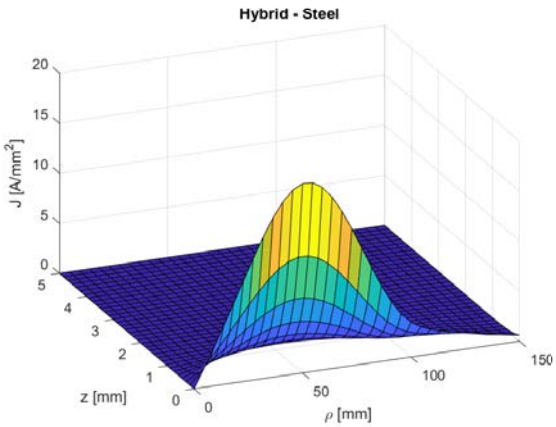

Figure 5.17: Surface current density in AISI steel 430 disk for hybrid system - 20 kHz - 1500 rpm.

disk the major contributor to the heating is the PMs disk whereas in the case of steel the heating power contribution from the PMs is just 13.7 W with respect 958 W given by the pancake inductor. In the case of copper the inductor worked ad 1 kHz while in the case of steel 20 kHz and the parameters of PMs disk are the same used in table 5.3 unless otherwise specified.

Since the several orders of magnitude of difference between the induced currents generated from inductor and PMs disk, figures 5.18 and 5.19 show the previous two graphs with the current density in logarithmic scale. We can note that the current along the

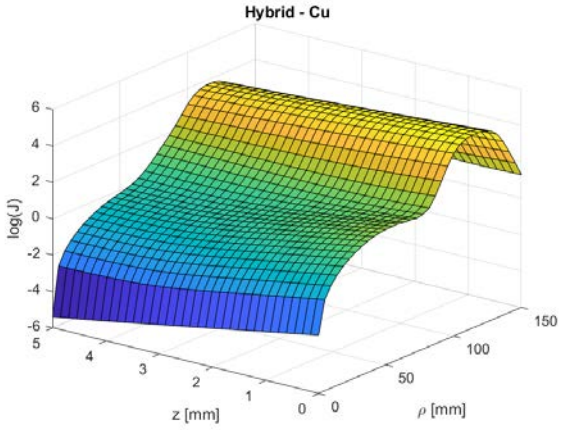

Figure 5.18: Surface current density in copper disk for hybrid system in log scale- 1 kHz - 1500 rpm.

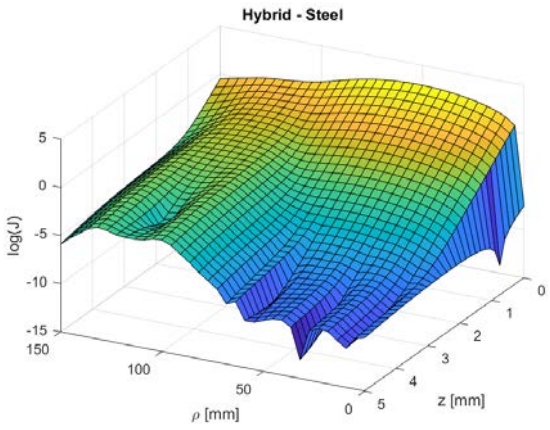

Figure 5.19: Surface current density in AISI steel 430 disk for hybrid system in log scale - 20 kHz - 1500 rpm.

thickness of the disk generated by the pancake decreases more than the current of the PMs and this is correlated by the frequency of the current which feeds the inductor i.e. the penetration depth. The current along the radial coordinate ρ of the metallic disk depends too by the azimuthal angle therefore it has been chosen the θ angle which maximize the current peak, this explains difference of the peaks current for the two system separately (100 A/mm^2 vs 15 A/mm^2). In fact while the eddy current generated by the inductor are independent from the azimuthal angle and the heating is more uniform than with PMs which has a number of $2p$ (poles number) local heat sources.
The advantages of the hybrid system are thus the possibility to heat different type of metals magnetic and non-magnetic, good conductors or not with a global sufficient efficiency. The drawbacks derives by the necessity to have a mechanical system based on motor and a electrical system based on inverter, capacitors which supply the inductor. This kind of system would have interesting domestic applications because it avoid the necessity to buy specific induction pots if it were not for axial force and the torque applied to the pot and generated with the rotation of the PMs.
With this hybrid system we extend the range applicability and, implementing control and feedback systems, we should obtain not an induction heating system but an "induction heating device" where the choice of the load is semi-independent by the heating.

Remarks and Future trends

Among the conclusions and overall considerations that have been written at the end of each chapter, some remarks must be given.
The analytical model for pancake inductors predicts the trend of the power transferred to the load with an error of a few percentage points. This error increases with increasing frequency and magnetic permeability of the material. However, it is possible to make rough predictions on the power transferred for a wide range of frequencies with computational times significantly shorter than the FEM study. It has been seen that the heating of excellent conductors such as copper, brass and aluminium by means of a pancake coil is inefficient and limited in terms of transmitted power, i.e. induction heating (in general) is not suitable to heat these types of metals.
The innovative mechanical heating system with permanent magnets instead is much more effective for this kind of non-magnetic metals. The analytical model developed in this thesis work for this system is in excellent agreement with the FEM results in terms of power transfer to the load, axial force generated and torque. The computational time of the analytical model is inverse in the choice of parameters and much shorter than that of the FEM simulation which, especially for high rotational velocity, can be tens of hours.
The repulsive force and the mechanical moment to which the load is subjected considerably limit the applications of this system, currently only in the industrial field. With particular precautions, however, the torque and axial force can be elided with a consequent complication of the mechanical and control part. While for pancake inductors the technology is already present and studied and the purpose of the analytical model is to reduce the study time, the permanent magnet system is still little known and used. Here has been presented a configuration with axial flux which is useful to heat flat metal pieces but other types of configurations can be studied based on the shape of the workpiece to heat. In the case of heating cylindrical billets the most effective configuration can be with radial flux PMs as shown in figure 5.20.
In any cases the big issue is the axial force that limits the safety and applicability in the home, so future studies will have to solve or avoid this problem. A possible solution can be to put a ferrite layer on the top of the pot, in order to eliminate the axial force or better, to make the force attractive, in this way the friction between pot and hob plane will also avoid the torque.

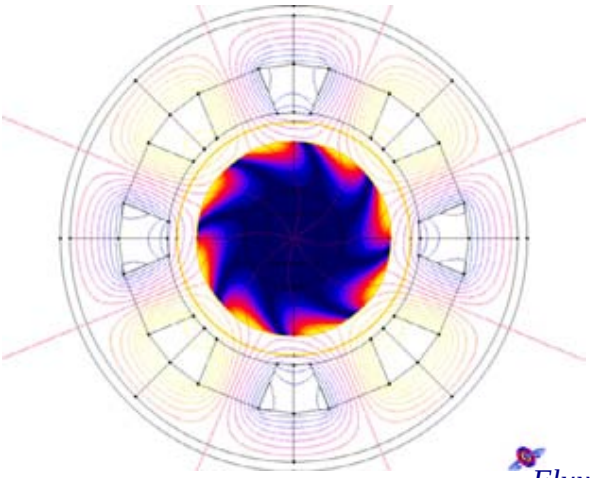

Figure 5.20: Induced current density distribution and equiux lines resulting in the steady-state condition of a transient FEM solution for a radial magnetic field [28].

Appendix A

A.1 Nodes and weights of the Gauss-Laguerre quadrature

i	x_i	w_i
1	0.070539889692	0.1687468018511
2	0.3721268180016	0.2912543620061
3	0.9165821024833	0.266686102867
4	1.7073065310283	0.1660024532695
5	2.7491992553094	0.074826064668792
6	4.048925313851	0.02496441730928
7	5.6151749708616	0.006202550844572
8	7.459017453671	0.0011449623864769
9	9.5943928695811	1.5574177302781E-4
10	12.038802546964	1.5401440865225E-5
11	14.814293442631	1.086486366518E-6
12	17.948895520519	5.330120909557E-8
13	21.47878824029	1.757981179051E-9
14	25.451702793187	3.725502402512E-11
15	29.932554631701	4.7675292515782E-13
16	35.01343424048	3.372844243362E-15
17	40.833057056729	1.1550143395E-17
18	47.619994047347	1.539522140582E-20
19	55.810795750064	5.28644272557E-24
20	66.524416525616	1.656456612499E-28

Table A.1: First 20 terms of Gauss-Laguerre's coefficients.

List of Figures

Bibliography

[1] Wikipedia contributors, *Induction heating — Wikipedia The Free Encyclopedia*, accessed 31-May-2020, https://en.wikipedia.org/w/index.php?title=Induction_heating&oldid=958969019, Online.

[2] GH group Induction atmosphere, *What is induction heating?*, Online content, accessed June 2020, http://www.gh-ia.com/induction_heating.html.

[3] Sergio Lupi, *Appunti di elettrotermia*, A.A. 2005-2006 - pag. 5.

[4] Industry association position on PEF revision, 2018, Online content, https://www.eurelectric.org/media/2382/2018_industry_association_position_on_pef_revision-2018-030-0114-01-e-h-216CBE01.pdf.

[5] Anke Esser (FhG-ISI), Frank Sensfuss (FhG-ISI), Review: Christof Amann (e7), Patxi Hernandez Iñarra (Tecnalia), *Evaluation of primary energy factor calculation options for electricity*, 13.05.2016.

[6] European commission directorate-general for energy- Directorate C. 2 New energy technologies, innovation and clean coal, *Mapping and analyses of the current and future (2020 - 2030) heating/cooling fuel deployment (fossil/renewables)*, Final report, September 2016.

[7] Induction chillers, *Explanation on how Induction Heating Works*, Online content, accessed June 2020, http://www.inductionchiller.com/induction-heating/.

[8] RDO Heating solution, *Components of induction heating*, Online content, accessed July 2020, https://www.rdoinduction.com/components-of-induction-heating.html.

[9] EFD Induction Inc.

[10] Thomas Bayerl, Miro Duhovic, Peter Mitschang, Debes Bhattacharyya, *The heating of polymer composites by electromagnetic induction*, A review, Composites Part A: Applied Science and Manufacturing, Volume 57, 2014, Pages 27-40, ISSN 1359-835X, https://doi.org/10.1016/j.compositesa.2013.10.024.

[11] Sergio Lupi - *Appunti di elettrotermia* - A.A. 2005-2006 - pag. 259.

[12] Bowman, Frank Introduction to Bessel Functions (Dover: New York, 1958).

[13] Dissegna Filippo, Prof. Fabrizio Dughiero, *A novel power control strategy for induction cooktops designed by means of analytical, circuital and FEM modelling*, Universita' degli Studi di Padova, Tesi di laurea magistrale, Anno accademico 2018/2019.

[14] S. Lupi, *The calculation of planar circular coils for the induction heating of bimetallic plates*, Archiv für Elektrotechnik, vol. 60, pp. 313318, Nov 1978.

[15] Abramowitz, M.; Stegun, I. A. *Handbook of Mathematical Functions*, Equation 25.4.45, Dover.

[16] A. Spagnolo, P. Bariani, G. Martinelli, S. Lupi, *Auto-adaptive multi-coil inductors for transverse flux induction heating of metal strips*, Scuola di Dottorato in Ingeneria Industriale, Universita' di Padova, XXII ciclo.

[17] T. Lubin, and A. Rezzoug, *Steady-state and transient performance of axial-field eddy-current coupling*, *IEEE Trans. Ind. Electron.*, vol. 62, no. 4, pp. 22872296, Apr. 2015.

[18] Z. Mouton, and M. J. Kamper, *Modeling and Optimal Design of an Eddy Current Coupling for Slip-Synchronous Permanent Magnet Wind. Generators*, *IEEE Trans. Ind. Electron.*, vol. 61, no. 7, pp. 33673376, Jul. 2014.

[19] Griffiths, David J. . *Introduction to Electrodynamics*, 3rd ed., Prentice Hall, p. 438, 1999.

[20] Thierry Lubin, Abderrezak Rezzoug, *3-D Analytical Model for Axial-Flux Eddy-Current Couplings and Brakes Under Steady-State Conditions*, Université de Lorraine, Groupe de Recherche en Electrotechnique et Electronique de Nancy, GREEN, F-54500 Vandoeuvre-lès-Nancy, France, *IEEE Transactions on Magnetics*, October 2015 - page 3-5.

[21] D. SPAEK, *Analytical electromagnetic field and forces calculation for linear, cylindrical and spherical electromechanical converters*, Bulletin of the polish academy of sciences, Technical sciences Vol. 52, No. 3, 2004.

[22] Thierry Lubin, Abderrezak Rezzoug, *3-D Analytical Model for Axial-Flux Eddy-Current Couplings and Brakes Under Steady-State Conditions*, Université de Lorraine, Groupe de Recherche en Electrotechnique et Electronique de Nancy, GREEN, F-54500 Vandoeuvre-lès-Nancy, France, *IEEE Transactions on Magnetics*, October 2015 - page 6.

[23] Manoharan, S., Devarajan, N., Deivasahayam, S.M., Ranganathan, G., *Review on efficiency improvement in squirrel cage induction motor by using DCR technology*. J. Electr. Eng. 2009.

[24] Trolleymotion Ebus Berlin., *Vergleich unterschiedlicher Antriebstechnologien für elektrische Busantriebe*, Berlin, 31.05.2016.

[25] A. Mohtar, Z. Nedic1 and J. Machotka, *A compact and affordable BLDC motor controller for a microelectronics remote laboratory*, School of Electrical and Information Engineering, University of South Australia, Adelaide, SA, Australia.

[26] M. P. Paranthaman, I. C. Nlebedim, F. Johnson, S. K. McCall, *Additive Manufacturing of Permanent Magnets*, Material Matters, 11.4.2016.

[27] Matthias Katter, *Industrial development of materials for sustainable development (magnets + magneto-caloric materials)*, September 2009

[28] F. Dughiero, M. Forzan, S. Lupi, M. Zerbetto and F. Nicoletti, *A new high efciency technology for the induction heating of non magnetic billets*,pag. 1531, Department of Electrical Engineering, University of Padua, Padova, Italy, and Inova Lab srl, Leinì, Italy.